Collider Signals of New Physics Beyond The Standard Model

A THESIS

submitted for the award of Ph.D. degree of

MOHANLAL SUKHADIA UNIVERSITY

in the

Faculty of Science

by

Pankaj Sharma

Under the Supervision of

Saurabh D. Rindani
Senior Professor
Theoretical Physics Division
Physical Research Laboratory
Ahmedabad, India

DEPARTMENT OF PHYSICS
MOHANLAL SUKHADIA UNIVERSITY
UDAIPUR
Year of submission: 2011

To

mummy, papa, munnu and manku

DECLARATION

*I **Mr. Pankaj Sharma**, S/o Mr. Tara Prakash Sharma, resident of 202, PRL Thaltej Hostel, Bodakdev, Ahmedabad 380009, hereby declare that the work incorporated in the present thesis entitled, **"Collider signals of new physics beyond the Standard Model"** is my own and original. This work (in part or in full) has not been submitted to any University for the award of a Degree or a Diploma. I solely own the responsibility for the originality of the entire document.*

Date :

(Pankaj Sharma)

CERTIFICATE

I feel great pleasure in certifying that the thesis entitled, **"Collider signals of new physics beyond the Standard Model"** embodies a record of the results of investigations carried out by Mr. Pankaj Sharma under my guidance.

He has completed the following requirements as per Ph.D. regulations of the University.

(a) Course work as per the university rules.

(b) Residential requirements of the university.

(c) Presented his work in the departmental committee.

(d) Published minimum of two research papers in a referred research journal.

I am satisfied with the analysis of data, interpretation of results and conclusions drawn.

I recommend the submission of thesis.

Date :

Saurabh D. Rindani
Senior Professor
(Thesis Supervisor)

Countersigned by
Head of the Department

Acknowledgements

It is a great pleasure to acknowledge those people who have helped me grow into the physicist I am today. First and foremost is my thesis supervisor, Prof. Saurabh D. Rindani, who has always encouraged me to learn invaluable techniques and skills, and shared with me many of his interesting ideas on which to pursue research. Dr. Namit Mahajan who has always provided invaluable guidance in research and always encouraged to pursue challenging problems. Apart from academics, he has been a great motivator and support during my stay here at PRL.

I would like to thank all my collaborators Prof. Katri Huitu, Prof. Rohini Godbole, Prof. M. Mullheitner, Dr. Rui Santos, Dr. Ritesh K. Singh, Dr. Kumar Rao, Dr. Santosh K. Rai, Dr. Sudhanshu Biswal, Christian Hangst, Miguel Won and Ketan Patel for providing opportunities to work with them. Working with them was really fun and interesting. In particular, working with Ketan and Sudhansu was really inspiring and sharing ideas with them provided great insight. I am also really thankful to Dr. Rui Santos for providing me a visit to HEP Group of Univ. of Southampton and for some really interesting discussions.

I would also like to acknowledge the support of all my colleagues at PRL with whom I spent five important years of my life, in particular, JRF06 batch. I am really grateful to Subimal da and Suman for giving me early lessons in Linux and patiently helping me. I thank Arvind, Ashwini, Debagnik, Vineet and Vimal for all the happy times together at Thaltej Hostel. The memories of the joyful time I spent at Tulip with Anand, Rabiul and Vimal are unforgettable. The company of Bhavik, T.K. Jha, Bhaswar, Ashok, Amzad, Sreekanth, Gyan and Alok at PRL main Hostel had been enjoyable. I also cherish the time spent with my younger colleagues (JRF09 and JRF10) at Thaltej Hostel. In particular, I cannot forget the taste of delicious food cooked by Yashpal and Naveen. Also, the time spent with them at Hospital after the Nal-Sarovar accident.

I am also grateful to PRL administration for all the support provided to me here. Specifically, I would like to acknowledge the support of Jigar Bhai, Parul Madam, Ghanshayam Bhai, Ranganathan sir (from Medical cell), Senthil bhai, who have been highly efficient.

Last but not the least, I would like to thank my parents, my younger brother Anant, and Shivani for their encouragement, love and support.

Pankaj Sharma

Abstract

The Standard Model (SM) has been extremely successful in explaining the fundamental interactions among elementary particles. However, the electroweak symmetry breaking (EWSB) sector of the SM remains untested yet as its central pillar, known as the Higgs boson, has not been discovered so far. That is why the most important goal of the current and future colliders like the Large Hadron Collider (LHC) at CERN and the International Linear Collider (ILC) is to discover the Higgs boson and study its properties with great precision so as to ascertain it to be the SM Higgs as different alternate scenarios beyond the SM (BSM) e.g., Minimal Supersymmetric Standard Model (MSSM), Two Higgs Doublet Model (THDM) etc. allow for a number of Higgs particles. Also, the top quark, because of its large mass (close to EWSB scale), is considered to play an important role in the probe of EWSB. In this thesis, we study Higgs boson and top quark couplings in various new physics (NP) scenarios and at different colliders to probe the EWSB utilizing the polarization of the final state top quark at the LHC and the polarization of the initial beams at the ILC.

In the case of the ILC, we study anomalous ZZH and γZH couplings in the process $e^+e^- \to ZH$ with polarized initial beams. We consider both electron and positron beams to be polarized simultaneously. Our main emphasis in this work is to obtain simultaneous limits on the anomalous couplings to the extent possible making use of combination of observables and/or polarizations. We study angular distributions of the Z using both longitudinally as well as transversely polarized beams and construct various asymmetries. We also study the angular correlations of the charged leptons coming from Z decay. Using the momenta of the charged leptons, we construct various correlations having definite CP and T transformation properties. We find that the longitudinal polarization helps to enhance the sensitivities of the couplings relative to the unpolarized case. The most remarkable result from the study of transverse polarization is that it helps to probe a specific coupling $\mathrm{Im}a_\gamma$ which is inaccessible in the distributions with longitudinally polarized as well as unpolarized beams.

In the context of the LHC, we focus on the study of NP involved in single-top production. First we study the single-top production in association with a W^- boson to study the sensitivity of the LHC to anomalous tbW couplings. Here we also consider the possibility of CP violation. Then we study single-top production in association with a charged Higgs in THDM of type II and probe the parameters

of the model at the LHC. In these studies, we utilize polarization of the final state top quarks since different NP scenarios give different predictions for top polarization. As a measure of top polarization, we look at various laboratory frame distributions of its decay products, viz., lepton angular and energy distributions and b-quark angular distributions, without requiring reconstruction of the rest frame of the top. In the charged Higgs case, we only study charged lepton angular distributions as they have been proven to be independent of any NP involved in top-decay and hence are the pure probes of parameters of THDM contributing only in the production. We construct certain asymmetries to study the sensitivity of these distributions to the NP involved in the single-top production. We find that these asymmetries are sensitive probes of the NP involved in the single-top production.

List of Publications

A. Papers related to thesis

1. **"Angular distributions as a probe of anomalous ZZH and gammaZH interactions at a linear collider with polarized beams"**
   S. D. Rindani and P. Sharma
   Phys. Rev. D **79**, 075007 (2009) [arXiv:0901.2821 [hep-ph]]

2. **"Decay-lepton correlations as probes of anomalous ZZH and gammaZH interactions in $e^+e^- \to ZH$ with polarized beams"**
   S. D. Rindani and P. Sharma
   Phys. Lett. B **693**, 134 (2010) [arXiv:1001.4931 [hep-ph]]

3. **"Probing anomalous tbW couplings in single-top production using top polarization at the Large Hadron Collider"**
   S. D. Rindani and P. Sharma
   arXiv:1107.2597 [hep-ph]

4. **"CP violation in tbW couplings at the LHC"**
   S. D. Rindani and P. Sharma
   arXiv:1108.4165 [hep-ph]

5. **"Probing top charged-Higgs production using top polarization at the Large Hadron Collider"**
   K. Huitu, S. K. Rai, K. Rao, S. D. Rindani and P. Sharma
   JHEP **1104**, 026 (2011) [arXiv:1012.0527 [hep-ph]]

B. Other Publications

1. **"Model-independent analysis of Higgs spin and CP properties in the process $e^+e^- \to t\bar{t}\Phi$"**
   R. M. Godbole, C. Hangst, M. Muhlleitner, S. D. Rindani and P. Sharma
   Eur. Phys. J. C **71**, 1681 (2011) [arXiv:1103.5404 [hep-ph]]

2. **"Forward-backward asymmetry in top quark production from light colored scalars in SO(10) model"**

K. M. Patel and P. Sharma
JHEP **1104**, 085 (2011) [arXiv:1102.4736 [hep-ph]]

C. Conference proceedings

1. **"Working group report: Physics at the Large Hadron Collider"**
   D. K. Ghosh *et al.*,
   Proceedings of WHEPP XI held at PRL on Jan 2-12, 2010,
   Pramana **76**, 707 (2011)

2. **"Probing anomalous ZZH and gammaZH interactions at an e+e- linear collider using polarized beams"**
   S. D. Rindani and P. Sharma
   arXiv:1007.3185 [hep-ph]
   To appear in the proceedings of International Linear Collider Workshop 2010 (LCWS10 & ILC10), Beijing, China, 26-30 Mar 2010

3. **"Constraining anomalous ZZH and gamma ZH interactions in the process $e^+e^- \to HZ$ at a linear collider with polarized beams "**
   S. D. Rindani and P. Sharma
   Proceedings of the XVIII DAE-BRNS (High Energy Physics Symposium),13-18 Dec 2008, Volume 18 (2008)

Abbreviations

BR	Branching Ratio
BSM	Beyond Standard Model
CKM	Cabbibo Kobayashi Maskawa
CLIC	Compact Linear Collider
CL	Confidence Level
cm	centre of mass
ev	electron-volts
EW	ElectroWeak
EWSB	ElectroWeak Symmetry Breaking
fb	femto barn
GUT	Grand Unification Theory
GeV	Giga Electron Volt
ILC	International Linear Collider
LC	Linear Collider
LEP	Large Electron-Positron Collider
LHC	Large Hadron Collider
LO	Leading Order
MeV	Mega Electron Volt
MSSM	Minimal Supersymmetric Standard Model
NLO	Next-to-Leading Order
NLL	Next-to-Leading Log
NP	New Physics
NWA	Narrow-Width Approximation
PDF	Parton-Distribution Function
pb	pico barn
RG	Renormalization Group
RGE	Renormalization-Group Evolution
SLAC	Stanford Linear Accelerator
SLC	SLAC Linear Collider
SLD	SLAC Large Detector
SM	Standard Model

SUSY	Supersymmetry
TeV	Tera Electron Volt
THDM	Two Higgs Doublet Model
QCD	Quantum Chromodynamics
QED	Quantum Electrodynamics
vev	vacuum expectation value

Contents

List of Tables

List of Figures

Chapter 1

Introduction

The Standard model (SM) of particle physics has been the most ambitious and the most organized efforts of many great particle physicists over the years to answer the question of what this universe is made up of. It has been a crown jewel of high energy particle physics for past several decades. However, there are various issues which cannot be explained in the SM, for example, the observed matter-antimatter asymmetry of the universe, experimentally observed neutrino mass etc. Also, the first-principle understanding of the mechanism of spontaneous electroweak symmetry breaking (EWSB) is not fully available to us. In the SM, masses of all the elementary particles are generated by introducing a scalar doublet into the theory which after acquiring the vacuum expectation value (vev) induce the EWSB. This mechanism is known as the Higgs mechanism which provides us three would-be Goldstone bosons corresponding to three broken generators, which appear as longitudinal polarizations of massive gauge bosons. The fourth degree of freedom of the scalar doublet is CP even and neutral, and corresponds to the "Higgs" boson [1]. So far, the Higgs boson has not been discovered. Therefore, the most important aim of current colliders, viz., the Large Hadron Collider (LHC) at CERN and the Tevatron at Fermilab; and future colliders, viz., the International linear collider (ILC) and the Compact Linear Collider (CLIC), is to probe the mechanism of EWSB through the study of interactions of Higgs with heavier particles like electroweak (EW) gauge bosons and the top quark.

The top quark is the heaviest elementary particle discovered so far. It has been discovered at the Tevatron which is a proton-antiproton collider. Because of its large mass, it is widely considered to be closely related to the mechanism of EWSB and provides a natural window to probe the hypothesis concerning the EWSB. The top quark is unique in the sense that it decays before its hadronization and hence provides a way to study the polarization of top quarks through the distribution of its decay products.

In this thesis, we explore different possible ways to probe the mechanism of EWSB through the studies of Higgs boson and top quarks at colliders. We utilize the polarization as a tool to probe the new physics responsible for EWSB. In the case of ILC we utilize the facility of beam polarization which we expect to be available there at the time of its operation. In the context of LHC, we study the polarization of top quarks in various single top production processes and construct various laboratory frame observables to probe couplings of top quarks and Higgs bosons related to EWSB. We have followed model independent approach in our analysis to probe the Higgs and the top quark couplings.

We begin this chapter with a brief overview of the SM and its Lagrangian. We then give an overview of EWSB and then study the Higgs boson couplings with the EW gauge bosons and fermions. We also give a brief introduction to the issue of polarization studies at colliders.

1.1 Standard Model (SM)

The SM [2] is a quantum field theory of the fundamental building blocks of the universe. These fundamental building blocks include fermions interacting with each other through interaction mediators known as gauge bosons. These gauge bosons arise by requiring the theory to be locally gauge invariant under transformations in the SM gauge group $SU(3)_C \times SU(2)_L \times U(1)_Y$.

We begin with a brief overview of construction of a Lagrangian invariant under local gauge transformations. This idea forms the building block of all gauge theories. The Lagrangian in a non-interacting $SU(N)$ gauge theory, also known as Yang-Mills theory [3], of a fermion of mass m is given by

$$\mathcal{L} = \bar{\Psi}\left(i\partial_\mu\gamma^\mu - m\right)\Psi \tag{1.1}$$

where Ψ is a N-plet of fermion fields ψ^a. It can be easily checked that the Lagrangian 1.1 is invariant under the phase transformation $\Psi(x) \to e^{i\alpha^a T^a}\Psi(x)$, where α^a $(a = 1, \ldots, N)$ are constant parameters and $T^a(a = 1, \ldots, N)$ are the generators of the $SU(N)$ group represented by Hermitian matrices which obey the commutation relations

$$\left[T^a, T^b\right] = if^{abc}T^c. \tag{1.2}$$

This invariance is known as 'global' $SU(N)$ gauge invariance. Now, let the phase parameters α^a depend upon space-time i.e., $\alpha^a = \alpha^a(x)$. Now the Lagrangian 1.1 is not invariant under such a local gauge transformation. To make it local gauge invariant, we must introduce vector fields into the theory which is accomplished through the definition of covariant derivative as :

$$\mathcal{D}_\mu \equiv \partial_\mu + igT^a A^a_\mu(x) \tag{1.3}$$

where A^a_μ transforms according to

$$T^a A^a_\mu(x) \to e^{i\alpha^a(x)T^a} \left\{ T^b A^b_\mu(x) - \frac{i}{g}\partial_\mu \right\} \left(e^{i\alpha^c(x)T^c} \right)^\dagger , \tag{1.4}$$

ensuring that $\mathcal{D}\Psi$ transforms exactly like Ψ under the gauge group $SU(N)$. This leads to the locally gauge invariant Lagrangian in terms of Dirac fields:

$$\mathcal{L} = i\bar{\Psi}\gamma^\mu \mathcal{D}_\mu \Psi - m\bar{\Psi}\Psi, \tag{1.5}$$

The covariant derivative brings in interaction between fermion fields and vector fields. For dynamical vector fields, it must have kinetic terms in the Lagrangian. We write kinetic term for vector field as :

$$\mathcal{L} = -\frac{1}{4}\mathcal{G}^a_{\mu\nu}\mathcal{G}^{\mu\nu}_a, \tag{1.6}$$

where

$$\mathcal{G}^a_{\mu\nu} = \partial_\mu G^a_\nu - \partial_\nu G^a_\mu - gf^{abc}G_{b\mu}G_{c\nu}, \tag{1.7}$$

to ensure that the kinetic term for non-abelian vector fields G^a_μ be invariant under gauge transformation. g is the same coupling that appears in the covariant derivative for the fermion. In the Lagrangian for vector fields, we cannot write mass terms for them explicitly because mass terms break gauge invariance.

As the basic recipe to construct a local gauge invariant Lagrangian has been explained, we now write the Lagrangian for the SM. The particle content in the SM is given in Table 1.1. In the SM, the left-chiral fermions and the right-chiral fermions have different quantum numbers, with the left-chiral fields arranged in doublets,

$$L_L = \begin{pmatrix} \nu_e \\ e \end{pmatrix}_L , \qquad Q_L = \begin{pmatrix} u \\ d \end{pmatrix}_L , \tag{1.8}$$

and the right-fermion fields in singlets,

$$e_R, \quad u_R, \quad d_R. \tag{1.9}$$

	Particles	electric charge	spin
Quarks	u, c, t	+2/3	1/2
	d, s, b	−1/3	1/2
Leptons	e, μ, τ	−1	1/2
	ν_e, ν_μ, ν_τ	0	1/2
Gauge bosons	γ, Z , gluons	0	1
	$W^{\pm}$	± 1	1
Scalar	Higgs	0	0

Table 1.1: *Particle content of the SM*

The Lagrangian describing the fundamental particles and their interactions in the SM is invariant under the transformations of the group $SU(3)_C \times SU(2)_L \times U(1)_Y$ as well as Lorentz invariant. We write the SM Lagrangian in the following form :

$$\mathcal{L}_{SM} = \mathcal{L}_{EW} + \mathcal{L}_{QCD} \tag{1.10}$$

where

$$\mathcal{L}_{QCD} = \bar{\Psi}\left[ig_s\frac{\lambda^a}{2}A^a_\mu\gamma^\mu\right]\Psi - \frac{1}{4}\mathcal{G}^{a\mu\nu}\mathcal{G}^a_{\mu\nu} \tag{1.11}$$

and $\mathcal{L}_{EW}$ is further written as :

$$\mathcal{L}_{EW} = \mathcal{L}_F + \mathcal{L}_G + \mathcal{L}_Y + \mathcal{L}_S, \tag{1.12}$$

with

$$\begin{aligned}
\mathcal{L}_F &= \sum_{i=1}^{3}\bar{\psi}^i_L\gamma_\mu\mathcal{D}^\mu_L\psi^i_L + \sum_{i=1}^{3}\bar{\psi}^i_R\gamma_\mu\mathcal{D}^\mu_R\psi^i_R, &(1.13)\\
\mathcal{L}_G &= -\frac{1}{4}\mathcal{W}^{a\mu\nu}\mathcal{W}^a_{\mu\nu} - \frac{1}{4}\mathcal{B}^{\mu\nu}\mathcal{B}_{\mu\nu}, &(1.14)\\
\mathcal{L}_Y &= -\mathcal{Y}^{ij}_u\bar{q}^i_L\tilde{\phi}u^j_R - \mathcal{Y}^{ij}_d\bar{q}^i_L\phi d^j_R - \mathcal{Y}^{ij}_e\bar{L}^i_L\phi e^j_R, &(1.15)\\
\mathcal{L}_S &= \left(\mathcal{D}^\mu_L\phi\right)^\dagger\left(\mathcal{D}_{L\mu}\phi\right) - \mathcal{V}(\phi). &(1.16)
\end{aligned}$$

In the Lagrangian of spin-half matter fields $\mathcal{L}_F$, the sum runs for all three generations of lepton and quark fields. In the Lagrangian of gauge fields $\mathcal{L}_G$, $\mathcal{W}^a_{\mu\nu}$ and $\mathcal{B}_{\mu\nu}$ are the field strength tensors for the vector fields of $SU(2)_L$ and $U(1)_Y$ gauge groups respectively. In the Yukawa Lagrangian $\mathcal{L}_Y$, $\mathcal{Y}^{ij}_u$, $\mathcal{Y}^{ij}_d$ and $\mathcal{Y}^{ij}_e$ are the Yukawa matrices for up-type quarks, down-type quarks and charged leptons respectively. The fermions couple to gauge bosons through covariant derivatives which are defined as:

$$\mathcal{D}_L^\mu = \left(i\partial^\mu - \frac{g_2}{2}\tau^a W^{a\mu} - \frac{g_1}{2} Y B^\mu\right), \tag{1.17}$$

$$\mathcal{D}_R^\mu = \left(i\partial^\mu - \frac{g_1}{2} Y B^\mu\right). \tag{1.18}$$

In the Lagrangian of Dirac and vector fields, there are no mass terms for them as they are forbidden by the gauge symmetries. We will see in the next section how the particle masses are generated by the spontaneous breakdown of $SU(2)_L \times U(1)_Y$ to $U(1)_Q$ (known as Higgs mechanism).

1.2 Electroweak Symmetry breaking (EWSB) in the SM

The gauge invariance under $SU(2)_L$ forbids mass terms for the fermions. Similarly, gauge boson mass terms $m_A^2 A^\mu A_\mu$ are also not allowed by gauge invariance. As we demand the SM Lagrangian to be gauge invariant, these explicit mass terms cannot be accommodated in the Lagrangian. Since all these particles are found to be massive in nature, we need to have some mechanism to generate masses of all the particles without spoiling gauge invariance. This problem is cured by introducing a hypercharge $Y = 1$ scalar $SU(2)_L$ doublet into the SM and when this scalar acquires a vev, it induces a spontaneous symmetry breaking, thereby generating the masses of all the particles in the SM. This mechanism is known as the Higgs-Brout-Englert-Guralnik-Hagen-Kibble mechanism of spontaneous symmetry breaking (SSB) [1] or simply "the Higgs mechanism". Under SSB, the Lagrangian remains invariant under the gauge transformations but the vacuum state do not respect the symmetry.

In the SM, SSB is induced by a Higgs doublet which is a hypercharge $Y = 1$ scalar $SU(2)_L$ doublet. The Higgs interacts with fermions through Yukawa couplings written in Eq. 1.15 and couples to gauge bosons through covariant derivative in the kinetic terms in the Lagrangian $\mathcal{L}_S$ of Eq. 1.16. The Higgs potential in Eq. 1.16 can be written as

$$\mathcal{V}(\phi) = -m^2\phi^\dagger\phi + \lambda|\phi^\dagger\phi|^2. \tag{1.19}$$

It can be easily checked that the wrong sign in the mass term leads to non-zero constant vev for the scalar field. We choose vev ϕ_0 of the Higgs field to be

$$\phi_0 = \frac{1}{\sqrt{2}} \begin{pmatrix} 0 \\ v \end{pmatrix} \tag{1.20}$$

and expand ϕ in terms of fluctuation around ϕ_0 as

$$\phi = \frac{1}{\sqrt{2}} \begin{pmatrix} 0 \\ v + H(x) \end{pmatrix} \exp\left[i\overrightarrow{\tau} \cdot \overrightarrow{\eta}(x)/v\right] \tag{1.21}$$

with $v = \sqrt{m^2/\lambda}$, $\overrightarrow{\eta}(x)$ being three Goldstone bosons and $h(x)$ being the Higgs boson.

1.2.1 Generation of gauge boson masses

The masses of the gauge bosons are generated through the covariant derivative of the scalar field. Using Eq. 1.21, we write the $\mathcal{L}_S$ of Eq. 1.16 in terms of the expansion 1.21 of the scalar field (given in Eqn. 1.21) as

$$|\mathcal{D}^L_\mu \phi|^2 = \frac{1}{2}\left(\partial_\mu H\right)^2 + \frac{1}{8}\left(v + H\right)^2 \left[g_2^2 |W^1_\mu + iW^2_\mu|^2 + |g_2 W^3_\mu - g_1 B_\mu|^2\right] \tag{1.22}$$

We define new fields $\mathcal{W}^\pm_\mu$, $\mathcal{Z}_\mu$ and $\mathcal{A}_\mu$ by

$$W^\pm_\mu = \frac{\left(W^1_\mu \mp W^2_\mu\right)}{\sqrt{2}}, Z_\mu = \frac{\left(g_2 W^3_\mu - g_1 B_\mu\right)}{\sqrt{g_1^2 + g_2^2}}, A_\mu = \frac{\left(g_1 W^3_\mu + g_2 B_\mu\right)}{\sqrt{g_1^2 + g_2^2}}, \tag{1.23}$$

and rewrite the Eq. 1.22 in terms of these fields as

$$|\mathcal{D}_\mu \phi|^2 = \frac{1}{2}\left(\partial_\mu H\right)^2 + \frac{1}{8}\left(v + H\right)^2 \left[2g_2^2 W^+_\mu W^{\mu -} + \left(g_1^2 + g_2^2\right) Z_\mu Z^\mu\right]. \tag{1.24}$$

Hence, from Eq. 1.24, the masses of the EW gauge bosons are

$$m_W = \frac{1}{2} g_2 v; \qquad m_Z = \frac{1}{2} v \sqrt{g_1^2 + g_2^2}, \qquad m_A = 0; \tag{1.25}$$

The appearance of mass terms for the gauge bosons after SSB can be explained by gauge bosons absorbing (eating) the would-be Goldstone bosons, η^i, which serve as longitudinal polarizations of the gauge bosons. Thus, after SSB, the local gauge group $SU(2)_L \times U(1)_Y$ is broken down to $U(1)_Q$ and since photon, A_μ corresponds to unbroken group $U(1)_Q$, it remains massless.

As mentioned previously, the SSB has mixed the B_μ and W^3_μ gauge bosons and the mass eigenstates consist of the massive Z boson and massless photon A_μ,

$$\begin{pmatrix} Z_\mu \\ A_\mu \end{pmatrix} = \begin{pmatrix} \cos\theta_W & -\sin\theta_W \\ \sin\theta_W & \cos\theta_W \end{pmatrix} \begin{pmatrix} W^3_\mu \\ B_\mu \end{pmatrix} \tag{1.26}$$

where the mixing angle θ_W is defined as

$$\tan\theta_W = \frac{g_1}{g_2}. \tag{1.27}$$

It is customary to define SM couplings in terms of the weak mixing angle, θ_W, coupling of the photon, e, mass of the Z, m_Z, and mass of the Higgs boson, m_H, rather than parameters μ^2, λ, g_1 and g_2. It is trivial to relate these two sets of parameters and the relations among the two sets of parameters are:

$$\sin\theta_W = \frac{g_1}{\sqrt{g_1^2+g_2^2}}, \quad \cos\theta_W = \frac{g_2}{\sqrt{g_1^2+g_2^2}}, \quad m_Z = \frac{m_W}{\cos\theta_W}, \quad e = g_1\sin\theta_W. \tag{1.28}$$

1.2.2 Generation of fermion masses

We have seen how SSB generates masses of the gauge bosons. In the SM, the same mechanism provides masses for the fermions through Yukawa interactions of Eqn. 1.15. As can be seen from the Eqn. 1.15, there is only one term for lepton while there are two terms for quarks in the Lagrangian. This is because of the fact that there are no right handed neutrinos in the SM. After SSB, if we write Higgs field ϕ in terms of physical fields in Eqn. 1.15, we obtain

$$\begin{aligned}
\mathcal{L} &= -\mathcal{Y}_e^{ij}\left[\frac{v}{\sqrt{2}}\left(\bar{e}^i_L e^j_R + \bar{e}^i_R e^j_L\right) + \frac{H}{\sqrt{2}}\left(\bar{e}^i_L e^j_R + \bar{e}^i_R e^j_L\right)\right] && (1.29)\\
&- \mathcal{Y}_d^{ij}\left[\frac{v}{\sqrt{2}}\left(\bar{d}^i_L d^j_R + \bar{d}^i_R d^j_L\right) + \frac{H}{\sqrt{2}}\left(\bar{d}^i_L d^j_R + \bar{d}^i_R d^j_L\right)\right] && (1.30)\\
&- \mathcal{Y}_u^{ij}\left[\frac{v}{\sqrt{2}}\left(\bar{u}^i_L u^j_R + \bar{u}^i_R u^j_L\right) + \frac{H}{\sqrt{2}}\left(\bar{u}^i_L u^j_R + \bar{u}^i_R u^j_L\right)\right] && (1.31)
\end{aligned}$$

From Eqn. 1.29, the terms involving the vev of the Higgs field are the mass terms for the lepton. Since there are no right-handed neutrinos, one can choose a basis where Yukawa matrix for lepton $\mathcal{Y}_e^{ij}$ is diagonal and the mass of leptons are given by

$$m_e^i = \frac{\mathcal{Y}_e^{ii}\, v}{\sqrt{2}}. \tag{1.32}$$

The scene is somewhat complicated for the quark sector. Because of the presence of right-handed up quarks in the SM, the diagonalization of the up and down quark Yukawa matrices $\mathcal{Y}_u^{ij}$ and $\mathcal{Y}_d^{ij}$ is not trivial. One can choose a basis where $\mathcal{Y}_u^{ij}$ is diagonal. This implies choosing a basis where up quark, charm quark and top quark are the physical particles. However, the matrix $\mathcal{Y}_d^{ij}$ need not be diagonal in this basis. This is a new feature, not encountered for leptons, since there was only one kind of matrix in the leptonic case which could always be taken as diagonal.

To obtain physical states for down type quarks, we then need to diagonalize this mass matrix. This task is executed by doing bi-unitary transformation. It implies that for any matrix $\mathcal{Y}^{ij}$, it is possible to find two unitary matrices $\mathcal{K}$ and $\mathcal{K}'$ such that $\bar{\mathcal{Y}} = \mathcal{K}'\mathcal{Y}\mathcal{K}$ is diagonal. The diagonal elements are then interpreted as the masses of physical down type quarks identified as down quark, strange quark and bottom quark. Hence the masses of down and up type quarks are written as

$$(m_d)_{ii} = \frac{\bar{\mathcal{Y}}_d v}{\sqrt{2}} \bar{\mathcal{D}}_L^i \mathcal{D}_R^i, (m_u)_{ii} = \frac{\bar{\mathcal{Y}}_u v}{\sqrt{2}} \bar{\mathcal{U}}_L^i \mathcal{U}_R^i, \tag{1.33}$$

where $\mathcal{U}^i$ and $\mathcal{D}^i$ are the physical states for up and and down type quarks respectively and are defined as:

$$\mathcal{U}_L^i = \mathcal{K}_u^{ij\dagger} \mathcal{U}_L^j, \;\; \mathcal{U}_R^i = \mathcal{K}_u'^{ij\dagger} \mathcal{U}_R^j \tag{1.34}$$

$$\mathcal{D}_L^i = \mathcal{K}_d^{ij\dagger} \mathcal{D}_L^j, \;\; \mathcal{D}_R^i = \mathcal{K}_d'^{ij\dagger} \mathcal{D}_R^j \tag{1.35}$$

This has an interesting consequence on the gauge interactions of quarks. The interaction of W with quarks in terms of mass eigenstates can be written as:

$$\mathcal{L}^W = \frac{g}{\sqrt{2}} \sum_{ij} \left[\bar{\mathcal{U}}_L^i (\mathcal{K}_L^\dagger K_R')_{ij} \gamma^\mu \mathcal{D}_R^j W_\mu^+ + h.c. \right]. \tag{1.36}$$

The matrix $\mathcal{V}_{ij} = (\mathcal{K}_L^\dagger K_R')_{ij}$ is known as the Cabbibo-Kobayashi-Maskawa (CKM) matrix and is related to the generational rotation. The CKM matrix is parameterized by three real rotational angles and one CP-violating phase. The form of the neutral current interaction is the same when written either in terms of gauge or in terms of mass eigenstates. This implies that there is no mixing matrix analogous to the CKM matrix in the neutral current sector.

1.3 The Higgs boson phenomenology

The study of the Higgs boson involves the measurement of its mass, decay widths, spin and couplings to various particles. There are predictions of Higgs boson couplings with other particles in the framework of a model. However, the Higgs mass remains an independent parameter in any model and only bounds on it are predicted assuming its couplings in that model.

1.3.1 Bounds on the Higgs boson mass

Mass of the Higgs boson is one of the parameters that cannot be predicted in the SM. However it is possible to obtain the theoretical bounds on it by using unitarity of scattering amplitudes, triviality of scalar field theory and stability of the vacuum. We give a brief overview of these bounds. (See Ref. [4] for details.)

The cross section of $W_L^+ W_L^-$ scattering has a bad high energy behavior if one does not include Higgs exchange diagram in the theoretical calculation. In principle, the amplitude of $W_L^+ W_L^- \to W_L^+ W_L^-$ violates unitarity at very high energies and hence to restore unitarity, one needs to include the Higgs exchange diagram. Writing the cross section of process $W_L^+ W_L^- \to W_L^+ W_L^-$ by decomposing scattering amplitude $\mathcal{A}$ in terms of partial wave amplitudes a_ℓ as

$$\sigma = \frac{16\pi}{s} \sum_{0}^{\infty} (2\ell + 1)|a_\ell|^2 \tag{1.37}$$

and using optical theorem

$$\sigma = \frac{1}{s} \mathrm{Im}[\mathcal{A}(\theta = 0)], \tag{1.38}$$

where $\mathcal{A}(\theta = 0)$ is the scattering amplitude in forward direction, we get

$$|a_\ell|^2 = |\mathrm{Re}a_\ell|^2 + |\mathrm{Im}a_\ell|^2 = \mathrm{Im}a_\ell \Rightarrow |\mathrm{Re}a_\ell| \leq \frac{1}{2}. \tag{1.39}$$

The Higgs contributes to the $J = 0$ partial wave amplitude for the process and in the high energy limit ($s \gg m_H^2$), we obtain $a_0 = -\frac{m_H^2}{8\pi v^2}$ which leads to upper bound on Higgs mass to be 870 GeV. The same analysis can be carried out for processes $W_L^+ W_L^- \to Z_L Z_L$, $Z_L Z_L \to Z_L Z_L$ etc. and combining scattering amplitudes of all such process further restricts the upper bound on the Higgs mass to 710 GeV.

The other theoretical bounds on the Higgs mass come from the Renormalization Group (RG) evolution of the Higgs quartic coupling. In a pure scalar $\lambda\phi^4$ theory, the quartic coupling λ at scale Q^2 using RGE equation is written as

$$\frac{\mathrm{d}}{\mathrm{dlog}Q^2} \lambda(Q^2) = \frac{3}{4\pi^2} \lambda^2(Q^2) + \text{higher order terms}. \tag{1.40}$$

However, in the SM, the running of the Higgs self-coupling gets contribution from fermions and gauge bosons. Including these contributions, RGE for the quartic coupling is written as :

$$\begin{aligned} \frac{\mathrm{d}}{\mathrm{dlog}Q^2} \lambda(Q^2) &= \frac{1}{16\pi^2} \Big[12\lambda^2 + 6\lambda\lambda_t - 3\lambda_t^2 - \frac{3}{2}\lambda(3g_2^2 + g_1^2) \\ &+ \frac{3}{16}(2g_2^4 + (g_2^2 + g_1^2)^2) \Big] \end{aligned} \tag{1.41}$$

where λ_t is the top Yukawa coupling and the mass of the Higgs is related to its self coupling λ by $m_H = 2\lambda v^2$.

For large Higgs self-coupling λ i.e., for large Higgs mass, the first term in Eqn. 1.41 dominates and hence for heavy Higgs, the quartic coupling at scale Q^2 can be approximately written as

$$\lambda(Q^2) = \frac{\lambda(v^2)}{\left[1 - \frac{3}{4\pi^2}\lambda(v^2)\log\frac{Q^2}{v^2}\right]}. \tag{1.42}$$

Hence, for large energy, the coupling λ grows and eventually diverges at

$$Q_c = v\exp\left(\frac{2\pi^2}{3\lambda}\right) = v\exp\left(\frac{4\pi^2 v^2}{3m_H^2}\right). \tag{1.43}$$

The point where λ diverges is called the Landau pole. On the other hand, at very small energy scale, $Q \ll v$, the coupling λ becomes very small and eventually goes to zero making the Higgs theory non-interacting or trivial. Thus, for a theory to be perturbative upto some scale, one can choose a Higgs mass such that λ remains finite over entire range and avoids the Landau pole. Using Eqn. 1.43, one can find the upper limit on Higgs mass as:

$$m_H^2 < \frac{8\pi^2 v^2}{3\log(\frac{Q^2}{v^2})} \tag{1.44}$$

where Q is the scale of new physics. For $Q \sim 10^6$, one requires $m_H \leq 200$ GeV and for $Q \sim 10^3$, the Higgs mass can be as large as 1 TeV, still avoiding the Landau pole.

For small quartic coupling λ the top quark contribution can be dominant and could lead the coupling to a negative value, thus making the vacuum of the theory unstable. This vacuum stability condition puts a lower bound on the Higgs mass

$$m_H^2 \geq \frac{v^2}{8\pi^2}\left[-12\frac{m_t^4}{v^4} + \frac{3}{16}(2g_2^2 + (g_1^2 + g_2^2)^2)\right] \log\frac{Q^2}{v^2}. \tag{1.45}$$

The lower bound on the Higgs mass depends on the scale of new physics Q. For example, at $Q \sim 10^3$ GeV, we have $m_H > 70$ GeV and for $Q \sim 10^6$ GeV, the lower limit on Higgs mass is 130 GeV (For a recent discussion, see [5].).

The direct constraints on the Higgs mass come from LEP-I and LEP-II experiments at CERN. At LEP-I, the Higgs boson has been searched at cm energy $\sqrt{s} \sim m_Z$ in the s-channel process $e^+e^- \to ZH$ with Z being off-shell and decaying to fermion-antifermion pair. Absence of any Higgs signal at LEP-I set a limit of

$m_H \gtrsim 65.2$ GeV at 95% CL. At LEP-II, the same process, but now with an on-shell Z, was reviewed at $\sqrt{s} = 209$ GeV and no Higgs signal has been found which put a limit of $m_H > 114.4$ GeV at 95 % CL (For details, see [6].). The combined results from CDF and D0 on direct search for a SM Higgs boson in the channel $p\bar{p} \to VH$, where $V = W, Z$ exclude the mass range $160 < m_H < 170$ GeV at 95 % CL [7]. The EW precision measurements also put an upper bound on the Higgs mass. The global χ^2 fit to all the EW measurements as a function of the Higgs mass put a 95% CL upper bound on m_H to be $m_H \lesssim 163$ GeV [8].

1.3.2 Higgs boson couplings

The Higgs couplings to the SM particles are determined by the mass of the particles to which it couples. The Higgs couplings to the EW gauge bosons can be read from the Eqn. 1.22 by expanding $(v + H)^2$ and keeping the terms linear in H:

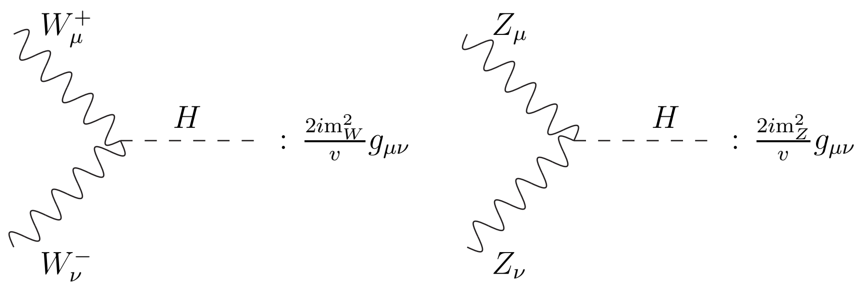

Figure 1.1: *SM couplings of the Higgs boson to EW gauge bosons.*

The Higgs boson couplings to the SM fermions can be written from Eqns. 1.29, 1.30 and 1.31 as

$$\Gamma_{f\bar{f}H} = \frac{\mathcal{Y}_f^{ii}}{\sqrt{2}} = \frac{m_f}{v} \tag{1.46}$$

where f can be any of the fermions i.e., charged lepton, down-type quarks and up-type quarks.

Once the Higgs boson is discovered, it would require a detailed and precise measurement of its fundamental properties, i.e., its spin, its mass and more importantly its couplings to heavier particles, to establish it as the SM Higgs. Since almost all BSM theories predict the existence of more than one Higgs boson, it would be essential to analyze the experimental data with the most general Higgs interactions encompassing various BSM models. Therefore, it is apt to adopt a model independent or effective Lagrangian approach to perform this sort of analysis in a more general and unambiguous manner.

Anomalous Higgs boson couplings to vector bosons

As mentioned earlier, Higgs couplings are proportional to masses of the particles which it couples. Hence, it is appropriate to study Higgs interactions with heavier particles like the massive EW vector bosons $W^\pm$ and Z. We study interactions of EW bosons with the Higgs in a model-independent approach and write the most general VVH ($V = W/Z/\gamma$) interactions consistent with the Lorentz invariance as

$$\Gamma^V_{\mu\nu} = g_V m_Z \left[a_V \, g_{\mu\nu} + \frac{b_V}{m_Z^2} \left(k_{1\nu} k_{2\mu} - g_{\mu\nu} k_1 \cdot k_2 \right) + \frac{\tilde{b}_V}{m_Z^2} \, \epsilon_{\mu\nu\alpha\beta} k_1^\alpha k_2^\beta \right] , \tag{1.47}$$

where $k_i's$ denote the momenta of the two vector bosons. In general, the couplings a_V, b_V and $\tilde{b}_V$ are complex. The couplings a_V and b_V are CP even while the coupling $\tilde{b}_V$ is CP odd. Hence the simultaneous presence of both the couplings would signal CP violation.

However, there is an alternative approach for the model independent analysis where the effective Lagrangian for an interaction is originated when all the dynamical degrees of freedom above a particular cut-off scale Λ are integrated out in an underline theory. This results in a series of higher-dimensional operators in the effective Lagrangian. The operators in the effective Lagrangian are suppressed by powers of Λ and are weighted by real coefficients which are known as Wilson coefficients.

The effective Lagrangian for the VVH interactions is written as

$$\mathcal{L}^{\text{eff}}_{HVV} = \sum_i \frac{f_i}{\Lambda^2} \mathcal{O}_i + \sum_i \frac{\tilde{f}_i}{\Lambda^2} \tilde{\mathcal{O}}_i \tag{1.48}$$

where $\mathcal{O}_i$ and $\tilde{\mathcal{O}}_i$ are the CP-even and CP-odd dimension-6 operators satisfying $SU(2)_L \times U(1)_Y$ and are listed below:

$$\begin{aligned}
\mathcal{O}_{WW} &= \Phi^{\dagger}\mathcal{W}_{\mu\nu}\mathcal{W}^{\mu\nu}\Phi, \\
\mathcal{O}_{WW} &= \Phi^{\dagger}\mathcal{B}_{\mu\nu}\mathcal{B}^{\mu\nu}\Phi, \\
\mathcal{O}_{WW} &= \Phi^{\dagger}\mathcal{B}_{\mu\nu}\mathcal{W}^{\mu\nu}\Phi, \\
\mathcal{O}_{W} &= \left(\mathcal{D}_L^{\mu}\Phi\right)^{\dagger}\mathcal{W}_{\mu\nu}\left(\mathcal{D}_L^{\nu}\Phi\right), \\
\mathcal{O}_{B} &= \left(\mathcal{D}_L^{\mu}\Phi\right)^{\dagger}\mathcal{B}_{\mu\nu}\left(\mathcal{D}_L^{\nu}\Phi\right), \\
\mathcal{O}_{\Phi,1} &= \left(\mathcal{D}_{L\mu}\Phi\right)^{\dagger}\Phi^{\dagger}\Phi\left(\mathcal{D}_L^{\mu}\Phi\right),
\end{aligned} \tag{1.49}$$

$$\begin{aligned}
\tilde{\mathcal{O}}_{WW} &= \frac{1}{2}\epsilon_{\mu\nu\alpha\beta}\Phi^{\dagger}\mathcal{W}_{\mu\nu}\mathcal{W}^{\alpha\beta}\Phi, \\
\tilde{\mathcal{O}}_{WW} &= \frac{1}{2}\epsilon_{\mu\nu\alpha\beta}\Phi^{\dagger}\mathcal{B}_{\mu\nu}\mathcal{B}^{\alpha\beta}\Phi, \\
\tilde{\mathcal{O}}_{WW} &= \frac{1}{2}\epsilon_{\mu\nu\alpha\beta}\Phi^{\dagger}\mathcal{B}_{\mu\nu}\mathcal{W}^{\alpha\beta}\Phi, \\
\tilde{\mathcal{O}}_{W} &= \frac{1}{2}\epsilon_{\mu\nu\alpha\beta}\left(\mathcal{D}_L^{\mu}\Phi\right)^{\dagger}\mathcal{W}^{\alpha\beta}\left(\mathcal{D}_L^{\nu}\Phi\right), \\
\tilde{\mathcal{O}}_{B} &= \frac{1}{2}\epsilon_{\mu\nu\alpha\beta}\left(\mathcal{D}_L^{\mu}\Phi\right)^{\dagger}\mathcal{B}^{\alpha\beta}\left(\mathcal{D}_L^{\nu}\Phi\right),
\end{aligned} \tag{1.50}$$

where covariant derivative $\mathcal{D}_L^{\mu}$ is defined in Eqn. 1.17. These operators contribute to anomalous W^+W^-H, ZZH, γZH and $\gamma\gamma H$ couplings in Eqn. 1.47. One specific practical aspect in which our approach differs from that of effective Lagrangians is that while the couplings are all taken to be real in the latter approach, we allow the couplings to be complex, and, in principle, momentum-dependent form factors.

In the next two chapters, we will investigate the sensitivity of 500 GeV ILC to these anomalous VZH ($V = Z,\ \gamma$) couplings utilizing the facility of both longitudinal and transverse beam polarizations. A brief introduction about beam polarizations at a linear collider has been given in the next section.

1.4 Beam polarization at linear collider

The full potential of a linear collider can only be achieved through polarized beams as it would lead to search for new physics with high sensitivity. Already the Stanford Linear Collider (SLC) has highlighted the importance of polarized electron beams in the SLAC Large Detector (SLD) experiment through the detailed and precise measurements of parity violation in weak neutral current interaction by studying e^+e^- collisions at the Z resonance [9]. The electron beam was 75% polarized in the SLD experiment which provided enhancement in statistical power of a factor of 25 for left-right forward-backward asymmetry. In particular the SLD experiment determined best individual measurement of the weak mixing angle θ_W.

In our work, we consider both electron and positron beams to be polarized at ILC. A high degree of polarization of at least 80% for electron beams and 30% for positron beams has already been achieved at a test facility [10]. New results indicate that 60% polarization for positron beams should be achievable [11]. The dominant processes in e^+e^- collisions are annihilation (s-channel) and scattering (t- and u-channel) processes. In annihilation processes, the helicities of initial electron and positron are correlated by the spin of the particle exchanged in the channel. Suitable combinations of electron and positron polarizations can be tuned to enhance the signal process and also suppress background processes. In scattering processes, the helicities of electron and positron are directly related to the properties of final state particles. Hence, tuning the polarizations of both the beams simultaneously may provide unique probes to new physics. Having both beams polarized would significantly increase the number of measurable observables, providing more powerful diagnostics tools which may be indispensable for revealing the structure of new physics.

1.4.1 Polarized cross sections

The helicity amplitude of the process $e^+(p_{e^+}, \lambda_{e^+})e^-(p_{e^-}, \lambda_{e^-}) \to X$ can be written as

$$T_{\lambda_{e^-},\lambda_{e^+}} = \bar{v}(p_{e^+}, \lambda_{e^+})\Gamma u(p_{e^-}, \lambda_{e^-}), \tag{1.51}$$

where Γ is a combination of $(\gamma_\mu, \gamma_\mu\gamma_5, 1, \gamma_5, \sigma_{\mu\nu})$ which are the basis elements (V,A,S,P,T) of the Dirac algebra. The polarized electron/positron beam is described by a 2×2 spin-density matrix $\rho_{\lambda_{e^\pm},\lambda_{e^\pm}}$ so that the transition probability is given by:

$$\begin{aligned} |\mathcal{M}|^2 &= \sum_{\lambda_{e^+},\lambda_{e^-},\lambda'_{e^+},\lambda'_{e^-}} \rho_{\lambda_{e^+},\lambda'_{e^+}} \rho_{\lambda_{e^-},\lambda'_{e^-}} T_{\lambda_{e^-},\lambda_{e^+}} T^*_{\lambda'_{e^-},\lambda'_{e^+}} \\ &= \sum_{\lambda_{e^+},\lambda_{e^-},\lambda'_{e^+},\lambda'_{e^-}} \rho_{\lambda_{e^+},\lambda'_{e^+}} \rho_{\lambda_{e^-},\lambda'_{e^-}} \left[\bar{v}(p_{e^+}, \lambda_{e^+})\Gamma u(p_{e^-}, \lambda_{e^-})\right] \\ &\qquad \times \left[\bar{u}(p_{e^+}, \lambda'_{e^+})\bar{\Gamma} v(p_{e^-}, \lambda'_{e^-})\right] \end{aligned} \tag{1.52}$$

To evaluate Eqn. 1.52, we use projection operators defined by

$$u(p,\lambda')\bar{u}(p,\lambda) = \frac{1}{2}\left[\delta_{\lambda,\lambda'} + \gamma_5 s^a_\mu \sigma_{\lambda,\lambda'}\right](\not{p}+m) \tag{1.53}$$

$$v(p,\lambda')\bar{v}(p,\lambda) = \frac{1}{2}\left[\delta_{\lambda',\lambda} + \gamma_5 s^a_\mu \sigma_{\lambda',\lambda}\right](\not{p}-m), \tag{1.54}$$

where σ^a, $a = 1,2,3$ are the Pauli matrices. The three four-component spin vectors s^a_μ and p^μ/m form an orthogonal system.

In the high energy limit $p_{e^\pm} \gg m_{e^\pm}$, the Eqns. 1.53 and 1.54 are written as

$$\begin{aligned} u(p_{e^\pm},\lambda'_{e^\pm})\bar{u}(p_{e^\pm},\lambda_{e^\pm}) &= \frac{1}{2}\Big[(1+\lambda_{e^\pm}\gamma_5)\,\delta_{\lambda_{e^\pm},\lambda'_{e^\pm}} \\ &+ \gamma_5\{s^1_{e^\pm}\sigma^1_{\lambda_{e^\pm},\lambda'_{e^\pm}} + s^2_{e^\pm}\sigma^2_{\lambda_{e^\pm},\lambda'_{e^\pm}}\}\Big]\not{p}_{e^\pm} \end{aligned} \tag{1.55}$$

$$\begin{aligned} v(p_{e^\pm},\lambda'_{e^\pm})\bar{v}(p_{e^\pm},\lambda_{e^\pm}) &= \frac{1}{2}\Big[(1-\lambda_{e^\pm}\gamma_5)\,\delta_{\lambda'_{e^\pm},\lambda_{e^\pm}} \\ &+ \gamma_5\{s^1_{e^\pm}\sigma^1_{\lambda'_{e^\pm},\lambda_{e^\pm}} + s^2_{e^\pm}\sigma^2_{\lambda'_{e^\pm},\lambda_{e^\pm}}\}\Big]\not{p}_{e^\pm} \end{aligned} \tag{1.56}$$

The 2×2 density matrix for electron (positron) can be expanded in terms of Pauli's matrices as :

$$\rho_{\lambda_{e^\pm},\lambda'_{e^\pm}} = \frac{1}{2}\left[\delta_{\lambda_{e^\pm},\lambda'_{e^\pm}} + P^1_{e^\pm}\sigma^1_{\lambda_{e^\pm},\lambda'_{e^\pm}} + P^2_{e^\pm}\sigma^2_{\lambda_{e^\pm},\lambda'_{e^\pm}} + P^3_{e^\pm}\sigma^3_{\lambda_{e^\pm},\lambda'_{e^\pm}}\right]. \tag{1.57}$$

Here, $P^3_{e^\pm}$ is the degree of longitudinal polarization with $P^3_{e^\pm} > 0$ corresponding to right handed polarization while $P^3_{e^\pm} < 0$ corresponds to left handed polarization. $P^1_{e^\pm}$ and $P^2_{e^\pm}$ are the degrees of polarization perpendicular to the scattering plane and in the scattering plane respectively. $P^T_{e^\pm} = \sqrt{(P^1_{e^\pm})^2 + (P^2_{e^\pm})^2}$ is the degree of transverse polarization.

1.4.2 Longitudinally polarized beams

With longitudinally polarized beams, the cross section, σ_{pol}, at an e^+e^- collider can be subdivided into

$$\begin{aligned} \sigma_{pol} &= \frac{1}{4}\Big[(1+P_L)\big(1+\overline{P}_L\big)\sigma_{RR} + (1-P_L)\big(1-\overline{P}_L\big)\sigma_{LL} \\ &+ (1+P_L)\big(1-\overline{P}_L\big)\sigma_{RL} + (1-P_L)\big(1+\overline{P}_L\big)\sigma_{LR}\Big] \end{aligned} \tag{1.58}$$

where P_L and $\overline{P}_L$ are the degrees of longitudinal polarization for electron and positron beams respectively and σ_{RL} stands for the cross section if electron and positron beams are completely right handed ($P_L = +1$) and left handed ($\overline{P}_L = -1$) polarized respectively. The other cross sections, σ_{RR}, σ_{LL} and σ_{LR} are defined analogously.

In case of annihilation diagrams, helicities of initial beams are coupled to each other and can only couple to spin-0 or spin-1 particles. In the SM, it would lead to $e^+e^- \to \gamma^*/Z$ in the chiral limit (the limit of vanishing electron mass). So, the cross section of e^+e^- annihilation into a vector particle with arbitrary longitudinally polarized beams is given by

$$\begin{aligned}
\sigma_{pol} &= \frac{1+P_L}{2}\frac{1-\overline{P}_L}{2}\sigma_{RL} + \frac{1-P_L}{2}\frac{1+\overline{P}_L}{2}\sigma_{LR}, \\
&= (1-P_L\overline{P}_L)\frac{\sigma_{RL}+\sigma_{LR}}{4}\left[1-\frac{P_L-\overline{P}_L}{1-P_L\overline{P}_L}\frac{\sigma_{LR}-\sigma_{RL}}{\sigma_{LR}+\sigma_{RL}}\right], \\
&= (1-P_L\overline{P}_L)\sigma_0\left[1-P_L^{\text{eff}}\mathcal{A}_{LR}\right], \qquad (1.59)
\end{aligned}$$

with

$$\begin{aligned}
\text{the unpolarized cross section: } \sigma_0 &= \frac{\sigma_{RL}+\sigma_{LR}}{4} \qquad (1.60) \\
\text{the left-right asymmetry: } \mathcal{A}_{LR} &= \frac{\sigma_{LR}-\sigma_{RL}}{\sigma_{LR}+\sigma_{RL}} \qquad (1.61) \\
\text{and, the effective polarization: } P_L^{\text{eff}} &= \frac{P_L-\overline{P}_L}{1-P_L\overline{P}_L}. \qquad (1.62)
\end{aligned}$$

The annihilation cross section can be enhanced if the both beams are polarized and if signs of P_L and $\overline{P}_L$ are opposite, see Eqn. 1.59. Introducing the effective luminosity, $\mathcal{L}_{eff}$ by

$$\mathcal{L}_{eff} = \frac{1}{2}(1-P_L\overline{P}_L)\mathcal{L}, \qquad (1.63)$$

Eqn. 1.59 can be written as

$$\sigma_{pol} = 2\sigma_0(\mathcal{L}_{eff}/\mathcal{L})[1-P_L^{\text{eff}}\mathcal{A}_{LR}]. \qquad (1.64)$$

Some values of effective polarization and effective luminosity are given in Table 1.2. Notice from the third row in Table 1.2 that the effective polarization is closer to 100% even though initial beam polarizations are rather low. Also, effective luminosity of the initial beams is increased upto 50%. Hence, it is desirable that beam polarizations at the ILC should have opposite signs.

		P_L^{eff}	$\mathcal{L}_{eff}/\mathcal{L}$
$P_L = 0,$	$\overline{P}_L = 0$	0%	0.50
$P_L = +80\%,$	$\overline{P}_L = 0$	+80%	0.50
$P_L = -80\%,$	$\overline{P}_L = +60\%$	−95%	0.74
$P_L = +80\%,$	$\overline{P}_L = +60\%$	+39%	0.26

Table 1.2: *Effective polarization and effective luminosity for realistic values of longitudinal beam polarization.*

1.4.3 Transversely polarized beams

At colliders, one can define the z-axis along the beam direction. If the initial beams are unpolarized or longitudinally polarized, we have a rotational symmetry around the beam axis and final state particles are distributed uniformly around the z-axis. The presence of transverse polarization breaks this cylindrical symmetry of the initial state by fixing a transverse direction in the lab frame. With this additional reference direction, it becomes possible to look for azimuthal distribution, even in a $2 \to 2$ processes, which is impossible otherwise.

For the transversely polarized beams, we take the e^- polarization to be along the x axis and that of the e^+ in the xy plane, making an angle of δ with the x axis, so that $\delta = 0$ corresponds to parallel e^- and e^+ transverse polarizations. With transversely polarized beams, cross section for $e^+e^- \to \gamma^*/Z^*$ is given by [12]

$$\begin{aligned}
\sigma_{pol} &= \frac{1}{4}\left[|\mathrm{T_{LL}}|^2 + |\mathrm{T_{RR}}|^2 + |\mathrm{T_{RL}}|^2 + |\mathrm{T_{LR}}|^2\right] \\
&- 2P_T\overline{P}_T\big\{ [\cos\delta\ \mathrm{Re}\,(\mathrm{T_{RR}T_{LL}^*}) + \cos(2\phi-\delta)\mathrm{Re}\,(\mathrm{T_{LR}T_{RL}^*})] \\
&- [\sin(2\phi-\delta)]\mathrm{Im}(\mathrm{T_{LR}T_{RL}^*}) - \sin\delta\ \mathrm{Im}(\mathrm{T_{RR}^*T_{LL}})\big\} \\
&+ P_T\big\{\cos\delta[\mathrm{Re}(\mathrm{T_{RL}T_{LL}^*}) + \mathrm{Re}(\mathrm{T_{RR}T_{LR}^*})] \\
&+ \sin\delta[\mathrm{Im}(\mathrm{T_{RL}^*T_{LL}}) + \mathrm{Im}(\mathrm{T_{RR}^*T_{LR}})]\big\} \\
&- \overline{P}_T\big\{\cos\delta[\mathrm{Re}(\mathrm{T_{LR}T_{LL}^*}) + \mathrm{Re}(\mathrm{T_{RR}T_{RL}^*})] \\
&+ \sin\delta[\mathrm{Im}(\mathrm{T_{LR}^*T_{LL}}) + \mathrm{Im}(\mathrm{T_{RR}^*T_{RL}})]\big\} \qquad (1.65)
\end{aligned}$$

where $\mathrm{T_{RL}}$ is the helicity amplitude for the process with completely right-handed and left-handed polarized electron and positron beams respectively and other helicity amplitudes are defined analogously. In the limit of vanishing electron mass, amplitudes $\mathrm{T_{LL}}$ and $\mathrm{T_{RR}}$ give zero contributions.

In a $2 \to 2$ process, the initial-state momenta are anti-parallel defining the beam axis and with one of the final-state momenta, one can suitably choose the $\phi = 0$ plane. With only two independent coplanar vectors, one can construct only few observables. Hence, one needs to include spins of the final state particles to construct more observables to probe new physics involved in the process. Since exact reconstruction of the spin of the final state particles is difficult, $2 \to 2$ processes are less informative. With transversely polarized beams, there is a possibility of studying the azimuthal distribution of final state particles even in the $2 \to 2$ process. Hence, the obvious advantage of transverse polarization over longitudinal polarization is the presence of a transverse reference direction, which can be used to construct azimuthal asymmetries with specific transformation properties under C, P and T.

1.5 Polarization of top quarks and its measurement at colliders

With a large mass of $\sim$ 172 GeV, the top quark has an extremely short lifetime, calculated in the SM to be $\tau_t = 1/\Gamma_t \sim 5 \times 10^{-25}$ s. This is an order of magnitude smaller than the hadronization time scale, which is roughly $1/\Lambda_{\rm QCD} \sim 3 \times 10^{-24}$ s. Thus, in contrast to lighter quarks, the top decays before it can form bound states with lighter quarks [13]. As a result, the spin information of the *bare* top, which depends solely on its production process, is reflected in characteristic angular distributions of its decay products. Thus, the degree of polarization of an ensemble of top quarks can provide important information about the underlying physics in its production, apart from usual variables like cross sections, since any couplings of the top to new particles can alter its degree of polarization and the angular distributions of its decay products[1].

The top polarization can be determined by the angular distribution of its decay products. In the SM, the dominant decay mode is $t \to bW^+$, with a branching ratio (BR) of 0.998, with the W^+ subsequently decaying to $\ell^+\nu_\ell$ (semileptonic decay, BR 1/9 for each lepton) or $u\bar{d}$, $c\bar{s}$ (hadronic decay, BR 2/3). The angular distribution of a decay product f for a top quark ensemble has the form (see for example [14]),

$$\frac{1}{\Gamma_f}\frac{\mathrm{d}\Gamma_f}{\mathrm{d}\cos\theta_f} = \frac{1}{2}(1 + \kappa_f P_t \cos\theta_f). \tag{1.66}$$

[1]For reviews on top quark physics and polarization see [14, 15, 16].

Here θ_f is the angle between f and the top spin vector in the top rest frame and

$$P_t = \frac{N_\uparrow - N_\downarrow}{N_\uparrow + N_\downarrow}, \tag{1.67}$$

is the degree of polarization of the top quark ensemble where $N_\uparrow$ and $N_\downarrow$ refer to the number of positive and negative helicity tops respectively. Γ_f is the partial decay width and κ_f is the spin analyzing power of f. Obviously, a larger κ_f makes f a more sensitive probe of the top spin. The charged lepton and d quark are the best spin analyzers with $\kappa_{\ell^+} = \kappa_{\bar{d}} = 1$, while $\kappa_{\nu_\ell} = \kappa_u = -0.30$ and $\kappa_b = -\kappa_{W^+} = -0.39$, at tree level [14]. Thus the ℓ^+ or d have the largest probability of being emitted in the direction of the top spin and the least probability in the direction opposite to the spin. Since at the LHC, leptons can be measured with high precision, we focus on leptonic decays of the top.

For hadronic $t\bar{t}$ production, spin correlations between the decay leptons from the t and $\bar{t}$ have been extensively studied in the SM and for BSM scenarios [14, 15, 17]. These spin correlations measure the asymmetry between the production of like and unlike helicity pairs of $t\bar{t}$ which can probe new physics in top pair production. However, this requires the reconstruction of the t and $\bar{t}$ rest frames, which results in large systematic errors and loss of statistics at the LHC. In this thesis, we investigate top polarization in the lab. frame, which would be more directly and easily measurable without having to construct the top rest frame.

1.6 Plan of the thesis

As stated earlier, the main emphasis of this thesis is to probe the mechanism of EWSB through the use of polarization studies at colliders. In the light of this, we have briefly introduced the need for beam polarization at a linear collider and elaborated the advantages of longitudinally and transversely polarized beams in the probe of new physics. We also introduced the idea of top polarization measurement at the colliders as a tool to probe new physics.

In chapter two, we study the role of longitudinally polarized beams to probe anomalous ZZH and γZH couplings at a linear collider in the process $e^+e^- \to ZH$. We construct various asymmetries from Z angular distributions. We also construct the correlations utilizing the momenta of Z-decay leptons having definite CP and T transformation properties. We find that longitudinal polarization helps in enhancing the sensitivities to these anomalous Higgs couplings.

In chapter three, we study transverse polarization of the beams at a linear collider in the context of anomalous ZZH and γZH couplings. In the presence of transverse polarization, we get additional reference direction enabling us to construct azimuthal asymmetries. The most remarkable result in this analysis is that a particular coupling Ima_γ can be probed with transversely polarized beams which is not possible otherwise. We also find that transverse polarization helps to put limits on anomalous couplings independent of each other.

In chapter four, we study single-top production in association with a W boson in the presence of anomalous tbW couplings. We look for the effect of top anomalous couplings on top polarization in the process. Since determination of top polarization requires reconstruction of top-rest frame which is a difficult task at the LHC, we focus on constructing observables in the laboratory frame which are easily measurable and are faithful probes of top polarization. In light of this, we study various distributions of top-decay products in the laboratory frame and construct various asymmetries to put limits on anomalous couplings.

In chapter five, we focus on the issue of CP violation in single-top production in the presence of anomalous tbW couplings. We study the asymmetries for both tW^- and $\bar{t}W^+$ production and decay. Any difference in the measurement of these asymmetries would be a signal of CP violation. We find that the difference is proportional to the product of the sine of CP-phase and the sine of absorptive phase. Hence, for non-zero CP violation, there must be CP and absorptive phases simultaneously present in the amplitude.

In chapter six, we study single-top production in association with a charged Higgs in a Two Higgs Doublet Model (THDM) of type II. We study top polarization as a tool to probe the parameters of THDM. Since charged-lepton angular distribution is a clean and pure probe of top polarization in any top production process, we focus on the angular distribution of the charged lepton. We study azimuthal distribution and construct an asymmetry from this distribution. We find that this asymmetry is a good probe of parameters of THDM at LHC energies.

Chapter 2

Anomalous VZH couplings with longitudinally polarized beams

As explained in the introduction, the EWSB sector of the SM is yet to be verified and its crucial component i.e., the SM Higgs boson, signaling the symmetry breaking in the SM, is yet to be discovered. It is expected that the currently operating LHC would most likely discover a scalar boson with the properties of the SM Higgs. However, there are a number of scenarios beyond the standard model like MSSM and THDM, which predict the existence of more than one scalar with different CP and weak isospin quantum numbers. Hence, ascertaining the mass and other properties of the scalar boson or bosons is an important task to establish it to be the SM Higgs boson. However, this task of studying Higgs properties precisely would prove extremely difficult for LHC due to large QCD backgrounds. The ILC with its much cleaner environment would be a much better place to perform precision studies of Higgs properties. The first step in the study of Higgs properties would be to determine the tensor structure of its couplings with other SM particles. Using various symmetry principles, one can write the most general structure of Higgs couplings. The anomalous parts in the couplings are assumed to arise from higher-order corrections in a renormalized theory or higher-dimensional operators in an effective theory.

In this chapter, we discuss in detail probes of Higgs couplings to two neutral EW gauge bosons viz., Z and γ, at the ILC using unpolarized and longitudinally polarized beams in the process $e^+e^- \to ZH$. We study how longitudinally polarized beams at ILC would help to increase the sensitivities to anomalous Higgs couplings. The dominant production mechanisms of the Higgs boson at a linear

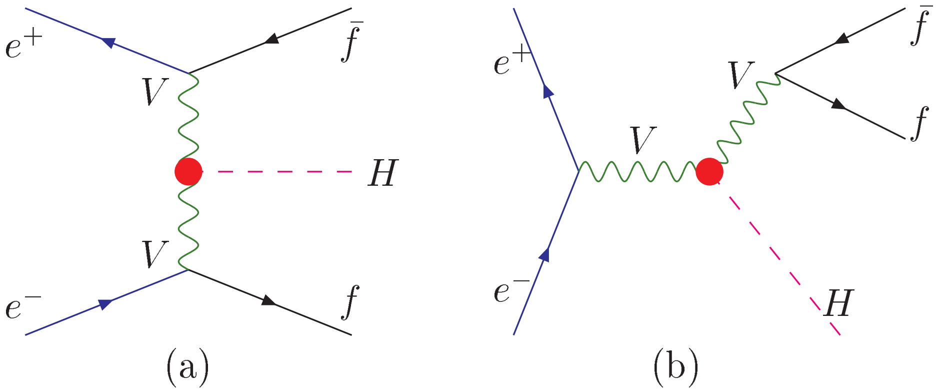

Figure 2.1: *Higgs production diagrams at e^+e^- linear collider (a) vector boson fusion diagram (b) Bjorken or Higgs-Strahlung diagram. For $f = e, \nu_e$, both (a) and (b) contribute while for all other fermions, only (b) contributes.*

e^+e^- collider are the following (also shown in Fig. 2.1):

1. the Higgs-strahlung process ($e^+e^- \to ZH$),
2. the WW-fusion process ($e^+e^- \to \nu_e\nu_e H$),
3. the ZZ-fusion process ($e^+e^- \to e^+e^-H$).

We consider in a general model-independent way the production of a Higgs mass eigenstate H in a possible extension of SM through the process $e^+e^- \to HZ$ mediated by s-channel virtual γ and Z. The process $e^+e^- \to HZ$ is generally assumed to get a contribution from a diagram with an s-channel exchange of Z. At the lowest order, the ZZH vertex in this diagram would be simply a point-like coupling. However, interactions beyond the SM can modify this point-like vertex by means of a momentum-dependent form factor, as well as by adding more complicated momentum-dependent forms of anomalous interactions considered in [20]-[30]. In Fig. 2.1, the anomalous ZZH vertex is denoted by a blob. There is also a diagram with a photon propagator and an anomalous γZH vertex, which does not occur in SM at tree level. This coupling vanishes in SM at tree level, but can get contributions at higher order in SM or in extensions of SM. Such anomalous γZH couplings were considered earlier in [22, 24, 29, 30].

The anoamlous VZH couplings have been searched for through the processes $e^+e^- \to H\gamma$, $e^+e^- \to HZ$ and $e^+e^- \to e^+e^-H$ at LEP by the L3 collaboration with 602 pb^{-1} of integrated luminosity at cm energies $\sqrt{s} = 189 - 209$ GeV [18]. The Higgs decay channels $H \to ZZ$ and $H \to Z\gamma$ were also considered and no evidence was found for anomalous Higgs production and decay. In the context of a linear collider, the anomalous ZZH couplings in the process $e^+e^- \to HZ$ have been addressed before in several works [20, 23, 25, 26, 28]. In Ref. [21], the authors have studied anomalous γZH couplings in the process $e^+e^- \to \tau^+\tau^-\gamma$ with the data provided by the L3 collaboration. They find an improvement of about an order of magnitude over the results obtained by the L3 collaboration. Refs. [22, 24, 29, 30] do take into account both γZH and ZZH couplings. However, they relate both to coefficients of terms of higher dimensions in an effective Lagrangian, whereas we treat all couplings as independent of one another. Moreover, [24] does not discuss effects of beam polarization. On the other hand, we attempt to seek ways to determine the couplings completely independent of one another. Refs. [29, 30] does have a similar approach to ours. They make use of optimal observables and consider only longitudinal electron polarization, whereas we seek to use simpler observables and asymmetries constructed out of the Z angular variables, and consider the effects of longitudinal and transverse polarization of both e^- and e^+ beams. The authors of [29] also include τ polarization and b-jet charge identification which we do not require. One specific practical aspect in which our approach differs from that of the effective Lagrangians is that while the couplings are all taken to be real in the latter approach, we allow the couplings to be complex, and in principle, momentum-dependent form factors.

Refs. [31, 32] considered a beyond-SM contribution represented by a four-point e^+e^-HZ coupling general enough to include the effects of the diagrams of Fig. 2.1, as well as additional couplings going beyond s-channel exchanges. By considering appropriate relations between those form factors and momentum dependencies, one can derive the expressions we consider here. While the four-point coupling is the most general, the dominant contributions are likely to arise from the three-point couplings considered here.

Our emphasis has been on simultaneous independent determination of couplings, to the extent possible, making use of a combination of asymmetries and/or polarizations. We have also tried to consider rather simple observables, conceptually, as well as from an experimental point of view. With this objective in mind, we use only Z angular distributions without including the polarization or the decay of the Z. This amounts to using the sum of the momenta of the Z decay products. Since we do not require charge determination, this has the advantage that one can include both leptonic and hadronic decays of the Z. On the other hand, if a measurement on the Higgs-boson decay products is made, we can also use the two-neutrino decay channels of Z since the missing energy-momentum would be fully determined.

When all couplings are assumed to be independent and nonzero, we find that angular asymmetries and momentum correlations are linear combinations of a certain number of anomalous couplings (in our approximation of neglecting terms quadratic in anomalous couplings). By using that many number of observables, for example, different asymmetries, or the same asymmetry measured for different beam polarizations, one can solve simultaneous linear equations to determine the couplings involved. This is the approach we follow here. A similar technique of considering combinations of different polarizations was made use of, for example, in [41].

2.1 Anomalous VZH couplings

Assuming Lorentz invariance, the general structure for the vertex corresponding to the process $V_\mu^*(k_1) \to Z_\nu(k_2)H$, where $V \equiv \gamma$ or Z, can be written as [23, 25, 26, 29]

$$\Gamma^V_{\mu\nu} = g_V m_Z \left[a_V\, g_{\mu\nu} + \frac{b_V}{m_Z^2}\,(k_{1\nu}k_{2\mu} - g_{\mu\nu}k_1\cdot k_2) + \frac{\tilde{b}_V}{m_Z^2}\,\epsilon_{\mu\nu\alpha\beta}k_1^\alpha k_2^\beta \right], \tag{2.1}$$

where a_V, b_V and $\tilde{b}_V$, are form factors, which are in general complex. We have omitted terms proportional to $k_{1\mu}$ and $k_{2\nu}$, which do not contribute to the process $e^+e^- \to HZ$ in the limit of vanishing electron mass. The constant g_Z is chosen to be $g/\cos\theta_W$, so that $a_Z = 1$ for SM. g_γ is chosen to be e. Of the interactions in Eqn. 2.1, the terms with $\tilde{b}_Z$ and $\tilde{b}_\gamma$ are CP violating, whereas the others are CP conserving. It may be noted that electromagnetic gauge invariance requires a_γ to vanish for $k_1^2 = 0$, and is therefore proportional to k_1^2. Henceforth we will write $a_Z = 1 + \Delta a_Z$, Δa_Z being the deviation of a_Z from its tree-level SM value. The other form factors are vanishing in SM at tree level. Thus the above "couplings," which are deviations from the tree-level SM values, could arise from loops in SM or from new physics beyond SM. We could of course work with a set of modified couplings where the anomalous couplings denote deviations from the tree-level values in a specific extension of the SM model, like a concrete two-Higgs doublet model. The corresponding modifications are trivial to incorporate.

2.2 The process $e^+e^- \to HZ$

The expression for the amplitude for the process

$$e^-(p_1) + e^+(p_2) \to Z^\alpha(q) + H(k), \tag{2.2}$$

arising from the SM diagram of Fig. 2.1 with a point-like ZZH vertex, is

$$M_{\rm SM} = -\frac{e^2}{4\sin^2\theta_W\cos^2\theta_W}\frac{m_Z}{s-m_Z^2}\overline{v}(p_2)\gamma^\alpha(g_V-\gamma_5 g_A)u(p_1), \tag{2.3}$$

where the vector and axial-vector couplings of the Z to electrons are given by

$$g_V^e = -1 + 4\sin^2\theta_W,\ g_A^e = -1, \tag{2.4}$$

and θ_W is the weak mixing angle.

While we have restricted the actual calculation to SM couplings in calculating M_{SM}, it should be borne in mind that in models with more than one Higgs doublet this amplitude would differ by an overall factor depending on the mixing among the Higgs doublets. Thus our results are trivially applicable to such extensions of SM, by an appropriate rescaling of the coupling. Our expressions are not, however, applicable for the case when the Higgs is a pure pseudoscalar in models conserving CP, since in that case, the SM-like lowest-order couplings are absent.

2.2.1 Differential cross sections

We obtain the differential cross section for the process (2.2) keeping the pure SM contribution, and the interference between the SM amplitude and the amplitudes with anomalous γZH and ZZH couplings respectively. We ignore terms bilinear in the anomalous couplings, assuming that the new-physics contribution is small. We treat the two cases of longitudinal and transverse polarizations for the electron and positron beams separately. In this chapter, we consider only the effects of longitudinally polarized beams and transversely polarized beams in process 2.2 will be considered in the next chapter.

Helicity amplitudes for the process were obtained earlier in the context of an effective Lagrangian approach [24, 22, 29, 30], and could be made use of for obtaining the differential cross section for the case of longitudinal polarization, and, with less ease, for the case of transverse polarization. We have used instead trace techniques employing the symbolic manipulation program 'FORM' [42]. We neglect the mass of the electron.

We choose the z axis to be the direction of the e^- momentum, and the xz plane to coincide with the HZ production plane in the case when the initial beams are unpolarized or longitudinally polarized. We then define θ to be the polar angle of the momentum $\vec{q}$ of the Z. We use the convention $\epsilon^{0123} = +1$ for the Levi-Civita tensor.

2.2.2 Angular distribution of Z

The angular distribution for the process (2.2) with longitudinal polarizations P_L and $\overline{P}_L$ respectively of the e^- and e^+ beams may be written as

$$\frac{d\sigma_L}{d\Omega} = \left(1 - P_L\overline{P}_L\right)[A_L + B_L \sin^2\theta + C_L \cos\theta], \tag{2.5}$$

where A_L, B_L, C_L are further written in terms of contributions from SM alone (superscript "SM"), interference between SM and ZZH terms (superscript Z), and interference between SM and γZH (superscript γ):

$$A_L = A_L^{\text{SM}} + A_L^Z + A_L^\gamma, \tag{2.6}$$
$$B_L = B_L^{\text{SM}} + B_L^Z + B_L^\gamma, \tag{2.7}$$
$$C_L = C_L^Z + C_L^\gamma. \tag{2.8}$$

In case of C_L, which is the coefficient of a CP-odd term, there is no contribution from SM. The expressions for the various terms used above are as follows.

$$A_L^{SM} = B_L^{\text{SM}}\frac{2m_Z^2}{|\vec{q}|^2} = (g_V^{e2} + g_A^{e2} - 2g_V^e g_A^e P_L^{\text{eff}})K^{SM}, \tag{2.9}$$
$$C_L^{\text{SM}} = 0, \tag{2.10}$$

where

$$K^{SM} = \frac{\alpha^2|\vec{q}|}{2\sqrt{s}\sin^4 2\theta_W}\frac{m_Z^2}{(s - m_Z^2)^2}. \tag{2.11}$$

We also have

$$
\begin{aligned}
A_L^Z &= 2\left(\text{Re }\Delta a_Z + \text{Re }b_Z \frac{\sqrt{s}q^0}{m_Z^2}\right)(g_V^{e2} + g_A^{e2} - 2g_V^e g_A^e P_L^{\text{eff}})K^{\text{SM}}, && (2.12)\\
B_L^Z &= 2\text{Re }\Delta a_Z \frac{|\vec{q}|^2}{2m_Z^2}(g_V^{e2} + g_A^{e2} - 2g_V^e g_A^e P_L^{\text{eff}})K^{\text{SM}}, && (2.13)\\
C_L^Z &= 2\text{Im }\tilde{b}_Z \frac{\sqrt{s}|\vec{q}|}{m_Z^2}\left((g_V^{e2} + g_A^{e2})P_L^{\text{eff}} - 2g_V^e g_A^e\right)K^{\text{SM}}, && (2.14)\\
A_L^\gamma &= \left(\text{Re }a_\gamma + \text{Re }b_\gamma \frac{\sqrt{s}q^0}{m_Z^2}\right)(g_V^e - g_A^e P_L^{\text{eff}})K^\gamma, && (2.15)\\
B_L^\gamma &= \text{Re }a_\gamma \frac{|\vec{q}|^2}{2m_Z^2}(g_V^e - g_A^e P_L^{\text{eff}})K^\gamma, && (2.16)\\
C_L^\gamma &= \frac{\sqrt{s}|\vec{q}|}{m_Z^2}\text{Im }\tilde{b}_\gamma\left(g_A^e - g_V^e P_L^{\text{eff}}\right)K^\gamma && (2.17)
\end{aligned}
$$

where

$$K^\gamma = \frac{\alpha^2|\vec{q}|}{\sqrt{s}\sin^2 2\theta_W}\frac{m_Z^2}{s(s-m_Z^2)}. \tag{2.18}$$

The expressions for the Z energy q^0 and the magnitude of its three-momentum $|\vec{q}|$ are

$$q^0 = \frac{s + m_Z^2 - m_H^2}{2\sqrt{s}}, \; |\vec{q}| = \frac{\sqrt{s^2 + (m_Z^2 - m_H^2)^2 - 2s(m_Z^2 + m_H^2)}}{2\sqrt{s}}. \tag{2.19}$$

Immediate inferences from these expressions are enumerated below:

1. If the six coefficients $A_L^{\gamma,Z}$, $B_L^{\gamma,Z}$ and $C_L^{\gamma,Z}$ could be determined independently using angular distributions and polarization, it would be possible to determine the six anomalous couplings $\text{Re}a_\gamma, \text{Re}\Delta a_Z, \text{Re}b_\gamma, \text{Re}b_Z, \text{Im}\tilde{b}_\gamma$ and $\text{Im}\tilde{b}_Z$.

2. Imaginary parts of a_γ, Δa_Z, b_γ, b_Z, and real parts of $\tilde{b}_\gamma$, $\tilde{b}_Z$ do not contribute to the angular distributions at this order, and hence remain undetermined.

3. Numerically g_V^e is small (about -0.12 for $\sin^2\theta_W = 0.22$), while $g_A^e = -1$. Hence, in the absence of polarization, from among the anomalous contributions, the terms A_L^Z, B_L^Z and C_L^γ dominate over the others. If these coefficients are determined from angular distributions, it would be possible to measure $\text{Re}\Delta a_Z, \text{Re}b_Z$ and $\text{Im }\tilde{b}_\gamma$ with greater sensitivity. On the other hand, there would be very low sensitivity to the remaining couplings, viz., $\text{Re}a_\gamma, \text{Re}b_\gamma$ and $\text{Im }\tilde{b}_Z$.

4. Within the combinations of couplings which appear in A_L^γ and A_L^Z, the contributions of Reb_γ and Reb_Z are enhanced because of the factor $\sqrt{s}q^0/m_Z^2$ multiplying them. This improves their sensitivity.

5. With longitudinal polarization turned on, with a reasonably large value of $P_L^{\rm eff}$, the coefficients C_L^Z, A_L^γ and B_L^γ would become significant. In that case, the sensitivity to R$e\ a_\gamma$, R$e\ b_\gamma$ and I$m\ \tilde{b}_Z$ would be improved.

6. In view of (5), it is clear that a combination of angular distributions for the polarized and unpolarized cases will help in disentangling the different couplings.

We now examine how the angular distributions in the presence of longitudinal polarization may be used to determine the various form factors.

2.2.3 Angular asymmetries of the Z boson

In this section we discuss observables like partial cross sections and angular asymmetries which can be used to determine the anomalous couplings.

An obvious choice of observable is the total cross section σ, which is even under C, P and T[1]. It would get contribution from the SM terms as well as a linear combination of the real parts of anomalous couplings ReΔa_Z, Rea_γ, Reb_Z and Reb_γ, provided the range in θ is forward-backward symmetric.

On the other hand, with longitudinal polarization, the cross section depends on a different linear combination of the real parts of the anomalous couplings. Thus, combining results of the measurement with unpolarized beams with those of the measurement with longitudinally polarized beams with e^- and e^+ polarizations of the same sign or opposite signs would give three relations with which to constrain the four couplings.

The expression for the partial cross sections in the longitudinal polarization case, in terms of the coefficients A_L and B_L used in the differential cross section, is

$$\sigma_L(\theta_0) = (1 - P_L\overline{P}_L)4\pi\cos\theta_0\left[A_L + \left(1 - \frac{1}{3}\cos^2\theta_0\right)B_L\right], \qquad (2.20)$$

where θ_0 is the cut-off angle.

[1]Henceforth, T will always refer to *naive* time reversal, i.e., reversal of all momenta and spins, without interchange of initial and final states.

The terms proportional to $\cos\theta$ can be determined using a simple forward-backward asymmetry:

$$A_{\rm FB}(\theta_0) = \frac{1}{\sigma(\theta_0)}\left[\int_{\theta_0}^{\pi/2}\frac{d\sigma}{d\theta}d\theta - \int_{\pi/2}^{\pi-\theta_0}\frac{d\sigma}{d\theta}d\theta\right], \tag{2.21}$$

where

$$\sigma(\theta_0) = \int_{\theta_0}^{\pi-\theta_0}\frac{d\sigma}{d\theta}d\theta, \tag{2.22}$$

and θ_0 is a cut-off in the forward and backward directions which could be chosen to optimize the sensitivity.

The expression for $A^L_{\rm FB}(\theta_0)$ for longitudinal polarization is

$$A^L_{\rm FB}(\theta_0) = \frac{C_L\cos\theta_0}{2\left[A_L^{\rm SM} + B_L^{\rm SM}\left(1-\frac{1}{3}\cos^2\theta_0\right)\right]}, \tag{2.23}$$

where we have used only the SM cross section in the denominator because we work to linear order in the anomalous couplings. This asymmetry is odd under CP and is proportional to C and therefore to a combination of Im$\tilde{b}_Z$ and Im$\tilde{b}_\gamma$. It should be noted that only imaginary parts of couplings enter. This is related to the fact that the CP-violating asymmetry $A_{\rm FB}(\theta_0)$ is odd under naive CPT. It follows that for it to have a non-zero value, the amplitude should have an absorptive part [44].

The asymmetry $A^L_{\rm FB}$, in the presence of longitudinal polarization, determines a different combination of the same couplings Im$\tilde{b}_Z$ and Im$\tilde{b}_\gamma$. Thus observing asymmetries with and without polarization, the two imaginary parts can be determined independently.

In the same way, a combination of the cross section for the unpolarized and longitudinally polarized beams can be used to determine two different combinations of the remaining couplings which appear in (2.5). However, one can get information only on the real parts of $\Delta a_Z, b_Z, a_\gamma, b_\gamma$, not their imaginary parts.

2.2.4 Numerical Calculations

We now evaluate various observables and their sensitivities for a linear collider operating at $\sqrt{s} = 500$ GeV. We assume that longitudinal beam polarizations of $P_L = \pm 0.8$ and $\overline{P}_L = \pm 0.6$ can be reached. With this choice of individual polarizations, the factor $1 - P_L\overline{P}_L$, occurring in the expression for the cross section, is 0.52 or 1.48 depending on whether the electron and positron have like-sign or unlike-sign polarizations. (We take the sign of polarization to be positive for right-handed polarization). The effective polarization $P_L^{\rm eff}$, defined in Eqn. 1.62, which appears in various expressions is then 0.385 or 0.946 in the two cases of like-sign and unlike-sign polarizations.

We have chosen $m_H = 120$ GeV for the main part of our calculations. We comment later on the results for larger Higgs masses.

We have made use of the following values of other parameters: $M_Z = 91.19$ GeV, $\alpha(m_Z) = 1/128$, $\sin^2\theta_W = 0.22$. For studying the sensitivity of the linear collider, we have assumed an integrated luminosity of $L \equiv \int \mathcal{L} dt = 500\,{\rm f}b^{-1}$.

Cross section

The simplest observable is the total rate that can be used to determine some combination of anomalous couplings. If we integrate the differential cross section with respect to polar and azimuthal angle over the full ranges, we would get a combination of the couplings ReΔa_Z, Reb_Z, Rea_γ and Reb_γ. Different combinations of these same couplings enter the unpolarized cross section and cross sections with same-sign or opposite-sign polarizations of the beams.

The anomalous part of the cross section in Eqn. 2.20 can be written as

$$\begin{aligned}\sigma_L(\theta_0) - \sigma_L^{\rm SM}(\theta_0) = \sigma_L^{\rm SM}(\theta_0) \Bigg[2 \left({\rm Re}\Delta a_Z + \frac{2\sqrt{s}q^0}{2m_Z^2 + \left(1 - \frac{1}{3}\cos^2\theta_0\right)|\vec{q}|^2} {\rm Re} b_Z \right) \\ + \frac{(g_V^e - g_A^e P_L^{\rm eff})}{(g_V^{e2} + g_A^{e2} - 2 g_V^e g_A^e P_L^{\rm eff})} \frac{K_\gamma}{K_{\rm SM}} \left({\rm Re} a_\gamma + \frac{2\sqrt{s}q^0}{2m_Z^2 + \left(1 - \frac{1}{3}\cos^2\theta_0\right)|\vec{q}|^2} {\rm Re} b_\gamma \right) \Bigg]\end{aligned} \tag{2.24}$$

It can be seen that for fixed cut-off, measuring the cross section for two different polarization combinations can determine two combinations of two anomalous couplings each, viz.,

$$c_Z \equiv 2 \left({\rm Re}\Delta a_Z + \frac{2\sqrt{s}q^0}{2m_Z^2 + \left(1 - \frac{1}{3}\cos^2\theta_0\right)|\vec{q}|^2} {\rm Re} b_Z \right) \tag{2.25}$$

and

$$c_\gamma \equiv \frac{2 g_V^e \sin^2 2\theta_W}{g_V^{e2} + g_A^{e2}} \frac{s - m_Z^2}{s} \left({\rm Re} a_\gamma + \frac{2\sqrt{s}q^0}{2m_Z^2 + \left(1 - \frac{1}{3}\cos^2\theta_0\right)|\vec{q}|^2} {\rm Re} b_\gamma \right). \tag{2.26}$$

Further, using the same combinations of polarizations, c_Z and c_γ can again be determined for a different value of cut-off θ_0. This would give two equations for

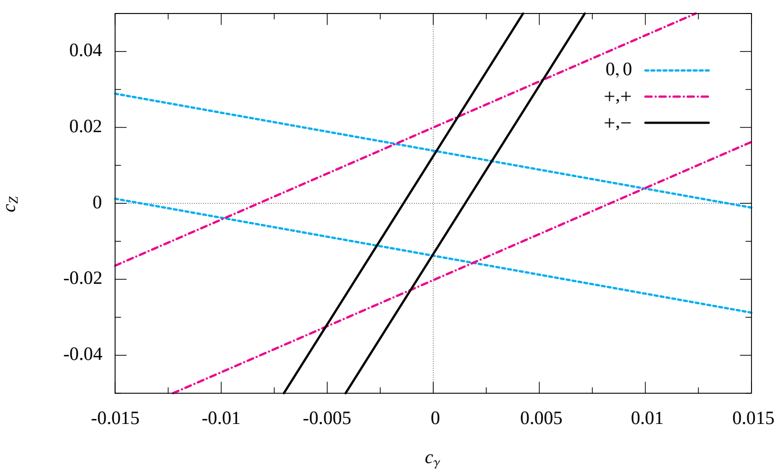

Figure 2.2: *The region in the $c_\gamma - c_Z$ plane accessible at the 95% CL with cross sections with different beam polarization configurations for integrated luminosity $L = 500$ fb^{-1}. $0,0$, $+,+$ and $+,-$ stand for the cases of zero, like-sign and opposite-sign e^- and e^+ polarizations. The cut-off θ_0 is taken to be $\pi/16$.*

each of c_Z and c_γ. It would then be possible to determine all four of $\mathrm{Re}\Delta a_Z$, $\mathrm{Re}b_Z$, $\mathrm{Re}a_\gamma$ and $\mathrm{Re}b_\gamma$ independent of one another.

Fig. 2.2 shows the 95% CL constraints in the $c_\gamma - c_Z$ plane from polarization combinations $(P_L, \overline{P}_L)$ of $(0,0)$, $(0.8,+0.6)$ and $(0.8,-0.6)$, using a cut-off $\theta_0 = \pi/16$. The lines correspond to the solutions of the equation

$$|\sigma_L(\theta_0) - \sigma_L^{\mathrm{SM}}(\theta_0)| = 2.45\sqrt{\sigma_L^{\mathrm{SM}}(\theta_0)/L} \tag{2.27}$$

for the three polarization combinations.

The best simultaneous limits on c_γ and c_Z are obtained using a combination of unpolarized beams and longitudinally polarized beams with opposite signs, viz.,

$$|\mathrm{Re}\ c_\gamma| \leq 0.00271, \ |\mathrm{Re}\ c_Z| \leq 0.0137. \tag{2.28}$$

The individual limits that can be obtained keeping one coupling to be nonzero at a time and setting the rest to be zero are shown in Table 2.1.

A direct procedure would of course be to determine all four couplings by solving four simultaneous equations obtained by using two combinations of polarization, each for two values of cut-off. Applying this approach for polarization combinations $P_L = \overline{P}_L = 0$ and $(P_L, \overline{P}_L) = (0.8, -0.6)$, and the cut-off values $\theta_0 = \pi/16$ and $\theta_0 = \pi/4$, we find the 95% CL limits of

$$|\mathrm{Re}a_\gamma| \leq 0.320; \quad |\mathrm{Re}\Delta a_Z| \leq 0.128; \quad |\mathrm{Re}b_\gamma| \leq 0.0721; \quad |\mathrm{Re}b_Z| \leq 0.0287. \tag{2.29}$$

	$\lvert \mathrm{Re} a_\gamma \rvert$	$\lvert \mathrm{Re}\Delta a_Z \rvert$	$\lvert \mathrm{Re} b_\gamma \rvert$	$\lvert \mathrm{Re} b_Z \rvert$
Unpolarized	0.0705	0.00553	0.0149	0.00117
$P_L = 0.8$, $\overline{P}_L = +0.6$	0.0423	0.00805;	0.00890	0.00169
$P_L = 0.8$, $\overline{P}_L = -0.6$	0.00741	0.00516	0.00156	0.00109

Table 2.1: *Individual 95% CL limits on the couplings* $\mathrm{Re} a_\gamma$, $\mathrm{Re}\Delta a_Z$, $\mathrm{Re} b_\gamma$, $\mathrm{Re} b_Z$ *obtained from the cross section for a cut-off* $\theta_0 = \pi/16$ *for different beam polarization combinations.*

The two other polarization combinations, viz., $P_L = \overline{P}_L = 0$ or $(P_L, \overline{P}_L) = (0.8, +0.6)$ used with $(P_L, \overline{P}_L) = (0.8, -0.6)$, give worse limits than these.

Forward-backward Asymmetry

As can be seen from Eqn. 2.23, the forward-backward asymmetry $A_{\rm FB}$ can be a probe of the combination of the couplings $\mathrm{Im}\tilde{b}_Z$ and $\mathrm{Im}\tilde{b}_\gamma$. We examine the accuracy to which this combination can be determined. The limits which can be placed at the 95% CL on the two parameters contributing to the asymmetry is given by equating the asymmetry to $2.45/\sqrt{N_{\rm SM}}$, where N_{SM} is the number of SM events. This leads to the relation

$$|A_{\rm FB}| = \frac{2.45}{\sqrt{L\sigma_L^{\rm SM}}}, \tag{2.30}$$

where L is the integrated luminosity.

We show in Fig. 2.3 a plot of the relation Eqn. 2.30 in the space of the couplings involved for unpolarized beams, and for the two combinations of longitudinal polarizations $(P_L, \overline{P}_L) \equiv (0.8, +0.6)$, denoted by $(+,+)$ and $(P_L, \overline{P}_L) \equiv (0.8, -0.6)$, denoted by $(+,-)$. The intersection of the lines corresponding to any two combinations gives a closed region which is the allowed region at 95% CL. The best simultaneous limits are obtained by considering the region enclosed by the intersections of the lines corresponding to $P_L = \overline{P}_L = 0$ and $(P_L, \overline{P}_L) = (0.8, -0.6)$. These limits are

$$|\mathrm{Im}\tilde{b}_\gamma| \leq 4.69 \times 10^{-3}; \ |\mathrm{Im}\tilde{b}_Z| \leq 5.61 \times 10^{-3}. \tag{2.31}$$

Individual limits on the two couplings obtained from the forward-backward asymmetry by setting one coupling to zero at a time for the three polarization combinations are shown in Table 2.2.

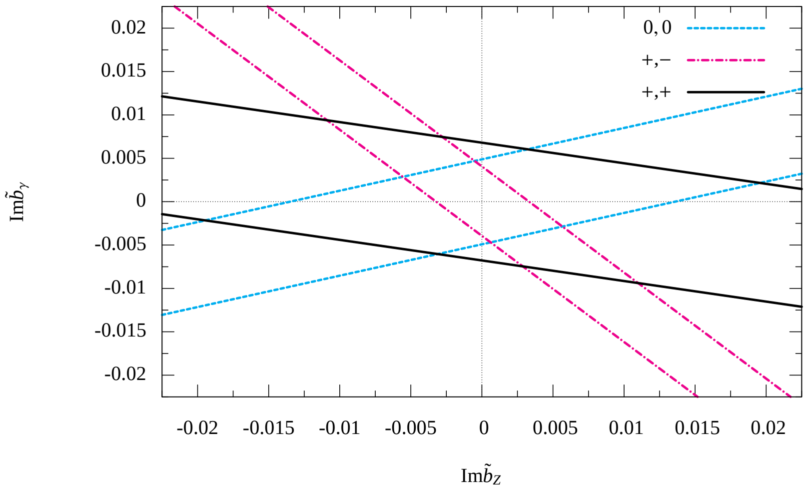

Figure 2.3: *The region in the* $\mathrm{Im}\tilde{b}_Z$-$\mathrm{Im}\tilde{b}_\gamma$ *plane accessible at the* 95% *CL with forward-backward asymmetry with different beam polarization configurations for integrated luminosity* $L = 500$ *fb*$^{-1}$. $0, 0$, $+, +$ *and* $+, -$ *stand for the cases of zero, like-sign and opposite-sign* e^- *and* e^+ *polarizations.*

	$\lvert\mathrm{Im}\tilde{b}_\gamma\rvert$	$\lvert\mathrm{Im}\tilde{b}_Z\rvert$
Unpolarized	0.00392	0.0108
$P_L = 0.8$, $\overline{P}_L = +0.6$	0.00543	0.0229
$P_L = 0.8$, $\overline{P}_L = -0.6$	0.00320	0.00262

Table 2.2: *Individual 95% CL limits on the couplings* $\mathrm{Im}\tilde{b}_\gamma$, $\mathrm{Im}\tilde{b}_Z$, *obtained from the forward-backward asymmetry for a cut-off* $\theta_0 = \pi/16$ *for different beam polarization combinations.*

It can be seen that the limit is improved considerably in the case of opposite-sign polarizations as compared to unpolarized beams for $\mathrm{Im}\tilde{b}_Z$, but only marginally in case of $\mathrm{Im}\tilde{b}_\gamma$. Like-sign polarizations make the limits worse.

2.3 The process $e^+e^- \to ZH \to \ell^+\ell^- H$

We now calculate the amplitude for the process

$$e^-(p_1) + e^+(p_2) \to Z^\alpha(q) + H(k) \to \ell^-(p_3)\ell^+(p_4)H, \tag{2.32}$$

where ℓ is either μ or τ. The expression for the amplitude for 2.32 arising from the SM diagram of Fig. 2.1 with a point-like ZZH vertex, is

$$\begin{aligned} M_{\rm SM} &= \frac{e^3 m_Z}{16\sin^3\theta_W\cos^3\theta_W(s-m_Z^2)(q^2-m_Z^2)} \\ &\times\left[\overline{v}(p_2)\gamma^\alpha(g_V-\gamma_5 g_A)u(p_1)\,\overline{u}(p_3)\gamma_\alpha(g_V-\gamma_5 g_A)v(p_4)\right], \end{aligned} \tag{2.33}$$

The corresponding amplitude for the diagram with an anomalous γZH vertex is

$$\begin{aligned} M_{\gamma ZH} &= \frac{e^2}{16\sin^2\theta_W\cos^2\theta_W s(q^2-m_Z^2)}\Gamma^{\gamma}_{\alpha\beta} \\ &\times\left[\overline{v}(p_2)\gamma^\alpha u(p_1)\,\overline{u}(p_3)\gamma^\beta(g_V-\gamma_5 g_A)v(p_4)\right], \end{aligned} \tag{2.34}$$

and the amplitude with an anomalous ZZH vertex is

$$\begin{aligned} M_{ZZH} &= \frac{e^2}{16\sin^2\theta_W\cos^2\theta_W(s-m_Z^2)(q^2-m_Z^2)}\Gamma^{Z}_{\alpha\beta} \\ &\times\left[\overline{v}(p_2)\gamma^\alpha(g_V-\gamma_5 g_A)u(p_1)\,\overline{u}(p_3)\gamma^\beta(g_V-\gamma_5 g_A)v(p_4)\right], \end{aligned} \tag{2.35}$$

where the anomalous vertex factors $\Gamma^V_{\alpha\beta}$ are given by eq. (2.1).

2.3.1 Differential cross sections

We now obtain the differential cross section for the process (2.32) keeping the pure SM contribution, and the interference between the SM amplitude of Eq. 2.33 and the amplitudes with anomalous γZH and ZZH couplings from Eqs. 2.34 and 2.35 respectively. We ignore terms bilinear in the anomalous couplings, assuming that the new-physics contribution is small. We neglect the mass of the electron.

The expression for the cross section with longitudinal polarizations P_L and $\overline{P}_L$ for e^- and e^+ beams respectively is

$$\begin{aligned} \sigma_L &= \int\frac{d^3p_3}{2p_3^0}\int\frac{d^3p_4}{2p_4^0}\left(\frac{e}{4\sin\theta_W\cos\theta_W}\right)^2 \\ &\times\frac{1}{(q^2-m_Z^2)^2+\Gamma_Z^2}(1-P_L\overline{P}_L)\left[\mathcal{F}^L_{SM}+\mathcal{F}^L_Z+\mathcal{F}^L_\gamma\right] \end{aligned}$$

where $\mathcal{F}^L_{SM}$, $\mathcal{F}^L_Z$ and $\mathcal{F}^L_\gamma$ are the contributions from the SM alone, interference between the SM and the ZZH terms and interference between the SM and the γZH terms respectively, full analytical expressions of which are given in Appendix I.

Inferences from expressions of distributions for longitudinally polarized beams:

1. Including decay of Z into charged leptons, we get additional contributions from anomalous couplings Imb_γ, Imb_Z, Re$\tilde{b}_\gamma$ and Re$\tilde{b}_Z$, which are absent in the distributions without Z decay,

2. Couplings Ima_γ and ImΔa_Z are still absent from distributions of decay leptons for longitudinally polarized beams.

2.3.2 Observables

We have evaluated the expectation values of the observables for unpolarized and longitudinally polarized beams. We have chosen e^- polarization to be equal to ± 0.8 and e^+ polarization to be ± 0.6. We have done phase space integrals numerically. We have used the expressions of the cross sections to leading order of anomalous couplings for the calculations of the expectation values of the observables in the formula

$$\langle O_i \rangle = \frac{1}{\sigma} \int O_i \frac{d\sigma}{d^3p_3 d^3p_4} d^3p_3 d^3p_4. \tag{2.36}$$

We construct observables based on their CP and T transformation properties. The various possible observables that we have used in our analysis, along with their CP and T transformation properties have been listed in Table 2.3. Observables which are even under CP get contributions from CP-even VZH couplings which are Δa_Z, a_γ, b_Z and b_γ; and observables which are odd under CP get contributions from CP-odd VZH anomalous couplings which are $\tilde{b}_Z$ and $\tilde{b}_\gamma$. The CPT theorem implies that observables which are CP even and T even would get contribution from real part of the couplings, as also those which are CP odd and T odd, implying that observables which are CPT even get contributions from real part of couplings. On the other hand, observables, which are CPT odd which means that they should either be CP odd and T even or CP even and T odd, get contributions from imaginary part of the couplings as they would require presence of absorptive part in the amplitude and hence require imaginary parts from couplings.

CP-even observables get contributions from Rea_V, Reb_V, if they are T even, and Ima_V, Imb_V, if they are T odd. CP-odd observables get contributions from Re$\tilde{b}_V$ or Im$\tilde{b}_V$, depending on whether they are T odd or T even.

The observables we have chosen are by no means exhaustive. They have been chosen based on simplicity, and with the idea of extracting information on all couplings, and if possible, placing limits on them independently of one another.

In the next section we discuss numerical evaluation of the cross sections and

Symbol	Observable	CP	T	Couplings
X_1	$(p_1 - p_2).q$	$-$	$+$	$\mathrm{Im}\tilde{b}_Z,\ \mathrm{Im}\tilde{b}_\gamma$
X_2	$P.(p_3 - p_4)$	$-$	$+$	$\mathrm{Im}\tilde{b}_Z,\ \mathrm{Im}\tilde{b}_\gamma$
X_3	$(\overrightarrow{p_3} \times \overrightarrow{p_4})_z$	$-$	$-$	$\mathrm{Re}\tilde{b}_Z,\ \mathrm{Re}\tilde{b}_\gamma$
X_4	$(p_1 - p_2).(p_3 - p_4)(\overrightarrow{p_3} \times \overrightarrow{p_4})_z$	$-$	$-$	$\mathrm{Re}\tilde{b}_Z,\ \mathrm{Re}\tilde{b}_\gamma$
X_5	$(p_1 - p_2).q(\overrightarrow{p_3} \times \overrightarrow{p_4})_z$	$+$	$-$	$\mathrm{Im}b_Z,\ \mathrm{Im}b_\gamma$
X_6	$P.(p_3 - p_4)(\overrightarrow{p_3} \times \overrightarrow{p_4})_z$	$+$	$-$	$\mathrm{Im}b_Z,\ \mathrm{Im}b_\gamma$
X_7	$[(p_1 - p_2).q]^2$	$+$	$+$	$\mathrm{Re}b_Z,\ \mathrm{Re}b_\gamma$
X_8	$[(p_1 - p_2).(p_3 - p_4)]^2$	$+$	$+$	$\mathrm{Re}b_Z,\ \mathrm{Re}b_\gamma$

Table 2.3: *Possible observables to constrain anomalous couplings, their CP and T properties and the couplings they probe. Here, $P = p_1 + p_2$ and $q = p_3 + p_4$*

.

asymmetries, and demonstrate how information using more than one observable, or one observable, but different polarization choices can be used to disentangle the different anomalous couplings. We will also study the numerical limits that can be put on the couplings at a linear collider.

We calculate the individual limits (taking all other couplings except one to be zero) which can be placed at the 95% CL on a coupling contributing to the correlation of O_i is given by following relation:

$$Lim = 1.96 \frac{\sqrt{\langle O_i^2 \rangle_{SM} - \langle O_i \rangle_{SM}^2}}{\langle O \rangle_1 \sqrt{L \sigma_L^{SM}}} \tag{2.37}$$

where $\langle O \rangle_1$ is the expectation value of the observable O for unit value of the coupling, L is the integrated luminosity, and σ_{SM} is the SM cross section.

The limits which can be placed at the 95% CL on the two parameters contributing to the expectation value of O_i is given by equating the deviation of the expectation value of the observable from the SM value with $2.45/\sqrt{N_{SM}}$, where N_{SM} is the number of SM events. This leads to the relation

$$|\langle O_i \rangle - \langle O_i \rangle_{SM}| = 2.45 \frac{\sqrt{\langle O_i^2 \rangle_{SM} - \langle O_i \rangle_{SM}^2}}{\sqrt{L \sigma_L^{SM}}} \tag{2.38}$$

As seen from Table 2.3, each observable chosen by us has dependence on a combination of a limited number of couplings, depending upon the transformation properties under CP and T. Thus any single observable can only be used to determine, or put limits on, a combination of couplings. We can determine, from a single observable, limits on individual couplings either under an assumption on the remaining couplings which contribute to the observable, or by combining the results from more than one observable, or more than one combination of polarization. We will refer to limits on a coupling as an individual limit if the limit is obtained on the assumption of all other couplings being zero. If no such assumption is made, and more than one observable is used simultaneously to put limits on all couplings contributing to these observables, we will refer to the limits as simultaneous limits.

2.3.3 Sensitivities with longitudinal beam polarization

The differential cross section with longitudinally polarized beams, apart from an overall factor $(1 - P_L\overline{P}_L)$, depends on the "effective polarization" $P_L^{\rm eff}$. Since $P_L^{\rm eff}$ is about 0.946 for $P_L = 0.8$, $\overline{P}_L = -0.6$, and 0.385 for $P_L = 0.8$, $\overline{P}_L = 0.6$, a high degree of effective polarization can be achieved using these partial polarizations for e^- and e^+ beams opposite in sign to each other, which are expected to be available at the ILC.

We now consider the effect of longitudinal polarization on the correlations and the sensitivities. We also suggest measurement of correlations with different combinations of polarization. Since these would give different combinations of couplings, their measurements may be used to put simultaneous limits on couplings, without assuming any coupling to be zero.

We can write expectation values of $X_1, \ldots, X_6$ schematically as :

$$\langle X_1\rangle \propto A_1[2g_Vg_A - (g_V^2 + g_A^2)P_L^{\rm eff}]{\rm Im}\tilde{b}_Z + B_1[g_VP_L^{\rm eff} - g_A]{\rm Im}\tilde{b}_\gamma \quad (2.39)$$
$$\langle X_2\rangle \propto A_2[2g_Vg_AP_L^{\rm eff} - (g_V^2 + g_A^2)]{\rm Im}\tilde{b}_Z + B_2[g_V - g_AP_L^{\rm eff}]{\rm Im}\tilde{b}_\gamma \quad (2.40)$$
$$\langle X_3\rangle \propto A_3[2g_Vg_A - (g_V^2 + g_A^2)P_L^{\rm eff}]{\rm Re}\tilde{b}_Z + B_3[g_VP_L^{\rm eff} - g_A]{\rm Re}\tilde{b}_\gamma \quad (2.41)$$
$$\langle X_4\rangle \propto A_4[2g_Vg_AP_L^{\rm eff} - (g_V^2 + g_A^2)]{\rm Re}\tilde{b}_Z + B_4[g_V - g_AP_L^{\rm eff}]{\rm Re}\tilde{b}_\gamma \quad (2.42)$$
$$\langle X_5\rangle \propto A_5[2g_Vg_AP_L^{\rm eff} - (g_V^2 + g_A^2)]{\rm Im}b_Z + B_5[g_V - g_AP_L^{\rm eff}]{\rm Im}b_\gamma \quad (2.43)$$
$$\langle X_6\rangle \propto A_6[2g_Vg_A - (g_V^2 + g_A^2)P_L^{\rm eff}]{\rm Im}b_Z + B_6[g_VP_L^{\rm eff} - g_A]{\rm Im}b_\gamma \quad (2.44)$$

where $A_i's$ and $B_i's$ are some kinematical coefficients.

From Eqns. 2.39, 2.41 and 2.44, we see that with unpolarized beams, the contributions of anomalous couplings ${\rm Im}\tilde{b}_Z$, ${\rm Re}\tilde{b}_Z$ and ${\rm Im}b_Z$ to expectation values of

X_1, X_3 and X_6 respectively are suppressed due to vector coupling g_V while with the longitudinally polarized beams, these couplings get an additional term in the expectation values which enhance their contributions to respective expectation values by a factor of $(g_V^2 + g_A^2)/(2g_Vg_A)$. Hence, with longitudinally polarized beams with opposite sign of beam polarization, the individual limits on the anomalous couplings Im$\tilde{b}_Z$, Re$\tilde{b}_Z$ and Imb_Z are enhanced by the factor of 5 relative to unpolarized beams as shown in Table 2.4.

Similarly from Eqns. 2.40, 2.42 and 2.43, we see that with unpolarized beams, the contributions of anomalous couplings Im$\tilde{b}_\gamma$, Re$\tilde{b}_\gamma$ and Imb_γ to expectation values of X_2, X_4 and X_5 respectively are suppressed due to vector coupling g_V while with the longitudinally polarized beams, these couplings get an additional term in the expectation values which enhance their contributions to respective expectation values by a factor of g_A/g_V. Hence, with longitudinally polarized beams with opposite sign of beam polarization, the individual limits on the anomalous couplings Im$\tilde{b}_\gamma$, Re$\tilde{b}_\gamma$ and Imb_γ are enhanced by the factor of 8 relative to unpolarized beams as shown in Table 2.4.

Observables X_7 and X_8 being CP even and T even get contributions from real parts of CP-even couplings. Since their expectaion values are nonzero in the SM, they will get contribution from anomalous couplings in the denominator. Their expectation values can be written schematically as :

$$\langle X_{7,8}\rangle = \frac{[a_{7,8}(1 + \text{Re}\Delta a_Z) + b_{7,8}\text{Re}b_Z + c_{7,8}\text{Re}a_\gamma + d_{7,8}\text{Re}b_\gamma]}{[a_{7,8}(1 + \text{Re}\Delta a_Z) + b'_{7,8}\text{Re}b_Z + c_{7,8}\text{Re}a_\gamma + d'_{7,8}\text{Re}b_\gamma]}. \tag{2.45}$$

As can be seen from Eqn. 2.45 that the numerator and denominator get equal contribution from couplings ReΔa_Z and Rea_γ. So, when we write $\langle X_{7,8}\rangle$ to linear order in anomalous couplings by expanding the denominator and keeping only the linear terms in anomalous couplings, we find that the contributions of the couplings ReΔa_Z and Rea_γ cancel exactly while the contributions of Reb_Z and Reb_γ survive. The expectation values of $X_{7,8}$ can be written in the linear order in couplings Reb_Z and Reb_γ as:

$$\langle X_7\rangle \propto A_7[2g_Vg_AP_L^{\text{eff}} - (g_V^2 + g_A^2)]\text{Re}b_Z + B_7[g_V - g_AP_L^{\text{eff}}]\text{Re}b_\gamma \tag{2.46}$$

$$\langle X_8\rangle \propto A_8[2g_Vg_AP_L^{\text{eff}} - (g_V^2 + g_A^2)]\text{Re}b_Z + B_8[g_V - g_AP_L^{\text{eff}}]\text{Re}b_\gamma. \tag{2.47}$$

Hence, the limits on the coupling Reb_γ are enhanced by a factor of $g_A/g_V \sim 8.3$ in the presence of longitudinally polarized beams utilizing X_7 and X_8 relative to unpolarized beams.

The 95% CL individual limits on anomalous ZZH and γZH couplings utilizing the observables listed in Table 2.3 using different beam polarizations are given in Table 2.4.

	Observable	Coupling	Limits for polarizations $P_L = 0$, $\overline{P}_L = 0$	$P_L = 0.8$, $\overline{P}_L = 0.6$	$P_L = 0.8$, $\overline{P}_L = -0.6$
X_1	$(p_1 - p_2).q$	$\text{Im}\tilde{b}_Z$	4.11×10^{-2}	8.69×10^{-2}	9.94×10^{-3}
		$\text{Im}\tilde{b}_\gamma$	1.49×10^{-2}	2.06×10^{-2}	1.22×10^{-2}
X_2	$P.(p_3 - p_4)$	$\text{Im}\tilde{b}_Z$	4.12×10^{-2}	5.99×10^{-2}	3.84×10^{-2}
		$\text{Im}\tilde{b}_\gamma$	5.23×10^{-1}	3.12×10^{-1}	5.52×10^{-2}
X_3	$(\vec{p_3} \times \vec{p_4})_z$	$\text{Re}\tilde{b}_Z$	1.41×10^{-1}	2.97×10^{-1}	3.40×10^{-2}
		$\text{Re}\tilde{b}_\gamma$	5.09×10^{-2}	7.05×10^{-2}	4.15×10^{-2}
X_4	$(p_1 - p_2).(p_3 - p_4)$	$\text{Re}\tilde{b}_Z$	2.95×10^{-2}	4.29×10^{-2}	2.75×10^{-2}
	$\times(\vec{p_3} \times \vec{p_4})_z$	$\text{Re}\tilde{b}_\gamma$	3.81×10^{-1}	2.24×10^{-1}	3.95×10^{-2}
X_5	$(p_1 - p_2).q(\vec{p_3} \times \vec{p_4})_z$	$\text{Im}b_Z$	7.12×10^{-2}	1.04×10^{-1}	6.64×10^{-2}
		$\text{Im}b_\gamma$	9.10×10^{-1}	5.42×10^{-1}	9.53×10^{-2}
X_6	$P.(p_3 - p_4)(\vec{p_3} \times \vec{p_4})_z$	$\text{Im}b_Z$	7.12×10^{-2}	1.50×10^{-1}	1.72×10^{-2}
		$\text{Im}b_\gamma$	2.58×10^{-2}	3.57×10^{-2}	2.10×10^{-2}
X_7	$[(p_1 - p_2).q]^2$	$\text{Re}b_Z$	1.75×10^{-2}	2.54×10^{-2}	1.63×10^{-2}
		$\text{Re}b_\gamma$	2.23×10^{-1}	1.34×10^{-1}	2.35×10^{-2}
X_8	$[(p_1 - p_2).(p_3 - p_4)]^2$	$\text{Re}b_Z$	1.53×10^{-2}	2.22×10^{-2}	1.42×10^{-2}
		$\text{Re}b_\gamma$	1.94×10^{-1}	1.16×10^{-1}	2.04×10^{-2}

Table 2.4: *The 95 % C.L. limits on the anomalous ZZH and γZH couplings, chosen nonzero one at a time, from various observables with unpolarized and longitudinally polarized beams for $\sqrt{s} = 500$ GeV and integrated luminosity $\int \mathcal{L}\, dt = 500$ fb^{-1}.*

We determine simultaneous limits on a pair of anomalous couplings through the measurement of a single observable using different polarization combinations for the measurement or through the measurements of more than one observable utilizing only unpolarized beams. For the sake of illustration for each case, we first consider observable X_1. The expectation value of X_1 gets contribution from two couplings $\text{Im}\tilde{b}_Z$ and $\text{Im}\tilde{b}_\gamma$ and is written in schematic form in Eqn 2.39. The different beam polarization combinations would give different expectation values for the observable. A graphical way of obtaining simultaneous limits with different combinations of polarization is illustrated for X_1 in Fig. 2.4 where relation Eqn. (2.38) is plotted in the space of the couplings involved for unpolarized beams denoted by $(0,0)$, and for the two combinations of longitudinal polarizations $(P_L, \overline{P}_L) \equiv (0.8, -0.6)$, and $(P_L, \overline{P}_L) \equiv (-0.8, 0.6)$, respectively denoted by $(+,-)$ and $(-,+)$. The lines corresponding to any two combinations gives a closed region which is the allowed region at 95% CL.

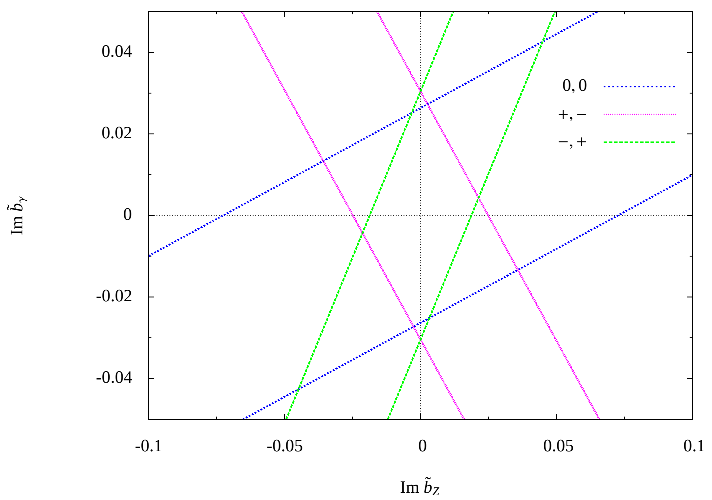

Figure 2.4: *The region in the* $\mathrm{Im}\tilde{b}_Z$-$\mathrm{Im}\tilde{b}_\gamma$ *plane accessible at the* 95% *CL with observable* X_1 *with different beam polarization configurations.* $(0,0)$, $(+,-)$ *and* $(-,+)$ *stand for* $(P_L, \overline{P}_L) = (0,0)$, $(0.8,-0.6)$ *and* $(-0.8, 0.6)$ *respectively.*

The best simultaneous limits on $\mathrm{Im}\tilde{b}_Z$ is obtained by considering the region enclosed by the lines corresponding to $(P_L, \overline{P}_L) = (0.8, -0.6)$ and $(P_L, \overline{P}_L) = (-0.8, 0.6)$, while on $\mathrm{Im}\tilde{b}_\gamma$, it is obtained by the region enclosed by the lines corresponding to $(P_L, \overline{P}_L) = (0,0)$ and $(P_L, \overline{P}_L) = (0.8, -0.6)$. These limits are

$$|\mathrm{Im}\tilde{b}_Z| \leq 2.72 \times 10^{-2}, |\mathrm{Im}\tilde{b}_\gamma| \leq 2.13 \times 10^{-2}. \tag{2.48}$$

Using the same strategy for all the observables $X_1, \ldots, X_8$, we obtain 95% CL simultaneous limits on all the couplings and these limits are given in Table 2.5.

We now illustrate how the measurements of two different observables can determine the simultaneous limits on a pair of anomalous couplings. For this, we consider observables X_1 and X_2. With unpolarized beams, X_1 and X_2 both probe different combinations of $\mathrm{Im}\tilde{b}_Z$ and $\mathrm{Im}\tilde{b}_\gamma$. We show in Fig. 2.5 a plot of relation Eq. 2.38 in the space of the couplings involved for observables X_1 and X_2 utilizing only unpolarized beams. The lines corresponding to two combinations gives a closed

Observable	Coupling	Limit on coupling for the polarization combination		
		$(0,0),(-,+)$	$(0,0),(+,-)$	$(-,+),(+,-)$
X_1	Im$\tilde{b}_Z$	4.50×10^{-2}	3.59×10^{-2}	2.14×10^{-2}
	Im$\tilde{b}_\gamma$	4.28×10^{-2}	2.74×10^{-2}	3.04×10^{-2}
X_2	Im$\tilde{b}_Z$	9.73×10^{-2}	7.56×10^{-2}	8.54×10^{-2}
	Im$\tilde{b}_\gamma$	3.06×10^{-1}	2.19×10^{-1}	1.37×10^{-1}
X_3	Re$\tilde{b}_Z$	1.54×10^{-1}	1.22×10^{-1}	7.29×10^{-2}
	Re$\tilde{b}_\gamma$	1.46×10^{-1}	9.31×10^{-2}	1.08×10^{-1}
X_4	Re$\tilde{b}_Z$	5.37×10^{-2}	6.89×10^{-2}	6.10×10^{-2}
	Re$\tilde{b}_\gamma$	1.56×10^{-1}	2.18×10^{-1}	9.78×10^{-2}
X_5	Imb_Z	1.67×10^{-1}	1.29×10^{-1}	1.48×10^{-1}
	Imb_γ	5.27×10^{-1}	3.76×10^{-1}	2.36×10^{-1}
X_6	Imb_Z	7.79×10^{-2}	6.18×10^{-2}	3.69×10^{-2}
	Imb_γ	7.39×10^{-2}	4.72×10^{-2}	5.27×10^{-2}
X_7	Reb_Z	2.53×10^{-2}	1.27×10^{-2}	3.11×10^{-2}
	Reb_γ	1.05×10^{-1}	5.74×10^{-2}	5.11×10^{-2}
X_8	Reb_Z	2.58×10^{-2}	2.05×10^{-2}	3.37×10^{-2}
	Reb_γ	1.15×10^{-1}	6.33×10^{-2}	5.26×10^{-2}

Table 2.5: *Simultaneous 95 % C.L. limits on the anomalous ZZH and γZH couplings from various observables using longitudinally polarized beams with different polarization combinations* $(0,0)$, *i.e.,* $P_L = 0, \overline{P}_L = 0$, $(\pm,\mp)$, *i.e.,* $(P_L = \pm 0.8, \overline{P}_L = \mp 0.6)$ *for* $\sqrt{s} = 500$ *GeV and integrated luminosity* $\int \mathcal{L}\, dt = 500$ *fb*$^{-1}$.

region which is the allowed region at 95% CL. The simultaneous limits obtained by considering the extremities of this closed region are

$$|\text{Im}\tilde{b}_Z| \leq 7.73 \times 10^{-2},\ |\text{Im}\tilde{b}_\gamma| \leq 5.44 \times 10^{-2}. \tag{2.49}$$

The intercepts on the two axes of each line give us the individual limits on the two couplings for that observable.

Similarly, with unpolarized beams, X_3 and X_4 both probe different combinations of Re$\tilde{b}_Z$ and Re$\tilde{b}_\gamma$ while X_5 and X_6 both probe different combinations of Imb_Z and Imb_γ. Analogous to Fig. 2.5, we can have a plot of relation Eq. 2.38 in the space of the couplings involved for observables X_3 and X_4 utilizing only

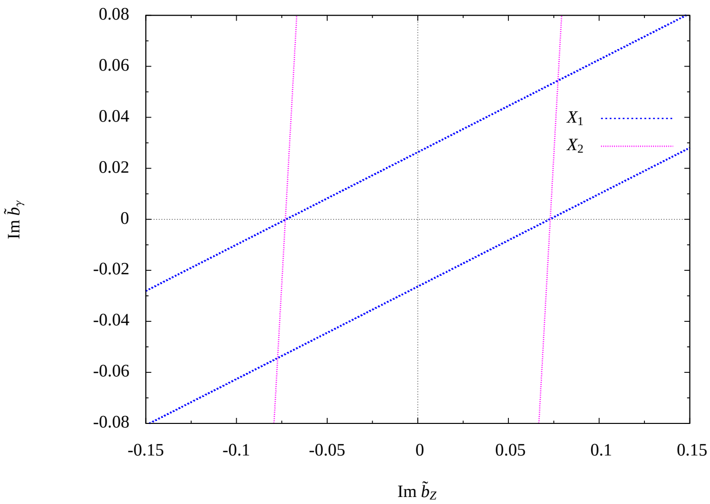

Figure 2.5: *The region in the* Im$\tilde{b}_Z$-Im$\tilde{b}_\gamma$ *plane accessible at the* 95% *CL with observables* X_1 *and* X_2 *with unpolarized beams for integrated luminosity* $L = 250$ *fb*$^{-1}$.

unpolarized beams. The 95 % CL simultaneous limits on couplings Re$\tilde{b}_Z$ and Re$\tilde{b}_\gamma$ obtained by considering the extremities of this closed region are

$$|\text{Re}\tilde{b}_Z| \leq 6.08 \times 10^{-2}, |\text{Re}\tilde{b}_\gamma| \leq 1.12 \times 10^{-1}. \tag{2.50}$$

Similarly, with X_5 and X_6, the 95% CL simultaneous limits on couplings Imb_Z and Imb_γ are

$$|\text{Im}b_Z| \leq 1.25 \times 10^{-1}, \ |\text{Im}b_\gamma| \leq 9.39 \times 10^{-2}. \tag{2.51}$$

With unpolarized beams, X_7 and X_8 both probe different combinations of Reb_Z and Reb_γ. Simultaneous limits on Reb_Z and Reb_γ from X_7 and X_8 are very bad since slopes of the two lines corresponding to X_7 and X_8 are of same sign and approximately equal in magnitude.

2.3.4 Effects of kinematical cuts

In practice, any measurement will need kinematical cuts for the identification of the decay leptons. We have examined the effect of kinematical cuts on our results using the following kinematical cuts [26]:

1. $E_f \geq 10$ GeV for each outgoing charged lepton,
2. $5^\circ \leq \theta_0 \leq 175^\circ$ for each outgoing charged lepton to remain away from the beam pipe,

3. $\Delta R_{ll} \geq 0.2$ for the pair of charged lepton, where $(\Delta R)^2 \equiv (\Delta\phi)^2 + (\Delta\eta)^2$, $\Delta\phi$ and $\Delta\eta$ being the separation in azimuthal angle and rapidity, respectively, for detection of the two leptons as separated.

In addition to this, we imposed a cut on the invariant mass of the $f\overline{f}$ so as to confirm the onshellness of the Z boson, which is

$$R1 \equiv |m_{f\overline{f}} - M_Z| \leq 5\Gamma_Z. \tag{2.52}$$

In addition to this, we impose a cut $|m_{l^-l^+} - M_Z| \leq 5\Gamma_Z$ on the invariant mass $m_{l^-l^+}$ of the lepton pair, so as to constrain the Z boson to be more or less on shell. This cut would allow us to test how well our results would simulate the results for a genuinely onshell Z. Moreover, the cut would also reduce contamination from $\gamma\gamma H$ couplings, which contribute in principle to the process (2.32), though not to $e^+e^- \to HZ$.

After imposing these cuts, we find that all observables except X_1 and X_2 are not very sensitive to these cuts. The limit on X_1 and X_2 change by $20 - 30\%$.

2.3.5 Sensitivities at different cm energies

Since the anomalous couplings b_Z, b_γ, $\tilde{b}_Z$ and $\tilde{b}_\gamma$ correspond to interactions which are momentum dependent, the sensitivity would be dependent on the cm energy. Naively, it is expected from eq. (3.22) that an increase by a factor of 2 in the cm energy as well as in the luminosity would result in an improvement in the limit by an overall factor $2\sqrt{2} \approx 3$. A factor of 4 improvement comes from the energy dependence of the anomalous term in the differential cross section contributing to the left-hand side of (3.22), an additional factor of $\sqrt{2}$ from the increase in the luminosity, but a decrease by a factor of 2 since $\sigma_{\rm SM}$ in denominator of the right-hand side falls by a factor 4. To investigate this, we have obtained sensitivities of all the observables to the anomalous couplings at $\sqrt{s} = 1000$ GeV with integrated luminosity $\int \mathcal{L}\, dt = 1000$ fb^{-1}.

We find that only X_3, X_4, X_5 and X_8 are more sensitive to anomalous couplings at higher energy and luminosity. It can be checked that the dominant contribution from longitudinally polarized Z produced at an anomalous γZH or ZZH vertex, which should grow with energy, actually vanishes, leaving a sub-dominant energy dependence which is the same as that in SM. Hence whether or not there is improvement in sensitivity with cm energy has to be studied on a case by case basis.

In the above, we have assumed a Higgs mass of 120 GeV. For larger values of m_H, for larger Higgs masses, we find decreased sensitivities.

2.3.6 Comparison with earlier works

It is appropriate to compare our results with those in works using the same parameterization as ours for the anomalous coupling and with an approach similar to ours. The paper of Han and Jiang [25] discuss limits on the CP-violating ZZH coupling $\text{Im}\tilde{b}_Z$ obtained using the forward-backward asymmetry of the Z. With identical values of $\sqrt{s}$ and integrated luminosity, Han and Jiang quote limits of 0.019 and 0.0028 for $\text{Im}\tilde{b}_Z$, respectively for unpolarized and longitudinally polarized beams with opposite-sign e^+ and e^- polarizations. The corresponding numbers we have form A_{FB} are 0.011 and 0.0026. The agreement is thus good, considering that Ref. [25] employs additional experimental cuts, which could reduce the nominal sensitivity. The limits on $\text{Im}\tilde{b}_Z$ and $\text{Im}\tilde{b}_\gamma$ we have from X_1 are 0.041 and 0.0099. The agreement with Ref. [25] is reasonable, after taking into account the facts that we use only one leptonic channel, and that they employ additional experimental cuts. The papers in [26] also deal only with anomalous ZZH couplings. The 3σ limit they quote for $\text{Im}\tilde{b}_Z$ is 0.064 for unpolarized beams, and 0.0089 for polarized beams. After correcting for the CL limit of 1.96σ which we use, and the inclusion of a single leptonic decay mode, their limits are still somewhat worse. This could be attributed to the stringent kinematic cuts imposed by them, and to the different luminosity choice in the case of polarized beams. Similarly, the limits quoted in [26] for $\text{Re}b_Z$ and $\text{Im}b_Z$ are worse compared to ours by a factor of order 2 or 3 in the unpolarized as well as the cases of longitudinally polarized beams. As for the case of γZH couplings, comparison with earlier works is not easy because of the different approach to parametrization of couplings.

2.4 Conclusions and discussion

We have obtained analytical expressions for angular distributions of the Z boson and differential cross sections of the charged leptons from Z-decay in the process $e^+e^- \to ZH \to \ell^+\ell^- H$ including anomalous γZH and ZZH couplings to linear order in the presence of unpolarized and longitudinally polarized beams. We have then looked at observables and asymmetries which can be used in combinations to disentangle the various couplings to the extent possible. We have also obtained the sensitivities of these observables and asymmetries to the various couplings for a definite configuration of the linear collider.

In certain cases where the contribution of a coupling is suppressed due to the fact that the vector coupling of the Z to e^+e^- is numerically small, longitudinal polarization helps to enhance the contribution of this coupling. As a result, longitudinal polarization improves the sensitivity.

We find that with a linear collider operating at a c.m. energy of 500 GeV with the capability of 80% electron polarization and 60% positron polarization with an integrated luminosity of 500 fb^{-1}, using the simple cross section and asymmetry measurements described above it would be possible to place 95% CL individual limits of the order of few times 10^{-3} or better on all couplings taken nonzero one at a time with use of an appropriate combination (P_L and $\overline{P}_L$ of opposite signs) of longitudinal beam polarizations. Polarization gives an improvement in sensitivity by a factor of 5 to 10 as compared to the unpolarized case for the real parts of γZH couplings, and the imaginary parts of ZZH couplings. The use of polarization also enables simultaneous determination (without any coupling being assumed zero) of all couplings which appear in the differential cross section, viz., ReΔa_Z, Rea_γ, Ima_γ, Reb_Z, Reb_γ, Im$\tilde{b}_\gamma$ and Im$\tilde{b}_Z$. The simultaneous limits are, as expected, less stringent, of the order of $0.1 - 0.3$ for Rea_γ and ReΔa_Z, and of the order of $0.03 - 0.07$ on Reb_γ and Reb_Z. The simultaneous limits on the CP-violating couplings Im$\tilde{b}_\gamma$ and Im$\tilde{b}_Z$ are a little better, being respectively 5×10^{-3} and 6×10^{-3}.

Chapter 3

Anomalous VZH couplings with transversely polarized beams

As explained in the introduction (Chapter 1), transverse polarization is useful because it provides an additional reference direction, thus enabling the study of azimuthal distributions of final-state particles even in $2 \to 2$ processes.

The question of whether transverse beam polarization, which could be obtained with the use of spin rotators, would be useful in probing new physics, has been addressed in recent times in the context of the ILC [31]-[39]. The cross section with transverse polarization generally provides combinations of the same couplings as longitudinal polarization. A marked exception is the angular dependence associated with the coupling $\mathrm{Im}a_\gamma$ – it is possible to use an azimuthal asymmetry which depends entirely on this coupling when the beams are transversely polarized, and its measurement would determine this coupling directly. Unpolarized or longitudinally polarized beams provide no access to $\mathrm{Im}a_\gamma$. Another azimuthal asymmetry in the presence of transverse polarization helps to isolate a combination of two couplings $\mathrm{Re}\Delta a_Z$ and $\mathrm{Re}b_Z$ out of the four which contribute to the differential cross section with longitudinal polarization. Transverse polarization can also help isolate other couplings, since, as it turns out, usually the contribution of one coupling dominates most observables.

In the last chapter, we studied the process in $e^+e^- \to HZ$ to probe the anomalous γZH and ZZH couplings utilizing angular asymmetries of the Z and the observables constructed with momenta of Z-decay leptons and initial e^+ and e^- momenta with longitudinal beam polarization. In this chapter, we study the role of transversely polarized beams in the process $e^+e^- \to ZH$ to probe anomalous

VZH couplings at a linear collider. We first consider the angular distribution of the Z and construct azimuthal asymmetries associated with it. We also consider the angular distribution of decay leptons from the Z. We utilize momenta of the decay leptons and spins and momenta of the initial electron and positron beams to construct various momentum correlations having specific CP and T transformation properties.

3.1 The process $e^+e^- \to HZ$

The expression for the amplitude for the process

$$e^-(p_1) + e^+(p_2) \to Z^\alpha(q) + H(k), \tag{3.1}$$

arising from the SM diagram with a point-like ZZH vertex, is

$$M_{\rm SM} = -\frac{e^2}{4\sin^2\theta_W\cos^2\theta_W}\frac{m_Z}{s-m_Z^2}\overline{v}(p_2)\gamma^\alpha(g_V-\gamma_5 g_A)u(p_1), \tag{3.2}$$

where the vector and axial-vector couplings of the Z to electrons are given by

$$g_V^e = -1 + 4\sin^2\theta_W,\ g_A^e = -1, \tag{3.3}$$

and θ_W is the weak mixing angle.

3.1.1 Angular distribution of Z with transversely polarized beams

For transversely polarized beams, we take the e^- polarization to be along the x axis and that of the e^+ in the xy plane, making an angle of δ with the x axis, so that $\delta = 0$ corresponds to parallel e^- and e^+ transverse polarizations. The expression for the differential cross section with transverse polarization P_T for the e^- beam and $\overline{P}_T$ for the e^+ beam is

$$\begin{aligned}\frac{d\sigma_T}{d\Omega} &= \big[A_T + B_T\sin^2\theta + C_T\cos\theta \\ &\quad + P_T\overline{P}_T\sin^2\theta\,\{D_T\cos(2\phi-\delta) + E_T\sin(2\phi-\delta)\}\big]\,,\end{aligned} \tag{3.4}$$

where A_T, B_T, C_T, D_T and E_T are further written in terms of contributions from SM alone (superscript "SM"), interference between SM and ZZH terms (superscript Z), and interference between SM and γZH (superscript γ), in exact analogy with expressions for A_L, B_L and C_L given in Chapter 2 for the longitudinal polarization case. The expressions for the separate contributions for these coefficients are as follows.

$$A_T^{\rm SM} = B_T^{\rm SM}\frac{2m_Z^2}{|\vec{q}|^2} = (g_V^{e2} + g_A^{e2})K^{\rm SM}, \tag{3.5}$$

$$C_T^{\rm SM} = 0,\ D_T^{\rm SM} = \frac{|\vec{q}|^2}{2m_Z^2}(g_V^{e2} - g_A^{e2})K^{\rm SM},\ E_T^{\rm SM} = 0, \tag{3.6}$$

$$A_T^Z = 2(g_V^{e2} + g_A^{e2})\left({\rm Re}\Delta a_Z + {\rm Re}b_Z\frac{\sqrt{s}q^0}{m_Z^2}\right)K^{\rm SM}, \tag{3.7}$$

$$B_T^Z = 2\frac{|\vec{q}|^2}{2m_Z^2}{\rm Re}\Delta a_Z(g_V^{e2} + g_A^{e2})K^{\rm SM},\ C_T^Z = 2{\rm Im}\tilde{b}_Z\frac{\sqrt{s}|\vec{q}|}{m_Z^2}2g_V^e g_A^e K^{\rm SM}, \tag{3.8}$$

$$D_T^Z = 2\frac{|\vec{q}|^2}{2m_Z^2}(-{\rm Re}\Delta a_Z)(g_V^{e2} - g_A^{e2})K^{\rm SM},\ E_T^Z = 0, \tag{3.9}$$

$$A_T^\gamma = \left({\rm Re}a_\gamma + {\rm Re}b_\gamma\frac{\sqrt{s}q^0}{m_Z^2}\right)(g_V^e)K^\gamma, \tag{3.10}$$

$$B_T^\gamma = \frac{|\vec{q}|^2}{2m_Z^2}{\rm Re}a_\gamma(g_V^e)K^\gamma,\ C_T^\gamma = \frac{\sqrt{s}|\vec{q}|}{m_Z^2}{\rm Im}\tilde{b}_\gamma\,(g_A^e)\,K^\gamma, \tag{3.11}$$

$$D_T^\gamma = \frac{|\vec{q}|^2}{2m_Z^2}{\rm Re}a_\gamma(-g_V^e)K^\gamma,\ E_T^\gamma = \frac{|\vec{q}|^2}{2m_Z^2}{\rm Im}a_\gamma(g_A^e)K^\gamma. \tag{3.12}$$

where K^{SM} and K^γ have been defined in Chapter 2.

Taking a look at the above equations, we note the following:

(i) For studying any effects dependent on transverse polarization, and therefore, of the azimuthal distribution of the Z, both electron and positron beams have to be polarized.

(ii) If the azimuthal angle ϕ of Z is integrated over, there is no difference between the transversely polarized and unpolarized cross sections [43]. Thus the usefulness of transverse polarization comes from the study of nontrivial ϕ dependence.

(iii) A glaring advantage of using transverse polarization would be to determine ${\rm Im}a_\gamma$ from the $\sin(2\phi - \delta)$ dependence of the angular distribution. It can be seen that E_T receives contribution only from E_T^γ, which determines ${\rm Im}a_\gamma$ independently of any other coupling. Moreover, ${\rm Im}a_\gamma$ does not contribute to unpolarized or longitudinally polarized cases.

(iv) The $\cos(2\phi - \delta)$ dependence of the angular distribution (the D_T term) determines a combination only of the couplings ${\rm Re}\Delta a_Z$ and ${\rm Re}a_\gamma$. On the other hand, in the case of unpolarized or longitudinally polarized beams the coefficient

B_L does depend only on Rea_γ and ReΔa_Z, and if measured, can give information on Rea_γ and ReΔa_Z independently of Reb_γ and Reb_Z. However, there is no simple asymmetry which allows B_L to be measured separately from A_L, which depends on a combination of all four of Rea_γ, ReΔa_Z, Reb_γ and Reb_Z.

(v) The real parts of the CP-violating couplings $\tilde{b}_Z$ and $\tilde{b}_\gamma$ remain undetermined with either longitudinal or transverse polarization without considering Z decay.

(vi) ImΔa_Z also remains undetermined.

3.1.2 Azimuthal asymmetries

Transversely polarized beams can in principle provide more information through the azimuthal angular distribution which has terms dependent on $\sin^2\theta \sin 2\phi$ and $\sin^2\theta\cos 2\phi$. The ϕ-dependent terms occur with the factor of $P_T\overline{P}_T$. Thus, both beams need to have transverse polarization for a nontrivial azimuthal dependence. We can construct observables which isolate terms dependent on $\sin^2\theta$ $\sin 2\phi$ and $\sin^2\theta\cos 2\phi$.

(a) The $\sin^2\theta\sin 2\phi$ term

We define an azimuthal asymmetry to separate out the $\sin^2\theta\sin 2\phi$ term:

$$\begin{aligned}\mathcal{A}^{\mathrm{T}}(\theta_0) = \frac{1}{\sigma_T^{SM}(\theta_0)}\Bigg[\int_{\theta_0}^{\pi-\theta_0} d\theta \quad &\Bigg(\int_0^{\pi/2} d\phi - \int_{\pi/2}^{\pi} d\phi \\ &+ \int_{\pi}^{3\pi/2} d\phi - \int_{3\pi/2}^{2\pi} d\phi\Bigg)\frac{d\sigma_T}{d\theta d\phi}\Bigg],\end{aligned} \tag{3.13}$$

where we use only the SM cross section in the denominators, since we work to first order in anomalous couplings.

The integrals in the above may be evaluated to yield

$$\mathcal{A}^{\mathrm{T}}(\theta_0) = \frac{2}{\pi}P_T\overline{P}_T\frac{(D_T\sin\delta + E_T\cos\delta)\left(1-\frac{1}{3}\cos^2\theta_0\right)}{A_T^{\mathrm{SM}} + B_T^{\mathrm{SM}}\left(1-\frac{1}{3}\cos^2\theta_0\right)}, \tag{3.14}$$

In the simplest scenario when $\delta = 0$ or π, we see that the asymmetry $\mathcal{A}^{\mathrm{T}}$ isolates a coefficient denoted by E_T in the expression of Eqn. (3.14). Since E_T^{SM} and E_T^Z are vanishing, this asymmetry uniquely determines E_T^γ, and hence the coupling Ima_γ. We thus have the important result that a measurement of $\mathcal{A}^{\mathrm{T}}(\theta_0)$ when the electron and positron polarizations are parallel to each other directly gives us a measurement of Ima_γ, which cannot be measured without the use of transverse polarization. This, in the present context, is the most important use of transverse polarization.

That ImΔa_Z does not contribute to asymmetry $\mathcal{A}^{\rm T}$ can be seen as follows. The transverse polarization dependent part of the differential cross section arises from the interference of amplitudes with a dissimilar e^- and e^+ helicity combination, and is proportional to Re $(e^{i2\phi}T_{LR}T^*_{RL})$ [43]. Here ϕ is the azimuthal angle of a final-state particle, and the subscripts on T denote the helicities. It is easy to check that in this expression, to first order in anomalous couplings, the ImΔa_Z contribution drops out. This is because the a_Z contribution is given by the SM contribution, which is real, multiplied by the coupling a_Z. This may also be inferred from the relevant tables in [40].

We can also choose to evaluate the expectation value of any operators which are odd functions of $\sin 2\phi$. We have chosen the three operators sign($\sin 2\phi$) whose expectation value corresponds to the asymmetry $\mathcal{A}^{\rm T}$, $\sin 2\phi$ and $\sin^3 2\phi$. The 95% CL limit that can be placed on Ima_γ was determined for each operator O using

$$|{\rm Im}a_\gamma| \leq 1.96 \frac{\sqrt{\langle O^2 \rangle}}{\langle O \rangle_1 \sqrt{L\sigma_T^{SM}}}, \tag{3.15}$$

where $\langle O \rangle_1$ is expectation value for unit value of the coupling. Table 3.1 shows limits on the $|{\rm Im}a_\gamma|$ at the 95% confidence level for various Higgs masses. It is seen

Operators	$M_H = 120$ GeV	$M_H = 200$ GeV	$M_H = 300$ GeV
sign($\sin 2\phi$)	0.0409	0.0522	0.101
$\sin 2\phi$	0.0368	0.0470	0.0913
$\sin^3 2\phi$	0.0388	0.0495	0.0963

Table 3.1: *Limits on* Ima_γ *for the various Higgs masses*

that the best limits are obtained using the operator $\sin 2\phi$.

(b) The $\sin^2\theta \cos 2\phi$ term

The coefficient of the $\cos 2\phi$ term, viz., D_T, is associated with ReΔa_Z and Rea_γ. We define an asymmetry

$$\begin{aligned} \mathcal{A}'^{\rm T}(\theta_0) = \frac{1}{\sigma_T(\theta_0)} \Bigg[\int_{\theta_0}^{\pi-\theta_0} d\theta \; \Bigg(& \int_{-\pi/4}^{\pi/4} d\phi - \int_{\pi/4}^{3\pi/4} d\phi \\ & + \int_{3\pi/4}^{5\pi/4} d\phi - \int_{5\pi/4}^{7\pi/4} d\phi \Bigg) \frac{d\sigma_T}{d\theta d\phi}\Bigg], \end{aligned} \tag{3.16}$$

to isolate the real parts of couplings Δa_Z and a_γ. In the definition of the asymmetry $\mathcal{A}'^{\rm T}$, we use total cross section including the anomalous VZH couplings in linear order since the asymmetry $\mathcal{A}'^{\rm T}$ itself gets contribution from the SM.

After performing the integrals in Eqn. 3.16, we get the following expression for $\mathcal{A}'_T$:

$$\mathcal{A}^{'\mathrm{T}}(\theta_0) = \frac{2}{\pi} P_T \overline{P}_T \frac{(D_T \cos\delta - E_T \sin\delta)\left(1 - \frac{1}{3}\cos^2\theta_0\right)}{A_T + B_T\left(1 - \frac{1}{3}\cos^2\theta_0\right)}. \tag{3.17}$$

When we expand the cross section in the denominator to obtain the expression for the asymmetry to linear order in anomalous couplings, we find that the denominator at linear order cancels the contribution of the coupling Rea_γ approximately, while introducing contributions of Reb_Z and Reb_γ, though the contribution of Reb_γ is found to be negligibly small. Thus, we conclude that asymmetry $\mathcal{A}^{'\mathrm{T}}$ probes the combination of couplings ReΔa_Z and Reb_Z.

As this asymmetry does not vanish for the SM, we use the following expression for determining the limit on the linear combination of couplings at 95% CL.

$$|\mathcal{A}^{'T} - \mathcal{A}^{'T\,SM}| \leq 2.45 \frac{\sqrt{1 - (\mathcal{A}^{'T\,SM})^2}}{\sqrt{L\sigma^{\mathrm{SM}}}}, \tag{3.18}$$

where $\mathcal{A}^{\mathrm{S}M}$ is the value of the asymmetry in SM.

As this asymmetry is proportional to the product $P_T\overline{P}_T$, changing the sign of polarization will only give a change of sign of the asymmetry. It is thus not possible to obtain two different combinations of the couplings ReΔa_Z and Reb_Z as in the earlier case of longitudinal polarization. However, it would be possible to obtain simultaneous limits on these couplings by choosing two different cut-offs on the azimuthal angle ϕ, which would give two equations. We have not attempted this in the present work.

The individual limits using $\mathcal{A}^{'\mathrm{T}}$ on ReΔa_Z and Reb_Z each taken nonzero by turns, are

$$|\mathrm{Re}\Delta a_Z| \leq 0.267, \ |\mathrm{Re}b_Z| \leq 0.113 \tag{3.19}$$

3.2 The process $e^+e^- \to ZH \to \ell^+\ell^- H$

In the previous section, we only focused on the angular distribution of the Z momentum which amounts to using the sum of the momenta of the Z-decay products. With only Z momentum, the angular distribution do not get contributions from couplings like Imb_Z, Im$\tilde{b}_Z$, Re$\tilde{b}_Z$, Imb_γ, Im$\tilde{b}_\gamma$ and Re$\tilde{b}_\gamma$. These couplings may contribute to the process $e^+e^- \to ZH$ if we consider the angular distributions of the decay leptons.

To explore this possibility, we now consider the Z decaying to charged leptons as:

$$e^-(p_1) + e^+(p_2) \to Z^\alpha(q) + H(k) \to \ell^-(p_3) + \ell^+(p_4) + H(k), \tag{3.20}$$

where ℓ is either μ or τ. Helicity amplitudes for the process were obtained earlier in the context of an effective Lagrangian approach [22, 29]. We have used instead trace techniques employing the symbolic manipulation program 'FORM' [42]. We neglect the mass of the electron.

We choose the z axis along the e^- momentum and the positive x axis is chosen to be along the direction of the e^- polarization (or the e^+ polarization taken to be parallel to the e^- polarization).

The amplitudes for the process 3.20 in the case of the SM and in the presence of anomalous ZZH and γZH couplings are given by Eqns. 2.33, 2.34 and 2.35 in Chapter 2. The expression for the cross section with transverse polarization P_T for e^- beam and $\overline{P}_T$ for e^+ beam is

$$\begin{aligned}\sigma_T &= \int \frac{d^3p_3}{2p_3^0}\frac{d^3p_4}{2p_4^0}\Big(\frac{e}{4\sin\theta_W\cos\theta_W}\Big)^2 \\ &\quad \frac{1}{(q^2-m_Z^2)^2+\Gamma_Z^2 m_Z^2}\left[\mathcal{F}_{SM}^T+\mathcal{F}_Z^T+\mathcal{F}_\gamma^T\right]\end{aligned} \tag{3.21}$$

where $\mathcal{F}_{SM}^T$, $\mathcal{F}_Z^T$ and $\mathcal{F}_\gamma^T$ are the contributions from the SM alone, interference between the SM and the ZZH terms and interference between the SM and the γZH terms respectively, full analytical expressions of which are given in Appendix II. The expression for the differential cross section with transverse polarization P_T for e^- beam and $\overline{P}_T$ for e^+ beam has terms either independent of the P_T and $\overline{P}_T$, or proportional to the product $P_T\overline{P}_T$. The phase space integrals of Eqn. 3.21 have been evaluated numerically.

3.2.1 Observables

We evaluate expectation values of the observables Y_i $(i = 1, 2, \ldots 6)$ for transversely polarized beams. The observables Y_i have definite transformation properties under CP and T. The definitions of Y_i with their CP and T transformation properties are given in Table 3.2.

Symbol	Observable	CP	T	Couplings
Y_1	$(q_x q_y)$	$+$	$-$	$\text{Im}a_\gamma$
Y_2	$(q_x^2 - q_y^2)$	$+$	$+$	$\text{Re}b_Z$, $\text{Re}a_\gamma$, $\text{Re}b_\gamma$
Y_3	$(p_3 - p_4)_x(p_3 - p_4)_y$	$+$	$-$	$\text{Im}a_\gamma$, $\text{Im}b_\gamma$
Y_4	$q_x q_y (p_3 - p_4)_z$	$-$	$-$	$\text{Re}\tilde{b}_Z$, $\text{Re}\tilde{b}_\gamma$
Y_5	$(p_3 - p_4)_x(p_3 - p_4)_y q_z$	$+$	$-$	$\text{Im}b_Z$, $\text{Im}b_\gamma$
Y_6	$[(p_3)_x^2 - (p_4)_x^2] - [(p_3)_y^2 - (p_4)_y^2]$	$-$	$+$	$\text{Im}\tilde{b}_Z$, $\text{Im}\tilde{b}_\gamma$

Table 3.2: *Possible observables to constrain anomalous couplings, their CP and T properties and the couplings they probe. Here, $P = p_1 + p_2$ and $q = p_3 + p_4$.*

3.2.2 Sensitivities with transverse beam polarization

For the purpose of numerical calculations, we have made use of the following values of parameters: $M_Z = 91.19$ GeV, $\alpha(M_Z) = 1/128$, $\sin^2\theta_W = 0.22$. We have evaluated expectation values of the observables and their sensitivities to the anomalous couplings for ILC operating at $\sqrt{s} = 500$ GeV having integrated luminosity $\int \mathcal{L}dt = 500$ fb^{-1}. We have assumed that transverse polarizations of $P_T = \pm 0.8$ and $\overline{P}_T = \pm 0.6$ would be accessible for e^- and e^+ beams respectively.

We have determined in each case the limit which can be placed at the 95% CL on a coupling contributing to the correlation of O_i using

$$|\langle O_i\rangle - \langle O_i\rangle_{\rm SM}| = f\,\frac{\sqrt{\langle O_i^2\rangle_{\rm SM} - \langle O_i\rangle_{\rm SM}^2}}{\sqrt{L\sigma_{\rm SM}}}, \tag{3.22}$$

where the subscript "SM" refers to the value in SM, and where f is 1.96 when only one coupling is assumed non-zero, and 2.45 when two couplings contribute.

The observables Y_i have vanishing expectation values in the absence of transverse polarization. As noted earlier, the differential cross section depends on transverse polarization through the product $P_T\overline{P}_T$. Hence both beams need to be polarized to observe the effects of these terms.

We have listed in Table 3.3 the results for individual limits obtained by utilizing transversely polarized beams. The most significant result is for the coupling $\text{Im}a_\gamma$. We find that the observable Y_1 can constrain $\text{Im}a_\gamma$ independent of all other couplings. This is particularly significant because Ima_γ can not be constrained with longitudinal polarization.

In the determination of $\langle Y_2 \rangle$ the numerator receives contribution only from ReΔa_Z and Rea_γ. However, the denominator at the linear order cancels the contribution of ReΔa_Z exactly and that of Rea_γ approximately, while introducing a dependence of $\langle Y_2 \rangle$ on Reb_Z and Reb_γ.

	Observable	Coupling	Limits for polarizations $P_T = 0.8$, $\overline{P}_T = \pm 0.6$
Y_1	$(q_x q_y)$	Ima_γ	1.98×10^{-1}
Y_2	$(q_x^2 - q_y^2)$	Rea_γ	8.15×10^{-1}
		Reb_Z	2.65×10^{-2}
		Reb_γ	3.41×10^{-1}
Y_3	$(p_3 - p_4)_x (p_3 - p_4)_y$	Ima_γ	9.62
		Imb_γ	4.72×10^{-2}
Y_4	$q_x q_y (p_3 - p_4)_z$	Imb_Z	1.58×10^{-1}
		Imb_γ	1.96
Y_5	$(p_3 - p_4)_x (p_3 - p_4)_y q_z$	Re$\tilde{b}_Z$	5.56×10^{-2}
		Re$\tilde{b}_\gamma$	6.89×10^{-1}
Y_6	$[(p_3)_x^2 - (p_4)_x^2] - [(p_3)_y^2 - (p_4)_y^2]$	Im$\tilde{b}_Z$	1.10×10^{-1}
		Im$\tilde{b}_\gamma$	1.36

Table 3.3: *The 95 % C.L. limits on anomalous ZZH and γZH couplings chosen nonzero one at a time from various observables with transverse polarization.*

The other observables listed in Table 3.3 do not allow limits on single couplings to be isolated. However, in each of these cases, if one assumes the couplings contributing to the expectation value to be of the same order of magnitude, then one of the couplings makes a dominant contribution to the expectation value, leading to an independent limit on that coupling. For example, Y_2, Y_3, Y_4, Y_5 and Y_6 can place independent limits on Reb_Z, Imb_γ, Imb_Z, Re$\tilde{b}_Z$ and Im$\tilde{b}_Z$, respectively.

3.2.3 Effects of kinematical cuts and change in cm energy

We employ the same cuts which we used in Chapter 2 for longitudinally polarized beams to identify the final-state particles. We find that except Y_6, for which limits on couplings change by $20-30\%$, other observables are not very sensitive to these cuts.

We also look at the effect on the sensitivity with the the change of cm energy. For this, we study the sensitivity of observables at $\sqrt{s} = 1000$ GeV and integrated luminosity of 1000 fb^{-1}. We find that observables Y_1, Y_2, Y_5 and Y_6 become less sensitive to anomalous couplings with higher cm energies while Y_4 is more sensitive to anomalous couplings at higher cm energies. Y_3 behaves differently relative to all other observables. While the limit on Ima_γ improves by about an order of magnitude, the limit on Imb_γ get worse with increase in cm energy. Thus, the naive expectation as discussed in Chapter 2 is not realized. The behaviour of sensitivities at high cm energies is non-trivial and requires more elaborate study which we have not attempted in our work.

3.2.4 Comparison with earlier works

The sensitivities on anomalous ZZH couplings with transversely polarized beams at a linear collider have been studied in Ref. [27]. The conclusion from their analysis is that transverse polarization helps to obtain limits on all anomalous ZZH couplings independent of one another. In our work, we widen this conclusion by incorporating the contribution of anomalous γZH couplings and show that transverse polarization indeed disentangles contributions of all ZZH and γZH couplings independent of one another. We find that the limits obtained in Ref. [27] are 2 to 3 times worse than that of ours. This can be attributed to the fact that they implement stringent cuts. Also, the limits obtained on anomalous couplings using transverse polarization are comparable to the ones obtained through the use of longitudinally polarized beams.

As for the case of γZH couplings, comparison with earlier work is not easy because of the different approach to parameterization of couplings. Also, there is no work dealing in transverse polarization with which we could make a comparison.

3.3 Conclusions and discussion

We have obtained angular distributions for the process $e^+e^- \to ZH \to \ell^+\ell^- H$ in the presence of anomalous γZH and ZZH couplings to linear order in these couplings in the presence of transverse beam polarizations. We find that transverse polarization probes a combination of couplings in which only one of the couplings dominates over others. In that case, it can be assumed that transverse polarization helps to determine the couplings almost independently of one another. The main advantage of transverse polarization is that it enables constraining Ima_γ which is not accessible without transverse polarization.

We have also obtained the sensitivities of these observables and asymmetries to the various couplings for a definite configuration of the linear collider. Transverse polarization enables the determination of Ima_γ independent of all other couplings, with a possible 95% CL limit of about 0.2. Independent limits on Reb_Z and Imb_γ of a few times 10^{-2} are possible, whereas those on Imb_Z, Re$\tilde{b}_Z$ and Im$\tilde{b}_Z$ would be somewhat larger, ranging upto about 0.1.

We consider only one leptonic decay mode of Z in our analysis in the Z-decay. Including both $\mu^+\mu^-$ and $\tau^+\tau^-$ modes would trivially improve the sensitivity. In case of observables like Y_1, Y_2, which do not need charge identification, even hadronic decay modes of Z can be included, which would considerably enhance the sensitivity. However considering a specific charged-lepton channel has enabled us to get a handle on Imb_γ, Imb_Z, Re$\tilde{b}_\gamma$ and Re$\tilde{b}_Z$, which were not accessible in using only Z distributions.

We have not included the decay of the Higgs boson in our analysis. For now, one could simply divide our limits by the square root of the branching ratios and detection efficiencies. Including the decay will entail some loss of efficiency.

Chapter 4

Anomalous tbW^- couplings in single-top production at the LHC

As has been discussed in Chapter 1 (Introduction), the EWSB sector of the SM is still not fully established. The top quark because of its heavy mass close to EWSB scale may play a special role in the understanding of the mechanism of EWSB. Since EWSB plays an important role in the generation of fermion masses, the effects from new physics (NP) would be more apparent in the top-quark sector than in any light-quark sector in the SM. A few examples have been discussed in Ref. [46] to illustrate that different models of EWSB mechanism will induce different interactions among the top quark and W and Z bosons. Therefore through the study of the top quark, one may eventually learn about symmetry breaking mechanism of the EW theory. The most significant consequence of the large mass of the top quark is that it decays before its hadronization and hence its spin information is preserved in its decay products. So, through the study of angular distributions of top-decay products, one can determine the degree of polarization of the top quarks in a top-quark ensemble. Different new physics models give different predictions for top polarization. Hence, top polarization may be used as a tool to study new physics involved in top production.

At the Large Hadron Collider (LHC), top quarks will be produced mainly in pairs dominantly through gluon fusion whose contribution to the cross section is 90%, while quark-antiquark annihilation contributes 10%. Both these production mechanisms proceed mainly through QCD interactions. Since gluon couplings are chirality-conserving, the polarization of top quarks can arise only through the Z-exchange contribution to $q\bar{q}$ annihilation channel, and is expected to be very small.

However, single-top production can also occur [54, 55, 56, 57, 58, 59, 60, 61, 64, 66], and has already been seen [67]. Since it proceeds via weak interactions, top quarks will have large polarization [60, 61]. At LHC energies, single-top quark events in the SM are expected to be produced via a) the t-channel ($bq \to tq'$) process, b) the s-channel process ($q\bar{q}' \to t\bar{b}$) and c) the tW associated production process ($bg \to tW^-$) [58]. In all these processes, there is at least one chiral vertex which gives rise to large top polarization. The three processes are completely different kinematically and can be separated from each other. The tW^- mode of single-top production is distinct from other two modes in the sense that it is affected by the new physics only in the tbW vertex while, in other modes, there may be exotic scalars or gauge bosons which can give additional contributions to the process. In this work, we study in detail the effect of anomalous tbW vertex on top polarization in associated production of the top quark with a W boson.

As discussed in Chapter I (Introduction), the most direct way to determine top polarization is by measuring the angular distribution of its decay products in its rest frame. However, at the LHC reconstructing the top-rest frame results in large systematic errors and loss in statistics. Our main aim in this work is to devise observables which can be measured in the lab frame and give a good estimate of top polarization and thence probe anomalous tbW couplings in single-top production. For this, we study various laboratory-frame distributions of the charged lepton and the b quark coming from top decay.

4.1 Single-top production

Single-top quark events can be produced by following mechanisms at the LHC

1. t-channel process, $bq \to tq'$ (shown in Fig. 4.1 (a)),
2. W-g fusion progess, $gq \to tbq'$ (shown in Fig. 4.1 (b)),
3. Drell-Yan type s-channel process, $q'\bar{q} \to W^* \to t\bar{b}$ (shown in Fig. 4.1 (c)),
4. tW associated production, $gb \to tW^-$ (shown in Fig. 4.2).

All these three mechanisms of single top productions are kinematically different and can be separated from each other. As can be seen from Fig. 4.1 and 4.2, in all three mechanisms of single-top production, there is at least one chiral tbW vertex which may enhance the polarization of the final state top quarks.

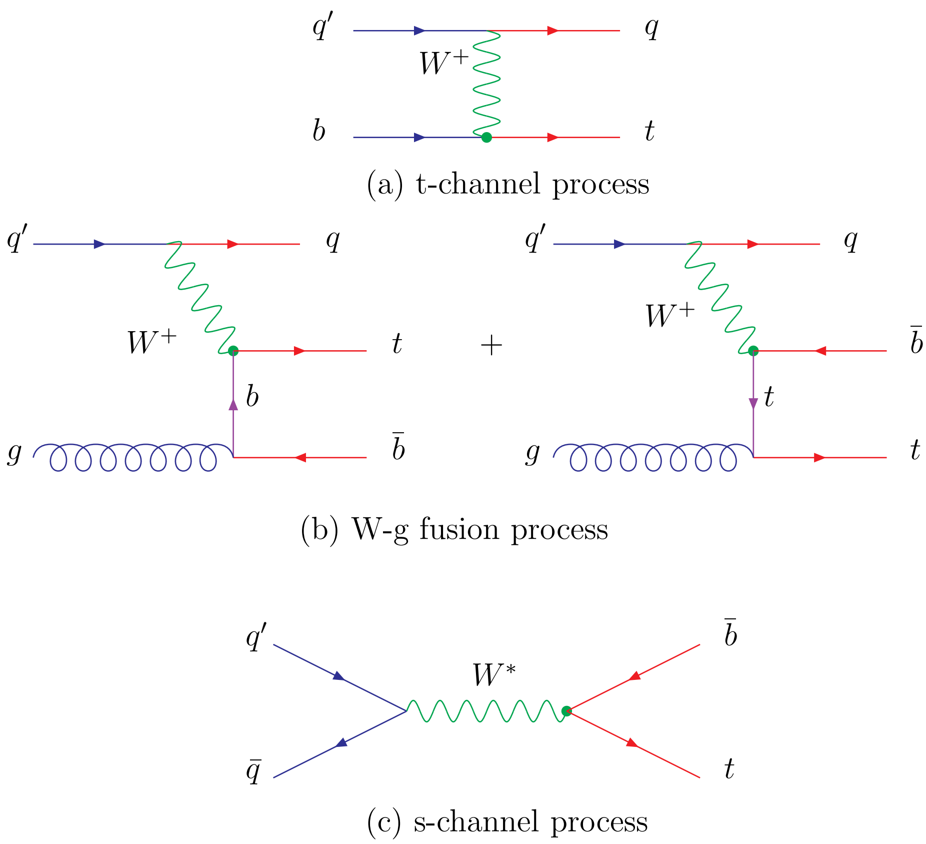

Figure 4.1: *Feynman diagrams for various single-top production processes.*

4.2 Anomalous tbW couplings

Among all top couplings to gauge and Higgs bosons, the tbW vertex deserves special attention since the top quark is expected to decay almost completely via this interaction. However, in several extensions of SM, as for example supersymmetry and models of dynamical symmetry breaking, sizable deviations are possible from the SM predictions and also new decays of top quarks are possible. These deviations of the tbW vertex may be observed in top decays. Single-top production is another source to study deviation in the tbW vertex.

For on-shell top, bottom and W, the most general effective vertices for the tbW interaction up to dimension five can be written as [68]

$$V_{t\to bW^+} = \frac{-g}{\sqrt{2}} V_{tb} \left[\gamma^\mu (\mathrm{f_{1L}} P_L + \mathrm{f_{1R}} P_R) - \frac{i\sigma^{\mu\nu}}{m_W} (p_t - p_b)_\nu (\mathrm{f_{2L}} P_L + \mathrm{f_{2R}} P_R) \right] \tag{4.1}$$

for the decay $t \to bW^+$, and

$$V_{b \to tW^-} = \frac{-g}{\sqrt{2}} V_{tb}^* \left[\gamma^\mu (\mathrm{f}_{1\mathrm{L}}^* P_L + \mathrm{f}_{1\mathrm{R}}^* P_R) - \frac{i\sigma^{\mu\nu}}{m_W} (p_t - p_b)_\nu (\mathrm{f}_{2\mathrm{R}}^* P_L + \mathrm{f}_{2\mathrm{L}}^* P_R) \right] \tag{4.2}$$

for tW^- production from a virtual b, where V_{tb} is the Cabibbo-Kobayashi-Maswkawa matrix element, and $\mathrm{f}_{1\mathrm{L}}$, $\mathrm{f}_{2\mathrm{L}}$, $\mathrm{f}_{1\mathrm{R}}$, $\mathrm{f}_{2\mathrm{R}}$ are couplings.

In the SM, $\mathrm{f}_{1\mathrm{L}} = 1$ and $\mathrm{f}_{1\mathrm{R}} = \mathrm{f}_{2\mathrm{L}} = \mathrm{f}_{2\mathrm{R}} = 0$. We have assumed all the anomalous couplings to be complex and consider real and imaginary parts of these couplings as independent parameters. We assume CP to be conserved in this analysis. Various extensions of the SM would have specific predictions for these anomalous couplings. For example, the contributions to these form factors in two Higgs doublet model (2HDM), minimal supersymmetric standard model (MSSM) and top-color assisted Technicolor model (TC2) have been evaluated in Ref. [69].

Tevatron provides the only existing direct limits on anomalous tbW couplings through W-polarization measurements. Recently, CDF II with 2.7 fb^{-1} of collected data reported results for the longitudinal and right-handed helicity fractions of the W boson in semileptonic top-decays [62]. D0 also reported results on W helicity fractions using a combination of semileptonic and dilepton decay channels [63]. These results on W-polarization measurements led to a limit of $[-0.3, 0.3]$ on $\mathrm{f}_{2\mathrm{R}}$ at the 95% confidence level (CL) [64] in single-top production. The CMS and ATLAS collaborations have also reported the W helicity fractions with early LHC data [65]. In Ref. [66], the authors have used the recent top-quark decay asymmetries from ATLAS and the t-channel single-top cross section from CMS to put the limits on tbW couplings. They find that despite the small statistics available, the early LHC limits of $[-0.6, 0.3]$ on $\mathrm{f}_{2\mathrm{R}}$ are not too far from the Tevatron limits.

Apart from direct measurements at the LHC and Tevatron, there are stringent indirect constraints coming from low-energy measurements of anomalous tbW couplings. The measured rate of $b \to s\gamma$ puts stringent constraints on the couplings $\mathrm{f}_{1\mathrm{R}}$ and $\mathrm{f}_{2\mathrm{L}}$ of about 4×10^{-3}, since their contributions to B-meson decay get an enhancement factor of m_t/m_b [70, 71, 72, 73]. The bound on the anomalous coupling $\mathrm{f}_{2\mathrm{R}}$ is very weak, $[-0.15, 0.57]$ at 95 % CL [73]. In Ref. [74], a slightly more stringent bound has been found on $\mathrm{f}_{2\mathrm{R}}$ utilizing $B_{d,s} - \bar{B}_{d,s}$ mixing. These bounds are obtained by taking one coupling to be non-zero at a time. However if one allows all couplings to be non-zero simultaneously, there is a possibility of cancellations among contributions of different couplings and the limits on these couplings could be very different.

4.3 The spin density matrix formalism for a generic top-production process

Let us consider a generic process of top production with X and subsequent semileptonic decay of t and inclusive decay of X, $AB \to tX \to b\ell^+\nu_\ell X$. Since $\Gamma_t/m_t \sim 0.008$, we can use the narrow width approximation (NWA) to write the cross section as a product of the $2 \to 2$ production cross section times the decay width of the top. However, in probing top polarization using angular distributions of the decay lepton, it is necessary to keep the top spin information in its decay arising from its production, thus requiring the spin density matrix formalism. As in [76], the amplitude squared can be factored into production and decay parts using the NWA as

$$\sum_{\text{spins}} \overline{|\mathcal{M}|^2} = \frac{\pi\delta(p_t^2 - m_t^2)}{\Gamma_t m_t} \sum_{\lambda,\lambda'} \rho(\lambda,\lambda')\Gamma(\lambda,\lambda'), \tag{4.3}$$

where $\rho(\lambda,\lambda')$ and $\Gamma(\lambda,\lambda')$ are the 2×2 top production and decay spin density matrices and $\lambda, \lambda' = \pm 1$ denote the sign of the top helicity. After phase space integration of $\rho(\lambda,\lambda')$ we get the resulting polarization density matrix $\sigma(\lambda,\lambda')$. The (1,1) and (2,2) diagonal elements of $\sigma(\lambda,\lambda')$ are the cross sections for the production of positive and negative helicity tops and $\sigma_{\rm tot} = \sigma(+,+) + \sigma(-,-)$ is the total cross section. We define the degree of *longitudinal* polarization P_t as

$$P_t = \frac{\sigma(+,+) - \sigma(-,-)}{\sigma(+,+) + \sigma(-,-)}. \tag{4.4}$$

The off-diagonal elements of $\sigma(\lambda,\lambda')$ are the production rates of the top with *transverse* polarization. We obtain the top-decay density matrix $\Gamma(\lambda,\lambda')$ for the process $t \to bW^+ \to b\ell^+\nu_\ell$ including anomalous tbW couplings and write it in a Lorentz invariant form. We find

$$\begin{aligned}
\Gamma(\pm,\pm) &= g^4\ |\Delta(p_W^2)|^2[m_t^2 - 2(p_t\cdot p_\ell)]\Big[|\mathrm{f_{1L}}|^2\Big\{(p_t\cdot p_\ell) \mp m_t(p_\ell\cdot n_3)\Big\} \\
&+ \ \mathrm{Ref_{1L}f_{2R}^*}\Big\{m_t m_W \mp \frac{m_t^2+m_W^2}{m_W}(p_\ell\cdot n_3) \mp \frac{2}{m_W}(p_b\cdot n_3)(p_t\cdot p_\ell)\Big\} \\
&+ \ \frac{|\mathrm{f_{2R}}|^2}{2}\Big\{m_W^2 + \frac{m_t^2 - 2p_t\cdot p_\ell}{2} \mp 2\left[(p_\ell\cdot n_3) + (p_b\cdot n_3)\right]\Big\}\Big],
\end{aligned} \tag{4.5}$$

for the diagonal elements and

$$\begin{aligned}
\Gamma(\mp,\pm) &= g^4\,|\Delta(p_W^2)|^2[m_t^2-2(p_t\cdot p_\ell)]\Big[|\mathrm{f}_{1\mathrm{L}}|^2\left\{-m_t[p_\ell\cdot(n_1\mp in_2)]\right\}\\
&- \mathrm{Re}\mathrm{f}_{1\mathrm{L}}\mathrm{f}_{2\mathrm{R}}^*\Big\{\frac{m_t^2+m_W^2}{m_W}[p_\ell\cdot(n_1\mp in_2)]-\frac{2}{m_W}[p_b\cdot(n_1\mp in_2)](p_t\cdot p_\ell)\Big\}\\
&- |\mathrm{f}_{2\mathrm{R}}|^2\Big\{\,[(p_\ell+p_b)\cdot(n_1\mp in_2)]\,\Big\}\Big], \qquad (4.6)
\end{aligned}$$

for the off-diagonal ones. Here $\Delta(p_W^2)$ is the W boson propagator, for which we will use the narrow-width approximations in our numerical calculations, and n_i^μ's $(i=1,2,3)$ are spin four-vectors for the top with four-momentum p_t corresponding to rest-frame spin quantization axes x, y and z respectively, with the properties $n_i\cdot n_j=-\delta_{ij}$ and $n_i\cdot p_t=0$. In the top rest frame they take the standard form $n_i^0=0$, $n_i^k=\delta_i^k$.

Using the NWA the differential cross section for top production and decay, with inclusive decay of X can be written as

$$\begin{aligned}
d\sigma &= \frac{1}{32\ \Gamma_t m_t}\,\frac{1}{(2\pi)^4}\left[\sum_{\lambda,\lambda'}d\sigma(\lambda,\lambda')\ \times\left(\frac{\Gamma(\lambda,\lambda')}{p_t\cdot p_\ell}\right)\right]E_\ell\ d\cos\theta_t\ d\cos\theta_\ell\ d\phi_\ell\\
&\times\ dE_\ell\ dp_W^2, \qquad (4.7)
\end{aligned}$$

where the lepton integration variables are in the lab frame and the b-quark energy integral is replaced by an integral over the invariant mass p_W^2 of the W boson. $d\sigma(\lambda,\lambda')$ is the differential cross section for the $2\to 2$ process of top production with indicated spin indices of the top. As shown in [76], by measuring the angular distributions of the decay lepton in the top rest frame (which requires reconstructing the top rest frame) analytic expressions for the longitudinal and transverse components of the top polarization can be obtained by a suitable combination of lepton polar and azimuthal asymmetries. However, as pointed out earlier, it would be useful and interesting to devise variables for the top-decay products in the laboratory frame, which are easily measured and are sensitive to probes of new physics responsible for top production.

4.4 Single-top production in association with a W boson

As stated earlier, single-top production at hadron colliders occurs through three different modes. All these three modes are distinct in terms of initial and final states and are in principle separately measurable. As mentioned earlier, the tW^- mode of single-top production is distinct from other two modes in the sense that it is affected by the new physics only in the tbW vertex while, in other modes, there may be exotic scalars or gauge bosons which can give additional contributions to the process. The tW^- mode of single-top production has been studied in detail in Ref. [58]. At the parton level, the tW^- production proceeds through a gluon

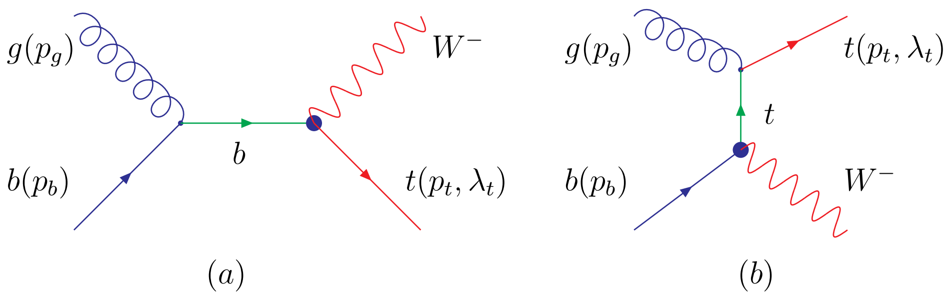

Figure 4.2: *Feynman diagrams contributing to associated tW^- production at the LHC.*

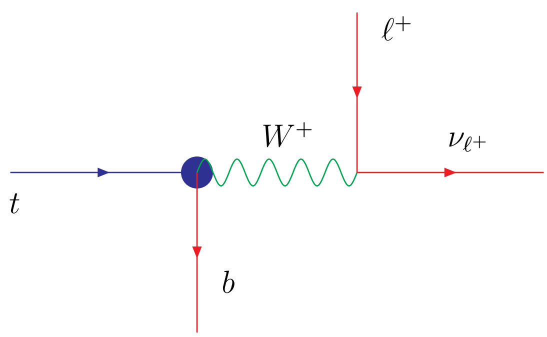

Figure 4.3: *Anomalous tbW couplings in top decay*

and a bottom quark each coming from a proton and gets contribution from two diagrams. Feynman diagrams for the process $g(p_g)b(p_b) \to t(p_t, \lambda_t)W^-$ are shown in Fig. 4.2, where $\lambda_t = \pm 1$ represent the top helicity and the blobs denote effective tbW vertices, including anomalous couplings, in the production process. These couplings are also involved in the decay of the top as shown in Fig. 4.3.

We obtain analytical expressions for the spin density matrix for tW production including anomalous couplings. Use was made of the analytic manipulation program FORM [78]. We find that at linear order, only the real part of the coupling $\mathrm{f}_{2\mathrm{R}}$ gives significant contribution to the production density matrix, whereas contributions from all other couplings are proportional to the mass of b quark (which we neglect consistently) and hence vanish in the limit of zero bottom mass. To second order in anomalous couplings, other anomalous couplings do contribute, but we focus only on $\mathrm{f}_{2\mathrm{R}}$, since its contribution, arising at linear order, is dominant. Expressions for the spin density matrix elements $\rho(\pm,\pm)$ and $\rho(\pm,\mp)$ for tW production, where $\pm$ are the signs of the top-quark helicity, are given in the Appendix III.

4.4.1 Production cross section

After integrating the density matrix given in the Appendix III over the phase space, the diagonal elements of this integrated density matrix, which we denote by $\sigma(+,+)$ and $\sigma(-,-)$, are respectively the cross sections for the production of positive and negative helicity tops and $\sigma_{\rm tot} = \sigma(+,+) + \sigma(-,-)$ is the total cross section.

For numerical calculations, we use the leading-order parton distribution function (PDF) sets of CTEQ6L [79] with a factorization scale of $m_t = 172.6$ GeV. We also evaluate the strong coupling at the same scale, $\alpha_s(m_t) = 0.1085$. We make use of the following values of other parameters: $M_W = 80.403$ GeV, the electromagnetic coupling $\alpha_{em}(m_Z) = 1/128$ and $\sin^2\theta_W = 0.23$. We set $\mathrm{f}_{1\mathrm{L}} = 1$ and $V_{tb} = 1$ in our calculations. We take only one coupling to be non-zero at a time in the analysis, except in Sec.4.7.

In Fig. 6.2, we show the cross section as a function of various anomalous tbW couplings for two different values of centre-of-mass (cm) energies of 7 TeV and 14 TeV for which the LHC is planned to operate. We show contributions of anomalous couplings to the cross section at linear order as well as without the approximation. From Fig. 4.4, one can infer that the cross section is very sensitive to negative values of $\mathrm{Ref}_{2\mathrm{R}}$. The linear approximation is seen to be good for values of anomalous coupling ranging from -0.05 to 0.05.

Since the cross section may receive large radiative corrections at the LHC, we focus on using observables like asymmetries which are ratios of some partial cross sections, and which are expected to be insensitive to such corrections.

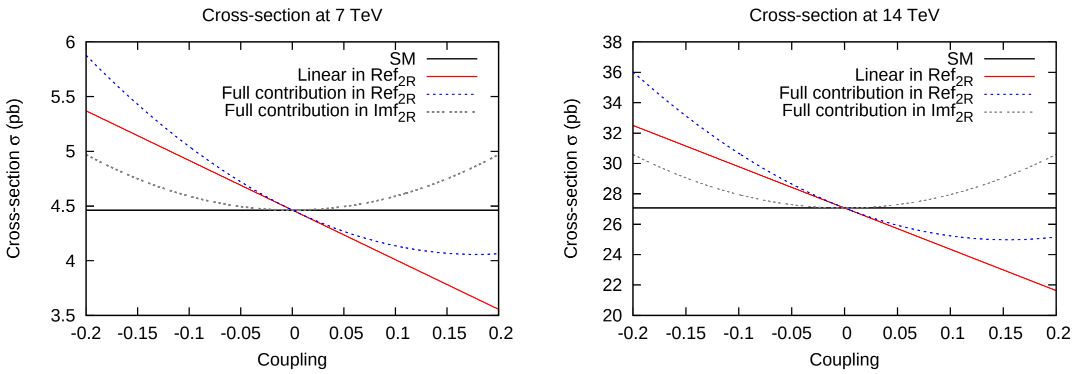

Figure 4.4: *The cross section for tW^- production at the LHC for two different cm energies, 7 TeV (left) and 14 TeV (right), as a function of anomalous tbW couplings.*

4.4.2 Top-angular distribution

The angular distribution of the top quark would be modified by anomalous couplings. Since the top quark is produced in a $2 \to 2$ process, its azimuthal distribution is flat. We can study its polar distribution with the polar angle defined with respect to either of the beam directions as the z axis. We find that the polar distribution is sensitive to anomalous tbW couplings. The normalized polar distribution

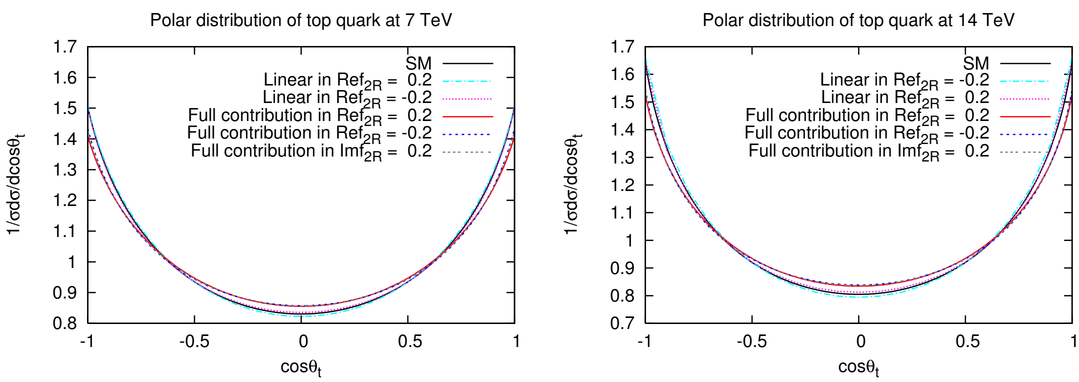

Figure 4.5: *The top-polar angular distributions for tW^- production at the LHC for two different cm energies, 7 TeV (left) and 14 TeV (right), for different anomalous tbW couplings.*

is plotted in Fig. 4.5 for cm energies 7 TeV and 14 TeV.

As can be seen from Fig. 4.5, the curves for the polar distributions for the

SM and for the anomalous couplings of magnitude 0.2 are separated from each other. The top distribution has no forward-backward asymmetry, the colliding beams being identical. However, we can define an asymmetry utilizing the polar distributions of the top quark as

$$\mathcal{A}_\theta^t = \frac{\sigma(|z| > 0.5) - \sigma(|z| < 0.5)}{\sigma(|z| > 0.5) + \sigma(|z| < 0.5)} \tag{4.8}$$

where z is $\cos\theta_t$. We plot this asymmetry as a function of anomalous tbW couplings

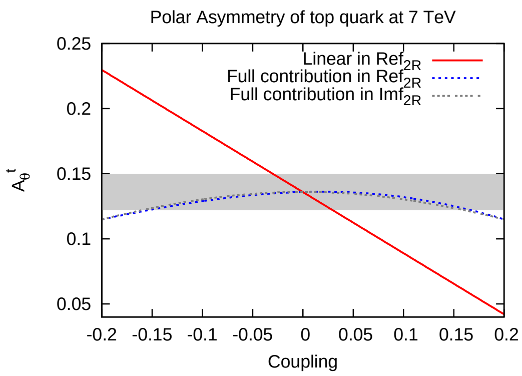

Figure 4.6: *The top polar asymmetries for tW^- production at the LHC for two different cm energies, 7 TeV (left) and 14 TeV (right), as a function of anomalous tbW couplings. The grey band corresponds to the top-polar asymmetry predicted in the SM with a 1 σ error interval.*

for two cm of energies $\sqrt{s}$ = 7 TeV and 14 TeV in Fig. 4.6. The asymmetry $\mathcal{A}_\theta^t$ requires accurate determination of the top direction in the lab frame and a quantitative estimate of its sensitivity to anomalous couplings needs details of the efficiency of reconstruction of the direction. We do not study this asymmetry any further, but proceed to a discussion of top polarization.

4.4.3 Top polarization

The degree of longitudinal polarization P_t of the top quark is given by Eqn. 4.4. This polarization asymmetry is shown in Fig. 4.7 as a function of anomalous couplings in the linear approximation, as well as without approximation, for $\sqrt{s}$ = 7 TeV and 14 TeV. As compared to the SM value of -0.256 for $\sqrt{s}$ = 14 TeV, the degree of longitudinal top polarization varies from -0.075 to -0.281 for Ref_{2R} varied over the range -0.2 to $+0.2$, while it varies from -0.139 to -0.256 for the

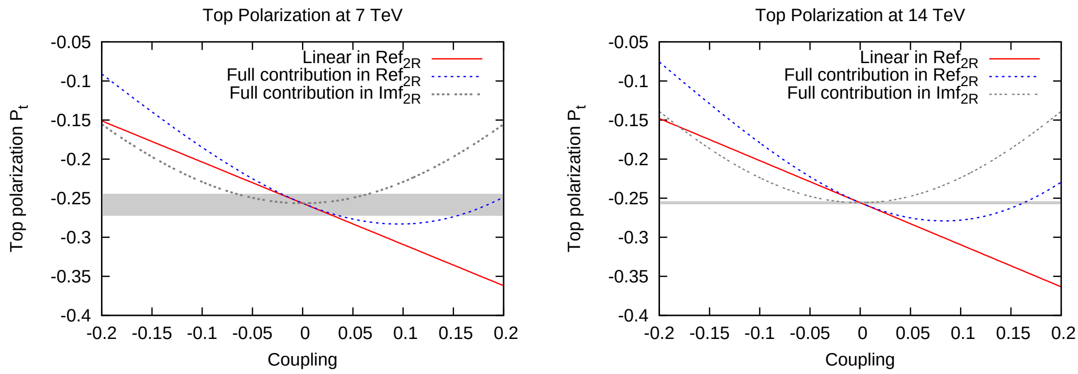

Figure 4.7: *The top polarization asymmetry for tW^- production at the LHC for two different cm energies, 7 TeV (left) and 14 TeV (right), as a function of anomalous tbW couplings. The grey band corresponds to the top-polarization asymmetry predicted in the SM with a 1 σ error interval.*

same range of $\mathrm{Im}f_{2\mathrm{R}}$, and is symmetric about $\mathrm{Im}f_{2\mathrm{R}} = 0$. We notice that just as for the total cross section, P_t is sensitive to negative values of $\mathrm{Re}f_{2\mathrm{R}}$. Also, P_t is equally sensitive to negative and positive values of $\mathrm{Im}f_{2\mathrm{R}}$. Thus P_t can be a very good probe of $\mathrm{Re}f_{2\mathrm{R}}$ and $\mathrm{Im}f_{2\mathrm{R}}$ if it can be measured at the LHC. However, the standard measurement of P_t requires reconstruction of the top-rest frame which is a difficult task, and would entail reduction in efficiency. We will therefore investigate lab-frame decay distributions for the measurement of anomalous couplings.

All the quantities considered so far, viz., the total cross section, the top polar distribution and the top polarization, can only be measured using information from the decay of the top. Both the polar distribution and the top polarization would play a role in determining the distributions of the decay products. Our main aim is to devise observables which can be measured in the lab frame and give a good estimate of top polarization and thence probe anomalous tbW couplings in single-top production. We proceed to construct such observables from kinematic variables of the charged lepton and b quark produced in the decay of the top.

4.5 Charged-lepton distributions

To preserve spin coherence while combining top production with decay, we make use of the spin density matrix formalism. Since $\Gamma_t/m_t \sim 0.008$, we can use the narrow width approximation (NWA) to write the cross section in terms of the product of the $2 \rightarrow 2$ production density matrix ρ and the decay density matrix Γ of the top as written in Eqn. 4.3. The top production spin density matrix $\rho(\lambda, \lambda')$ for process $gb \rightarrow tW^-$ is given in Appendix III. The top decay density matrix $\Gamma(\lambda, \lambda')$ for the process $t \rightarrow bW^+ \rightarrow b\ell^+\nu_\ell$ including anomalous tbW couplings is given in Eqns. 4.5 and 4.6 in a Lorentz invariant form.

The details of the factorization of the differential cross section for top production followed by its decay in a generic production process into production and decay parts has been elaborated earlier (See [76] for full details). We use the NWA for single-top production and its decay to write the partial cross section in the parton cm of frame as

$$\begin{aligned} d\sigma &= \frac{1}{32(2\pi)^4 \Gamma_t m_t} \int \left[\sum_{\lambda,\lambda'} \frac{d\sigma(\lambda,\lambda')}{d\cos\theta_t} \left(\frac{\langle \Gamma(\lambda,\lambda') \rangle}{p_t \cdot p_\ell} \right) \right] d\cos\theta_t \; d\cos\theta_\ell \; d\phi_\ell \\ &\times \; E_\ell dE_\ell \; dp_W^2, \end{aligned} \tag{4.9}$$

where the b-quark energy integral is replaced by an integral over the invariant mass p_W^2 of the W boson, its polar-angle integral is carried out using the Dirac delta function of Eqn. 4.3, and the average over its azimuthal angle is denoted by the angular brackets. $d\sigma(\lambda, \lambda')/d\cos\theta_t$ is proportional to $\rho(\lambda, \lambda')$, with the normalization chosen so that $d\sigma(\lambda, \lambda)/d\cos\theta_t$ is the differential cross section for the $2 \rightarrow 2$ process of tW^- production with helicity index λ of the top.

4.5.1 Angular distributions of charged leptons

We evaluate top decay in the rest frame of the top quark with the z axis as the spin quantization axis, which would also be the direction of the boost required to go to the parton cm frame. In the rest frame of the top quark, the diagonal and off-diagonal elements of decay density matrix, after averaging over the azimuthal angle of b quark w.r.t. the plane of top and lepton momenta, are given by

$$\begin{aligned}
\langle\Gamma(\pm,\pm)\rangle &= g^4 m_t E_\ell^0 |\Delta_W(p_W^2)|^2 (m_t^2 - 2p_t\cdot p_\ell)\left[\left\{|\mathrm{f_{1L}}|^2 + \mathrm{Re} \mathrm{f_{1L}}\mathrm{f_{2R}^*}\frac{m_t\, m_W}{p_t\cdot p_\ell}\right\}\right. \\
&\times\ (1\pm\cos\theta_\ell^0) - |\mathrm{f_{2R}}|^2\left(1-\frac{m_t^2+m_W^2}{2p_t\cdot p_\ell}\right)(1\mp\cos\theta_\ell^0) \\
&\pm\ \left.|\mathrm{f_{2R}}|^2\frac{m_W^2 m_t^2}{2(p_t\cdot p_\ell)^2}\cos\theta_\ell^0\right], \qquad (4.10)\\
\langle\Gamma(\pm,\mp)\rangle &= g^4 m_t E_\ell^0 |\Delta_W(p_W^2)|^2 (m_t^2 - 2p_t\cdot p_\ell)\sin\theta_\ell^0 e^{\pm i\phi_\ell^0}\left[|\mathrm{f_{1L}}|^2\right. \\
&+\ \left.\mathrm{Re}\mathrm{f_{1L}}\mathrm{f_{2R}^*}\frac{m_t\, m_W}{p_t\cdot p_\ell} + |\mathrm{f_{2R}}|^2\left\{1-\frac{m_t^2+m_W^2}{2p_t\cdot p_\ell}+\frac{m_W^2 m_t^2}{2(p_t\cdot p_\ell)^2}\right\}\right], \qquad (4.11)
\end{aligned}$$

where this averaging over the azimuthal angle of the b quark is most conveniently carried out in a coordinate system defined with the z axis along the lepton momentum direction.

In the limit of small anomalous coupling $\mathrm{f_{2R}}$, we see from Eqs. 4.10 and 4.11 that if we drop quadratic terms in $\mathrm{f_{2R}}$, $\langle\Gamma(\lambda,\lambda')\rangle$ factorizes into a pure angular part $\mathcal{A}(\lambda,\lambda')$, which depends on helicities, and a lepton-energy dependent part which does not depend on the helicities, where

$$\mathcal{A}(\pm,\pm) = (1\pm\cos\theta_\ell^0), \quad \mathcal{A}(\pm,\mp) = \sin\theta_\ell^0 e^{\pm i\phi_\ell^0}. \qquad (4.12)$$

The factorization of $\langle\Gamma(\lambda,\lambda')\rangle$ into $\mathcal{A}(\lambda,\lambda')$ and a helicity-independent part in the rest frame of the top quark implies that since the corrections from anomalous couplings reside in the helicity-independent part, they are identical to those of the total width appearing in the denominator of the angular distribution, and cancel. This leads to the result of [75, 76] that the energy averaged lepton angular distributions are insensitive to the new physics in top-quark decay in any top production process.

We study the angular distribution of the charged lepton in the lab frame both in the linear approximation of the anomalous couplings as well as with full contributions of the anomalous couplings without approximation.

We first obtain the angular distribution of the charged lepton in the parton cm frame, by integrating over the lepton energy, with limits given by $m_W^2 < 2(p_t\cdot p_\ell) < m_t^2$. This integral can be done analytically, giving the following expression for the

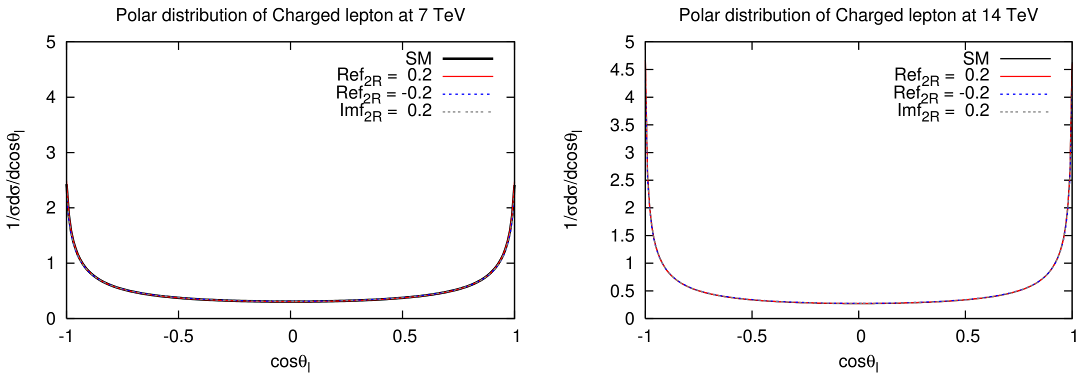

Figure 4.8: *The normalized polar distribution of the charged lepton in tW^- production at the LHC for two different cm energies, 7 TeV (left) and 14 TeV (right), for different anomalous tbW couplings.*

differential cross section in the parton cm frame:

$$\begin{aligned}\frac{d\sigma}{d\cos\theta_t\ d\cos\theta_\ell\ d\phi_\ell} &= \frac{1}{32\ \Gamma_t m_t}\ \frac{1}{(2\pi)^4}\int\left[\sum_{\lambda,\lambda'}\frac{d\sigma(\lambda,\lambda')}{d\cos\theta_t}g^4\mathcal{A}'(\lambda,\lambda')\right]\\ &\times\ |\Delta(p_W^2)|^2 dp_W^2,\end{aligned}\tag{4.13}$$

where

$$\begin{aligned}\mathcal{A}'(\pm,\pm) &= \frac{m_t^6}{24(1-\beta_t\cos\theta_{t\ell})^3E_t^2}\Big[(1-r^2)^2\big\{(1\pm\cos\theta_{t\ell})(1\mp\beta_t)\\ &\times\ \big[|\mathrm{f_{1L}}|^2(1+2r^2)+6r\mathrm{Ref_{1L}f_{2R}^*}\big]\\ &+\ |\mathrm{f_{2R}}|^2(2+r^2)(1\mp\cos\theta_{t\ell})(1\pm\beta_t)\big\}\\ &\mp\ 12r^2|\mathrm{f_{2R}}|^2\left(1-r^2+2\log r\right)(\cos\theta_{t\ell}-\beta_t)\Big],\qquad (4.14)\\ \mathcal{A}'(\pm,\mp) &= \frac{m_t^7}{24(1-\beta_t\cos\theta_{t\ell})^3E_t^3}\sin\theta_{t\ell}e^{\pm i\phi_\ell}\Big[(1-r^2)^2\big\{|\mathrm{f_{1L}}|^2(1+2r^2)\\ &+\ 6r\ \mathrm{Ref_{1L}f_{2R}^*}-|\mathrm{f_{2R}}|^2(2+r^2)\big\}-12r^2\ |\mathrm{f_{2R}}|^2\left(1-r^2+2\log r\right)\Big].\end{aligned}$$

Here $r=m_W/m_t$ and $\cos\theta_{t\ell}$ is the angle between the top quark and the charged lepton from the top decay in the parton cm frame, given by

$$\cos\theta_{t\ell}=\cos\theta_t\cos\theta_\ell+\sin\theta_t\sin\theta_\ell\cos\phi_\ell,\tag{4.15}$$

where θ_ℓ and ϕ_ℓ are the lepton polar and azimuthal angles. In the lab frame, the lepton polar angle is defined w.r.t. either of the beam direction and the azimuthal angle is defined with respect to the top-production plane chosen as the x-z plane, with beam direction as the z axis and the convention that the x component of the top momentum is positive. At the LHC, which is a symmetric collider, it is not possible to define a positive direction of the z axis. Hence lepton angular distribution is symmetric under interchange of θ_ℓ and $\pi - \theta_\ell$ as well as of ϕ_ℓ and $2\pi - \phi_\ell$. The lab frame expression for the differential cross section is obtained from Eq. 4.13 by an appropriate Lorentz transformation and integration over the parton densities.

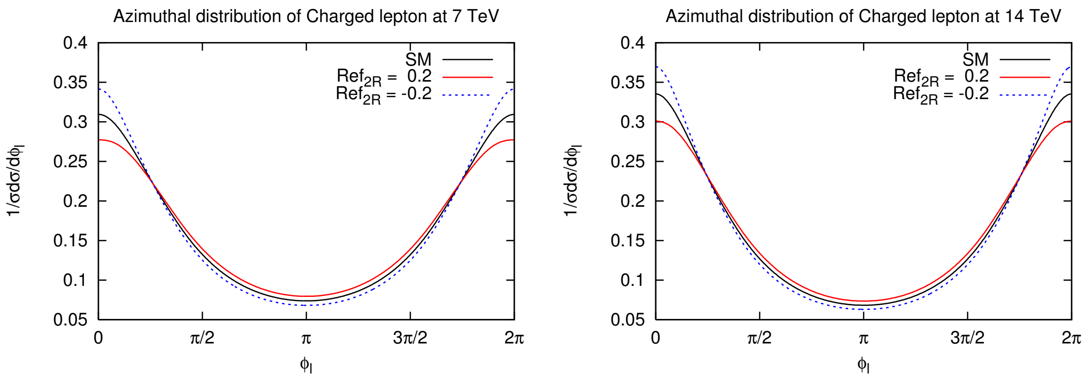

Figure 4.9: *The normalized azimuthal distribution of the charged lepton in tW^- production at the LHC for two different cm energies, 7 TeV (left) and 14 TeV (right), for different anomalous tbW couplings in the linear approximation.* $\mathrm{Imf_{2R}}$ *does not contribute in the linear order.*

We first look at the polar distribution of the charged lepton and the effect on it of anomalous tbW couplings. As can be seen from Fig. 4.8, where we plot the polar distribution for two cm of the LHC energies $\sqrt{s}$ = 7 TeV and 14 TeV, the normalized distributions are insensitive to anomalous tbW couplings.

We next look at the contributions of anomalous couplings to the azimuthal distribution of the charged lepton. In Fig. 4.9, we show the normalized azimuthal distribution of the charged lepton in a linear approximation of the couplings for $\sqrt{s} = 7$ TeV and 14 TeV for different values of $\mathrm{Ref_{2R}}$. At linear order, contributions of all other couplings vanish in the limit of vanishing bottom mass. In Fig. 4.10, we show the normalized azimuthal distribution of the charged lepton including higher-order terms in the couplings for $\sqrt{s}$ = 7 TeV and 14 TeV for different values of $\mathrm{Ref_{2R}}$ and $\mathrm{Imf_{2R}}$. We see that the curves for real and imaginary parts of the anomalous coupling $\mathrm{f_{2R}}$ peak near $\phi_\ell = 0$ and $\phi_\ell = 2\pi$. The curves are

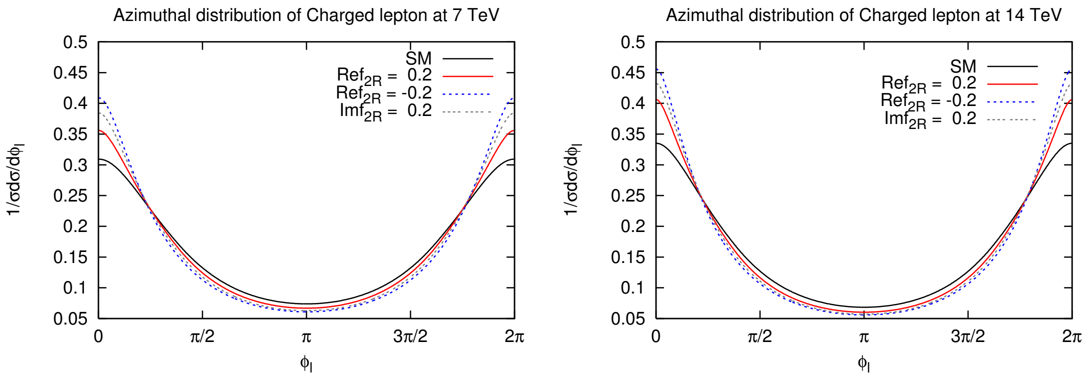

Figure 4.10: *The normalized azimuthal distribution of the charged lepton in tW^- production at the LHC for two different cm energies, 7 TeV (left) and 14 TeV (right), for different anomalous tbW couplings without the linear approximation*

well separated at the peaks for the chosen values of the anomalous tbW couplings and are also well separated from the curve for the SM. We define an azimuthal asymmetry for the lepton to quantify these differences in the distributions by

$$A_\phi = \frac{\sigma(\cos\phi_\ell > 0) - \sigma(\cos\phi_\ell < 0)}{\sigma(\cos\phi_\ell > 0) + \sigma(\cos\phi_\ell < 0)}, \tag{4.16}$$

where the denominator is the total cross section. Plots of A_ϕ as a function of the

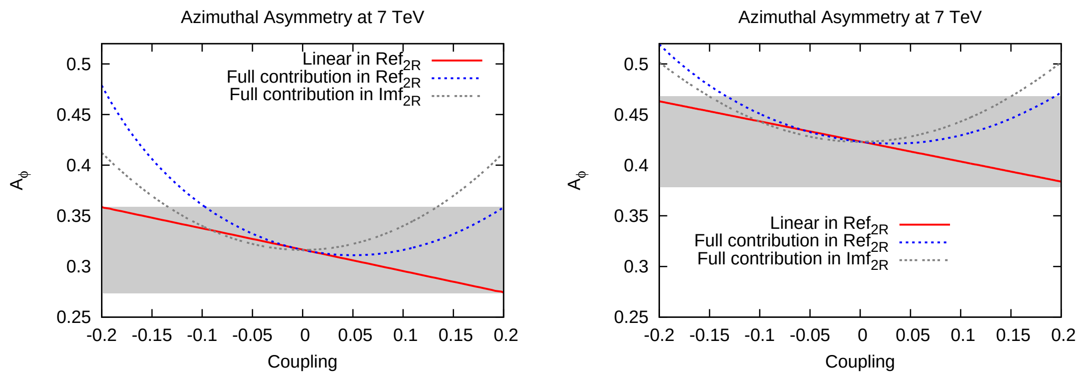

Figure 4.11: *The azimuthal asymmetries of the charged lepton in tW^- production at the LHC for cm energy 7 TeV without lepton cuts (left) and with cuts (right), as a function of anomalous tbW couplings. The grey band corresponds to the azimuthal asymmetry predicted in the SM with 1 σ error interval.*

couplings with and without cuts on the lepton momenta are shown in Fig. 4.11 for a cm energy of 7 TeV. In the former case, the rapidity and transverse momentum acceptance cuts on the decay lepton that we have used are $|\eta| < 2.5$, $p_T^\ell > 20$ GeV. The corresponding plots at $\sqrt{s}$ =14 TeV with and without lepton cuts are

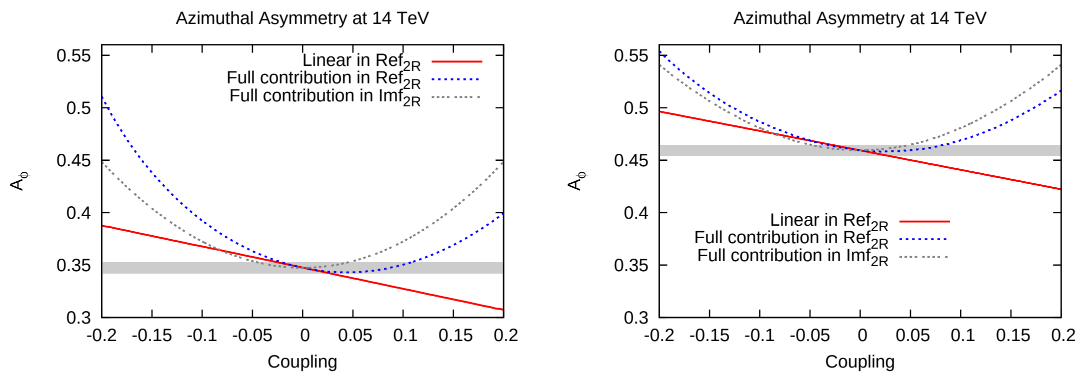

Figure 4.12: *The azimuthal asymmetries of the charged lepton in tW^- production at the LHC for cm energy 14 TeV without lepton cuts (left) and with cuts (right), as a function of anomalous tbW couplings. The grey band corresponds to the azimuthal asymmetry predicted in the SM with a 1σ error interval.*

shown in the Fig. 4.12. The lepton cuts increase the value of A_ϕ for the SM from 0.35 to around 0.45, and also increase A_ϕ substantially with anomalous couplings included. However, the cuts result in the reduction of signal events and from the Figs. 4.11 and 6.7, we see that these cuts actually decrease the sensitivity to anomalous couplings.

The azimuthal distribution depends both on top polarization and on a kinematic effect. According to Eqn. 1.66, the decay lepton is emitted preferentially along the top spin direction in the top rest frame, with $\kappa_f = 1$. The corresponding distributions in the parton cm frame are given by Eqn. 4.13 with the angular parts described by Eqs. 4.14 and 4.15. The rest-frame forward (backward) peak corresponds to a peak for $\cos\theta_{t\ell} = \pm 1$, as seen from the factor $(1 \pm \cos\theta_{t\ell})$ in the numerator of Eqn. 4.14. This is the effect of polarization. The kinematic effect is seen in the factor $(1 - \beta_t \cos\theta_{t\ell})^3$ in the denominator of Eqns. 4.14 and 4.15, which again gives rise to peaking for large $\cos\theta_{t\ell}$. Eqn. 4.15 therefore implies peaking for small ϕ_ℓ. This is borne out by the numerical results.

4.5.2 Energy distribution of charged leptons

We now study the energy distribution $d\sigma/dE_\ell$ of charged leptons to probe anomalous tbW couplings in single-top production and decay. In the rest frame of the top quark, the E_ℓ distribution of the decay density matrix $\Gamma(\lambda, \lambda')$ depends only on the combination of helicities, (λ, λ'). To linear order in the couplings, only the angular part of $\Gamma(\lambda, \lambda')$ depends on the helicities, and the energy dependence is the same for all helicity combinations, and is determined by the effective couplings occurring in decay. However, there is a weak dependence on the production differential cross section introduced because the boost to the parton cm frame is determined by $\theta_{t\ell}$. Thus, the E_ℓ distribution arises mainly from the decay process, and depends only weakly on the polarization.

We plot in Fig. 4.13 the E_ℓ distribution for $\sqrt{s} = 7$ and 14 TeV. We see

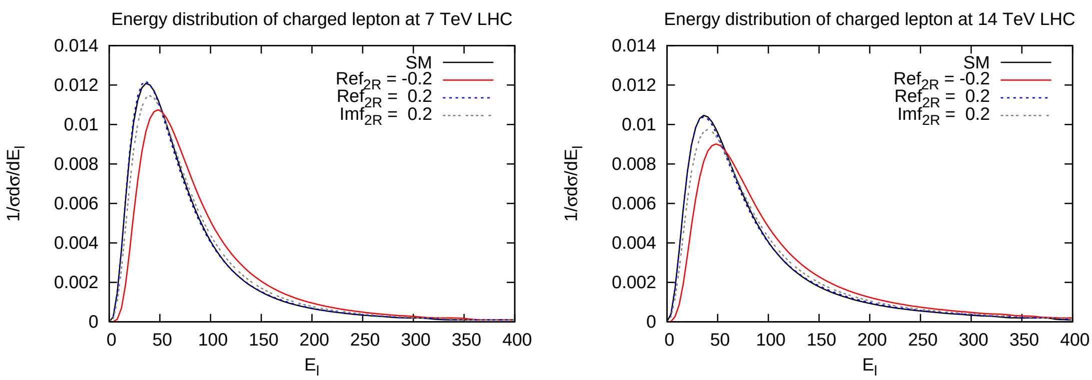

Figure 4.13: *The energy distribution of the charged lepton in tW^- production at the LHC for cm energies 7 TeV (left) TeV and 14 TeV (right) for different anomalous tbW couplings.*

that the distribution is peaked at low values of E_ℓ around 40-45 GeV, and all curves intersect at a particular value of $E_\ell \approx 62$ GeV. We also observe that the E_ℓ distribution is mainly sensitive to $\mathrm{Re}f_{2\mathrm{R}}$.

As seen from Fig. 4.13, the E_ℓ distribution is very sensitive to negative values of $\mathrm{Re}f_{2\mathrm{R}}$ and shows little sensitivity for positive values. The E_ℓ distribution at 7 TeV is peaked slightly more as compared to that for 14 TeV LHC, though the position of the peak for both is about the same.

The curves for the E_ℓ distribution for anomalous tbW couplings of ±0.2 and the SM are well separated from each other and intersect at $E_\ell^C = 62$ GeV. To quantify this difference and to make better use of statistics, we construct an asymmetry around the intersection point of the curves, defined by

$$A_{E_\ell} = \frac{\sigma(E_\ell < E_\ell^C) - \sigma(E_\ell > E_\ell^C)}{\sigma(E_\ell < E_\ell^C) + \sigma(E_\ell > E_\ell^C)}, \tag{4.17}$$

where the denominator is the total cross section. Plots for A_{E_ℓ} as a function the

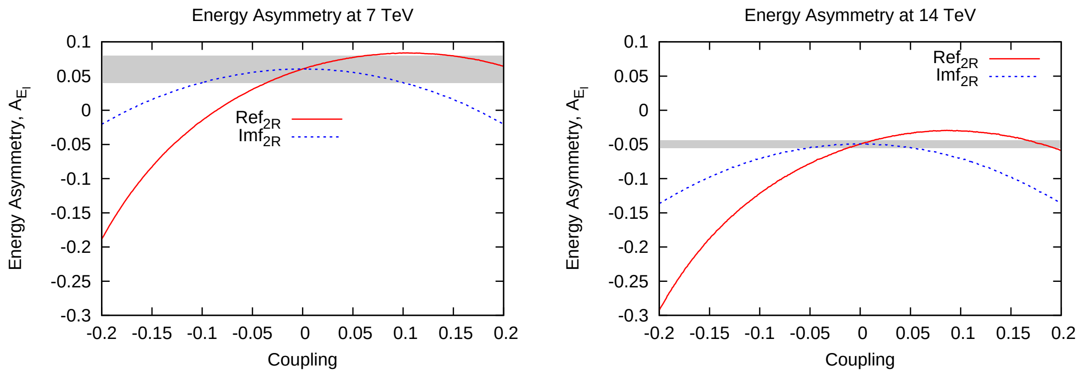

Figure 4.14: *The energy asymmetry of the charged lepton in tW^- production at the LHC for cm energy 14 TeV without lepton cuts (left) and with cuts (right), as a function of anomalous tbW couplings. The grey band corresponds to the energy asymmetry predicted in the SM with a 1σ error interval.*

coupling are shown in Fig. 4.14 for two cm energies of 7 TeV and 14 TeV. We can see from the figure that A_{E_ℓ} is very sensitive to $\text{Re}f_{2\text{R}}$ and hence can be a sensitive probe of this coupling. It is also seen from the figure that the A_{E_ℓ} for the SM is positive for $\sqrt{s} = 7$ TeV, but negative for $\sqrt{s} = 14$ TeV. This is in accordance with a sharper peaking of the energy distribution in the former case. Another difference between the asymmetries for the two cm energies is that A_{E_ℓ} changes sign with the sign for some value of $\text{Re}f_{2\text{R}}$ in case of $\sqrt{s} = 7$ TeV, but remains negative in case of $\sqrt{s} = 14$ TeV.

4.6 Angular distribution of b quarks

Although the charged-lepton azimuthal distribution provides a neat way to probe top polarization independent of new physics in the top-decay vertex, it suffers from low branching ratio of W and hence low number of events for the analysis. This situation can be improved upon by using b-quark angular distributions, without restricting only to the leptonic decays of the W coming from top decay, and thus utilizing all the single-top events. We thus assume, for purposes of this section, that the top quark can be identified in hadronic and semi-leptonic decays with sufficiently good efficiency to enable measurement of b-quark distribution in all of them.

As described earlier, we use NWA to factorize the full process into single-top production and top decay. Similar to Eqn. 4.7, we can write the full differential cross section for the process $g(p_g)b(p_b) \to t(p_t, \lambda_t)W^-$ followed by $t(p_t, \lambda_t) \to b(p'_b)W^+$ as

$$\begin{aligned} \frac{d\sigma}{d\cos_{\theta_t}\, d\Omega_b} &= \frac{1}{128(2\pi)^3 \hat{s}^{3/2}} \frac{|\overrightarrow{p_t}|}{\Gamma_t m_t} \frac{(m_t^2 - m_W^2)}{E_t^2(1-\beta_t \cos\theta_{bt})^2} \\ &\times \sum_{\lambda_t, \lambda'_t} \left[\rho(\lambda_t, \lambda'_t)\, \Gamma(\lambda_t, \lambda'_t)\right], \end{aligned} \tag{4.18}$$

where the polar angle θ_t of the top quark, and the polar and azimuthal angles θ_b and ϕ_b of the b quark produced in top decay, are measured with respect to the parton direction as the z axis, and with the xz plane defined as the plane containing the top momentum. θ_{bt} is the angle between the top momentum and the momentum of the decay b quark.

The density matrix for single-top production $\rho(\lambda_t, \lambda'_t)$ appearing in Eqn. 4.18 is given in the Appendix III. The decay density matrix for $t \to bW$ in the top-quark rest frame is given by [1]

$$\Gamma(\pm,\pm) = \frac{g^2 m_t^2}{2}\left[\mathcal{C}_1 \pm \mathcal{C}_2 \cos\theta_b^0\right], \tag{4.19}$$

$$\Gamma(\pm,\mp) = \frac{g^2 m_t^2}{2}\left[\mathcal{C}_2 \sin\theta_b^0 e^{\pm\phi_b^0}\right], \tag{4.20}$$

where

$$\mathcal{C}_1 = \frac{1}{2r^2}(1-r^2)\left[|\mathrm{f_{1L}}|^2(2r^2+1) + \mathrm{Ref_{1L}f_{2R}^*}\, 6r + |\mathrm{f_{2R}}|^2(2+r^2)\right], \tag{4.21}$$

$$\mathcal{C}_2 = \frac{1}{2r^2}(1-r^2)\left[|\mathrm{f_{1L}}|^2(2r^2-1) + \mathrm{Ref_{1L}f_{2R}^*}\, 2r + |\mathrm{f_{2R}}|^2(2-r^2)\right]. \tag{4.22}$$

The rest frame polar and azimuthal angles of the b, respectively θ_b^0 and ϕ_b^0, may be expressed in terms of the parton cm frame angles in a straightforward way.

Plots for the azimuthal distribution of the b quark for different values of anomalous couplings $\mathrm{Ref_{2R}}$ and $\mathrm{Imf_{2R}}$ are shown in Fig. 4.15. The curves for values ± 0.2

[1] The expressions for charged-lepton and b-quark angular distributions agree with those given in Ref. [83]

of these couplings are well separated from each other and from the SM curve. In the azimuthal distribution of the b quark, we get dependence on anomalous couplings both from production as well as decay. We find that the contributions from production and from decay come with opposite signs, partially cancelling each other.

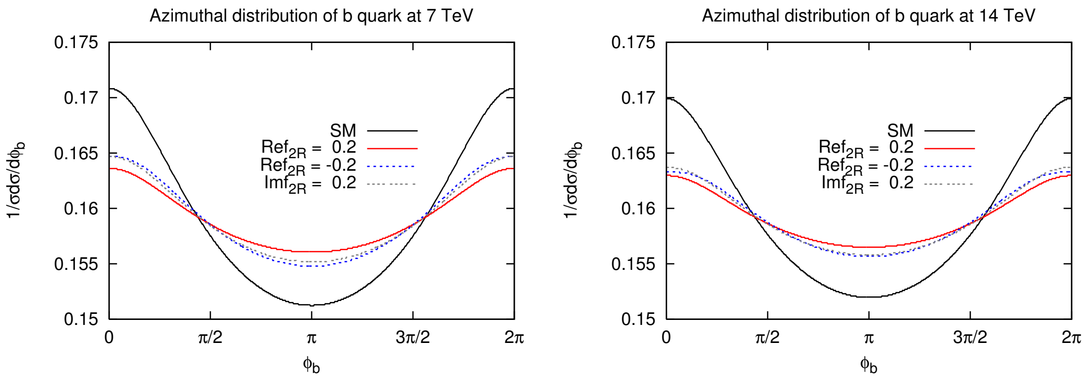

Figure 4.15: *The azimuthal distribution of the b quark in tW^- production at the LHC for cm energies 7 TeV and 14 TeV for different anomalous tbW couplings.*

To study the sensitivity and make the best use of azimuthal b-quark distribution, we construct an asymmetry A_b :

$$A_b = \frac{\sigma(\cos\phi_b > 0) - \sigma(\cos\phi_b < 0)}{\sigma(\cos\phi_b > 0) + \sigma(\cos\phi_b < 0)}. \tag{4.23}$$

The asymmetry A_b is plotted in Fig. 4.16 as a function of anomalous couplings for the cm energies $\sqrt{s} = 7$ TeV and 14 TeV. From the figure it is clear that A_b shows less sensitivity to couplings $\text{Ref}_{2\text{R}}$ and $\text{Imf}_{2\text{R}}$ as compared to other asymmetries. As stated earlier, this is due to the fact that the contributions of anomalous couplings to the asymmetry from the production and the decay are of opposite in sign and hence tend to cancel each other.

4.7 Sensitivity analysis for anomalous tbW couplings

We now study the sensitivities of the observables discussed in the previous sections to the anomalous tbW couplings at the LHC running at two cm of energies viz.,

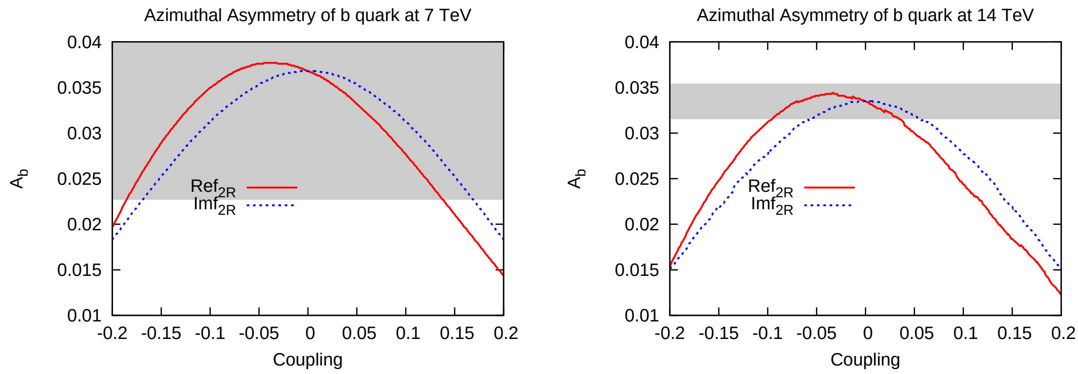

Figure 4.16: *The azimuthal asymmetry of the b quark in tW^- production at the LHC for cm energies 7 TeV and 14 TeV as a function of anomalous tbW couplings. The grey band corresponds to the asymmetry predicted in the SM with a 1σ error interval.*

7 TeV and 14 TeV, with integrated luminosities 1 fb^{-1} and 10 fb^{-1}, respectively. To obtain the 1σ limit on the anomalous tbW couplings from a measurement of an observable, we find those values of the couplings for which observable deviates by 1σ from its SM value. The statistical uncertainty σ_i in the measurement of any generic asymmetry $\mathcal{A}_i$ is given by

$$\sigma_i = \sqrt{\frac{1 - (\mathcal{A}_i^{SM})^2}{\mathcal{N}}}, \tag{4.24}$$

where $\mathcal{A}_i^{SM}$ is the asymmetry predicted in the SM and $\mathcal{N}$ is the total number of events predicted in the SM. We apply this to the various asymmetries we have discussed. In case of the top polarization asymmetry, the limits are obtained on the assumption that the polarization can be measured with 100% accuracy.

The 1σ limits on Ref$_{2R}$ and Imf$_{2R}$ are given in Table 4.1 where we assume only one anomalous coupling to be non-zero at a time. We have also assumed measurements on a tW^- final state. Including the $\bar{t}W^+$ final state will improve the limits by a factor of $\sqrt{2}$. In case of the lepton distributions, we take into account only one leptonic channel. Again, including other leptonic decays of the top would improve the limits further. The limits corresponding to a linear approximation in the couplings are denoted by the label "lin. approx.". Apart from the 1σ limits shown in Table 4.1, which correspond to intervals which include zero value of the coupling, there are other disjoint intervals which could be ruled out by null if no deviation from the SM is observed for P_t and A_{E_ℓ}. This is apparent from Figs.

4.7 and 4.14. The additional allowed intervals for $\mathrm{Ref_{2R}}$ from P_t measurement are [0.158, 0.205] and [0.160, 0.167] for cm energies of 7 TeV and 14 TeV, respectively. The corresponding intervals for A_{E_ℓ} are [0.147, 0.285] and [0.175, 0.185] [2].

	7 TeV		14 TeV	
Observable	$\mathrm{Ref_{2R}}$	$\mathrm{Imf_{2R}}$	$\mathrm{Ref_{2R}}$	$\mathrm{Imf_{2R}}$
P_t	[−0.025, 0.032]	[−0.072, 0.072]	[−0.004, 0.004]	[−0.034, 0.034]
P_t (lin. approx.)	[−0.027, 0.027]	–	[−0.004, 0.004]	–
A_ϕ	[−0.133, 0.194]	[−0.150,0.150]	[−0.034, 0.086]	[−0.050, 0.050]
A_ϕ (lin. approx.)	[−0.204, 0.204]	–	[−0.030, 0.030]	–
A_b	[−0.191, 0.147]	[−0.177, 0.177]	[−0.096, 0.035]	[−0.059, 0.059]
A_{E_ℓ}	[−0.044, 0.073]	[−0.114, 0.114]	[−0.006, 0.009]	[−0.038, 0.038]

Table 4.1: *Individual limits on real and imaginary parts of anomalous coupling* $\mathrm{f_{2R}}$ *which may be obtained by the measurement of the observables shown in the first column of the table at two cm of energies viz., 7 TeV and 14 TeV with integrated luminosities of 1* fb^{-1} *and 10* fb^{-1} *respectively. A dash "–" indicates that no limits are possible.*

It is seen that the azimuthal asymmetry A_ϕ and the energy asymmetry A_{E_ℓ} of the charged lepton are more sensitive to negative values of the anomalous couplings $\mathrm{Ref_{2R}}$. A_{E_ℓ} is the most sensitive of the asymmetries we consider. In fact, the sensitivity of A_{E_ℓ} to $\mathrm{Ref_{2R}}$ and $\mathrm{Imf_{2R}}$ is comparable to the sensitivity of top polarization to the same couplings, despite the fact that only one leptonic decay channel, with a branching fraction of about 1/9, is considered for A_{E_ℓ}. The additional contribution to A_{E_ℓ} of the $\mathrm{f_{2R}}$ coupling through the top decay channel seems to compensate for the low branching fraction. A_b is seen to have the lowest sensitivity, where there is partial cancellation of contributions to the asymmetry from production and from decay.

We also obtain simultaneous limits (taking both $\mathrm{Ref_{2R}}$ and $\mathrm{Imf_{2R}}$ non-zero simultaneously) on these anomalous couplings that may be obtained by combining the measurements of all observables. For this, we perform a χ^2 analysis to fit all the observables to within $f\sigma$ of statistical errors in the measurement of the observable. We define the following χ^2 function

$$\chi^2 = \sum_{i=1}^{n} \left(\frac{P_i - O_i}{\sigma_i} \right)^2 , \tag{4.25}$$

[2] [a, b] denotes the allowed values of the coupling f at the 1σ level, satisfying $a < f < b$.

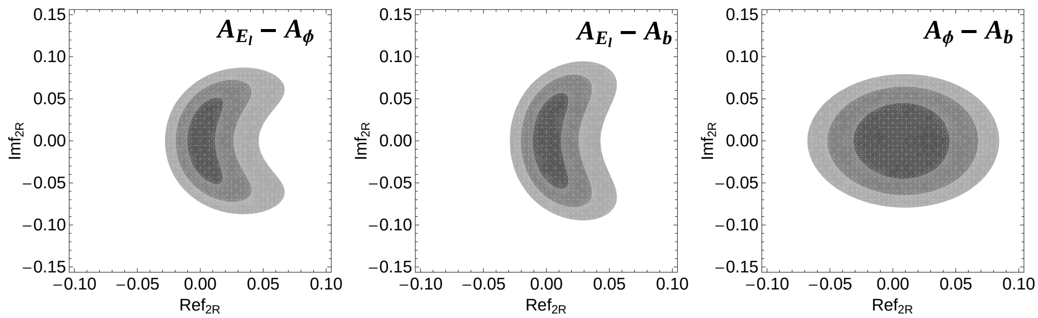

Figure 4.17: *The 1σ (central region), 2σ (middle region) and 3σ (outer region) CL regions in the* Ref_{2R}-Imf_{2R} *plane allowed by the combined measurement of two observables at a time. The left, centre and right plots correspond to measurements of the combinations* A_{E_ℓ}-A_ϕ, A_{E_ℓ}-A_b *and* A_ϕ-A_b *respectively. The* χ^2 *values for 1σ, 2σ and 3σ CL intervals are 2.30, 6.18 and 11.83 respectively for 2 parameters in the fit.*

where the sum runs over the n observables measured and f is the degree of the confidence interval. P_i's are the values of the observables obtained by taking both anomalous couplings non-zero (and are functions of the couplings Ref_{2R} and Imf_{2R}) and O_i's are the values of the observables obtained in the SM. σ_i's are the statistical fluctuations in the measurement of the observables, given in Eqn. 4.24.

In Fig. 4.17, we show the 1σ, 2σ and 3σ regions in Ref_{2R}-Imf_{2R} plane allowed by combined measurement of asymmetries A_{E_ℓ}, A_ϕ and A_b taken two at a time. For this, in the χ^2 function of Eqn. 4.25, we have taken only two of the three observables at a time. From among the three combinations shown in Fig. 4.17, we find that the strongest simultaneous limits come from the combined measurement of A_{E_ℓ} and A_ϕ, viz., $[-0.01, 0.02]$ on Ref_{2R} and $[-0.05, 0.05]$ on Imf_{2R}, at the 1σ level.

In Fig. 4.18, we show the 1σ, 2σ and 3σ regions in Ref_{2R}-Imf_{2R} plane allowed by combined measurement of all three asymmetries A_{E_ℓ}, A_ϕ and A_b simultaneously. We find that the combined measurement of all the observables provide the most stringent simultaneous limits on Ref_{2R} and Imf_{2R} of $[-0.010, 0.015]$ and $[-0.04, 0.04]$ respectively at 1σ. We find that the energy asymmetry A_{E_ℓ} plays a crucial role in determining the combined limits.

We now compare our results with those of other works on the determination of anomalous *tbW* couplings at the LHC. Refs. [57, 82, 83, 84, 59, 60, 66], have studied single-top production at the LHC in the context of anomalous *tbW* couplings.

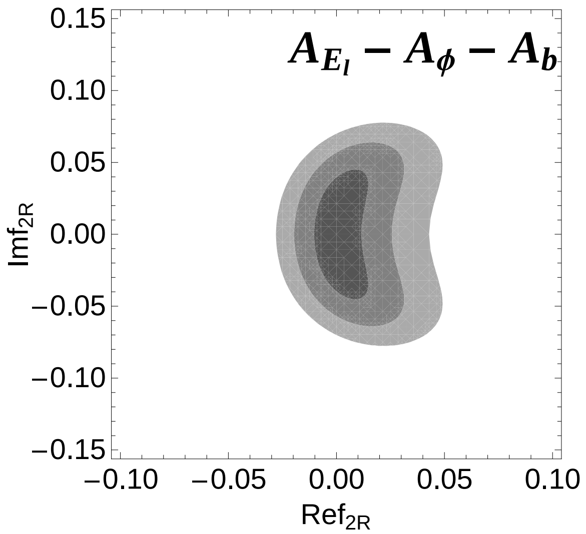

Figure 4.18: *The 1σ (central region), 2σ (middle region) and 3σ (outer region) CL regions in the* Ref$_{2R}$-Imf$_{2R}$ *plane allowed by the combined measurement of all the observables simultaneously.*

Boos et al. [57] find a limit of $0.12 < \mathrm{f}_{2R} < 0.13$ at the LHC with 100 fb^{-1} of luminosity. Refs. [59, 60] considered couplings f$_{1L}$ and f$_{1R}$ in their analysis and ignored f$_{2R}$ on which we focus. In Ref. [82], the authors have studied all three single-top production channels to probe anomalous tbW couplings and have utilized combinations of observables like cross sections, W polarization helicity fractions in top decay, and other angular asymmetries. They predict a 1σ limit of [−0.012, 0.024] on the coupling f$_{2R}$ with an integrated luminosity of 30 fb^{-1}. Ref. [83] determines expected 3σ limits on Ref$_{2R}$ to be [−0.056, 0.056] and on Imf$_{2R}$ to be [−0.115, 0.115], with 10 fb^{-1} of integrated luminosity. Najafabadi [84] has studied the tW channel for single-top production and determined the expected 1σ CL limits on anomalous coupling f$_{2R}$ to be in the range [−0.026, 0.017] with 20 fb^{-1} of integrated luminosity at 14 TeV LHC using the single-top production cross section.

Refs. [80, 81, 68] have studied various observables in $t\bar{t}$ pair production at the LHC with semileptonic decays of the top. Ref. [68] predict 1σ limit on f$_{2R}$ of $[-0.019, 0.018]$ with 10 fb^{-1} of integrated luminosity. Refs. [81, 80] study W polarization in top decay in top-quark pair production at the LHC to constrain the anomalous tbW couplings. They construct various asymmetries and helicity fractions to probe anomalous couplings in the decay of the top quark. Ref. [80]

quotes a 2σ limit of 0.04 on $\mathrm{f_{2R}}$ with full detector-level simulations including systematic uncertainties and with different observables. Ref. [81] obtain a limit on $\mathrm{f_{2R}}$ of $[-0.0260, 0.0312]$ with simulation of the ATLAS detector.

All these analyses except those of [68, 83] consider anomalous tbW couplings to be real parameters. In our analysis, we consider all anomalous couplings to be complex and find that only the real part of the coupling $\mathrm{f_{2R}}$ gives significant contribution to all observables at linear order in anomalous couplings. Without a linear approximation, other couplings also contribute at the quadratic level. However, we focus only on the $\mathrm{f_{2R}}$ since its contribution is dominant, occurring as it does at linear order. With integrated luminosity 10 fb^{-1} and cm energy 14 TeV, we find the most stringent limits possible on $\mathrm{Ref_{2R}}$ to be $[-0.006, 0.009]$ and on $\mathrm{Imf_{2R}}$ to be $\pm 3.8 \times 10^{-2}$, coming from the lepton energy asymmetry A_{E_ℓ}, which are nominally an order of magnitude better than the Tevatron direct search limit and better than the limits obtained in Refs. [57, 81, 82, 68, 80, 83]. Our estimate $[-0.044, 0.073]$ for limits on $\mathrm{Ref_{2R}}$ in the $\sqrt{s} = 7$ TeV run is comparable to the numbers obtained by the extrapolation of the result of [66] to an integrated luminosity of 1 fb^{-1}. It is of course true that including realistic detector efficiencies, especially for b tagging, will worsen our limits somewhat. But, the crucial point in our analysis is that we are able to determine limits on real and imaginary parts of coupling $\mathrm{f_{2R}}$ separately while others determine limits only on the magnitude of $\mathrm{f_{2R}}$.

4.8 Backgrounds and next-to-leading-order corrections

It is worthwhile to examine the dominant backgrounds to our signal process $gb \to tW^-$. Background estimation and extraction of the signal for this process has been studied in detail in Refs. [58, 85]. The main background for this signal would come from (a) processes which contain continuum of W^+W^-b involving an off-shell top quark, (b) top-pair production where one of the b quarks is missed as it lies outside the detector range, (c) processes containing W^+W^-j where lighter-quark jet j is misidentified as a b-quark jet (the probability being 1%). The contributions of the processes W^+W^-b and W^+W^-j, which are of order $O(\alpha_s\alpha_W^2)$, are much smaller than the tW^- signal, which is of order $O(\alpha_s\alpha_W)$. Tait [58] has considered both W's to decay leptonically and hence the final state consists of two hard charged leptons

+ one b jet + missing E_T (arising from two neutrinos). For such a signal, the process ZZj would also act as background where one of the Z decays into a pair of the charged leptons and the other Z decays into neutrinos. In Ref. [58], all the backgrounds are simulated at LO in the strong and weak couplings and standard acceptance cuts ($p_T > 15$ GeV and $\eta < 2$) are applied on all final state particles. To suppress large $t\bar{t}$ background, it is required that there should not be more than one hard b jet. After applying these cuts and with integrated luminosity less than 1 fb^{-1} at 14 TeV LHC, the conclusion of the Ref. [58] is that 5σ observation of single-top events in tW^- channel is possible.

The authors of Ref. [85] consider the situation where the W coming from the top quark decays leptonically and the other W decays into two light-quark jets. Therefore the signal would consist of three jets, one of which is a hard b jet, an isolated hard charged lepton and missing energy. The jet multiplicity requirement rejects a major part of the $t\bar{t}$ background. Also, the requirement of the two-jet invariant mass to be within the vicinity of the W mass (70 GeV-90 GeV) eliminates all backgrounds which do not have another W, as for example W+jets, other single-top and QCD processes. In all these analyses, b-tagging efficiency is assumed to be 60%. After applying all the cuts, it has been shown that 10% sensitivity can be achieved with 1 fb^{-1} by combining both electron and muon channels.

Turning to radiative corrections, NLO QCD corrections to the process $gb \to tW^-$ in the context of the 14 TeV LHC have been studied in detail in Ref. [86]. These corrections are substantial, up to 70% of the LO cross section. They are shown to be dependent on the factorization scale and increase steadily with the increment in the scale. For factorization scale $\mu = \mu_0/2 = (m_t + m_W)/2$, the K factor for the QCD correction is 1.4 while for $\mu = 2\mu_0 = 2(m_t + m_W)$, it is around 1.7. In our analysis, we have taken $\mu = m_t$, for which the K factor is expected to be about 1.5.

The complete NLO EW corrections have been calculated in Ref. [87] for $pp \to tW^- + X$ in the context of the LHC. The EW corrections are always positive and are maximum for tW invariant mass closed to threshold value. With increase in tW invariant mass, these EW corrections decrease. So, the maximum EW correction is around 7% at threshold and it goes down to 3.5% for tW invariant mass of 1200 GeV.

In our analysis, we have not included any K factor. Including NLO factors in our analysis would not change the asymmetries much, but would increase the signal and hence, the sensitivity on anomalous couplings would be enhanced.

4.9 Summary and discussion

We have investigated the sensitivity of the LHC to anomalous tbW couplings in single-top production in association with a W^- boson followed by semileptonic decay of the top. We derived analytical expressions for the spin density matrix of the top quark including contributions of both real and imaginary parts of the anomalous tbW couplings. We find that in the limit of vanishing b quark mass, only the real part of coupling $\mathrm{f_{2R}}$ contributes to the spin density matrix at linear order. Because of the chiral structure of the anomalous tbW couplings, the resulting top polarizations are vastly different from those expected in the SM. We find that substantial deviations, as much as 20-30%, in the degree of longitudinal top polarization from the SM value of -0.256 are possible even for anomalous couplings of magnitude 0.1. The degree of longitudinal top polarization varies from -0.075 to -0.281 for $\mathrm{Ref_{2R}}$ while for $\mathrm{Imf_{2R}}$ it is symmetric around the SM value and varies from -0.139 to -0.256 for the same range of $\mathrm{Imf_{2R}}$ as compared to the SM value of -0.256 for 14 TeV LHC.

Since top polarization can only be measured through the distributions of its decay products in top decay, we studied distributions of top-decay products. We consider the top to decay semi-leptonically, since this channel is expected to have the best accuracy and spin analyzing power. However, decay distributions can get contributions from anomalous couplings responsible for top polarization as well as for top decay. We find that normalized charged-lepton azimuthal and energy distributions and b-quark azimuthal distributions are sensitive to anomalous couplings $\mathrm{Ref_{2R}}$ and $\mathrm{Imf_{2R}}$. In each case, we define an asymmetry, whose deviation from the SM value would be a measure of the anomalous couplings. We find that the azimuthal asymmetry A_ϕ and the energy asymmetry A_{E_ℓ} of the charged lepton are more sensitive to negative values of the anomalous couplings $\mathrm{Ref_{2R}}$. A limit of $[-0.034, 0.086]$ on $\mathrm{Ref_{2R}}$ would be possible from A_ϕ for cm energy of 14 TeV at the LHC with integrated luminosities of 10 fb^{-1} respectively. For $\mathrm{Imf_{2R}}$ the corresponding limit is ± 0.050. A_{E_ℓ}, which is the most sensitive of the asymmetries we consider, probes $\mathrm{Ref_{2R}}$ and $\mathrm{Imf_{2R}}$ in the ranges $[-0.006, 0.009]$ and ± 0.038 respectively. Limits from A_b are the least stringent, though not much worse than those from A_{E_ℓ}.

The above results correspond to assuming only one coupling to be nonzero at a time. We also estimated simultaneous limits on $\mathrm{Ref_{2R}}$ and $\mathrm{Imf_{2R}}$ by combining measurements of all observables using a χ^2 analysis. The best possible 1σ limits on these couplings were found to be [−0.010, 0.015] and [−0.050, 0.050], respectively.

The limits we estimate for LHC with $\sqrt{s} = 7$ TeV and integrated luminosity 1 fb^{-1} are obviously worse. Nevertheless, they are comparable to those expected from an analysis of W helicities as carried out in [66].

In summary, our proposal will enable limits to be placed on $\mathrm{f}_{2\mathrm{R}}$ which are somewhat better than limits expected from other measurements at the LHC, and at least an order of magnitude better than the indirect limits.

Our results would be somewhat worsened by the inclusion realistic detection efficiencies for the b jet and for the detection of the W. However, we would like to emphasize that since we do not require accurate reconstruction of the full top-quark four-momentum, the limits are not likely to be much worse. On the other hand, inclusion of the $\bar{t}W^+$ final state, as well as additional leptonic channels in top decay would contribute to improving on our estimates of the limits. A more complete analysis including detector simulation would be worthwhile to carry out.

Chapter 5

CP-violation in single-top production

The phenomenon of CP violation (CPV) is important because it is believed to be a key in the understanding of the observed matter-antimatter or the baryon asymmetry of the universe. In the SM, the only source of CPV is the CKM phase associated with the CKM matrix for the inter-generational quark mixing. However, the amount of CPV predicted in the SM is insufficient to explain this asymmetry [88]. In many cases, extensions of the SM such as the THDM and the MSSM are able to supply the CPV required to produce such a baryon asymmetry in the early universe. In fact, in these models, it is precisely the CP-violating phases associated with the couplings of the top quark with scalar particles which drive baryogenesis [89]. Thus the study of CPV in the top-quark sector could shed light on these primordial processes.

In this chapter, we would like to examine to what extent CP violation, a distinctly weak interaction phenomenon, can be studied at the LHC in associated tW production. A number of extensions of SM, for example models with more than one Higgs doublet and CP-violating MSSM, have been proposed which incorporate new mechanisms of CP violation. In particular, it is expected that these would also modify tbW couplings. We extend the study of Chapter 4 to include both tW^- and $\bar{t}W^+$ production to find a way to probe CP-violating anomalous tbW couplings. While a comparison of the parton-level processes for the production of tW^- and $\bar{t}W^+$ states can immediately allow us to lay a finger on CP violation, the use of a pp initial state, which is not self-conjugate, involves some assumptions about parton distributions, as we shall see.

There are a number of proposals for the study of CP violation in top-pair production at lepton [90], photon [91] and hadron colliders [92]. However, CP violation in single-top production has received little attention [93]. The reason can be seen to be two-fold. For one, unlike in $t\bar{t}$ production, where the final state is self-conjugate, in single-top production, a process involving t has to be related to another involving $\bar{t}$, which is not straightforward. The other reason is the low event rate for single-top production expected at Tevatron. Single-top production at the LHC can be substantial, and it would be worthwhile attempting to extract information on CP violation, even though it needs more elaborate analysis than in the case of pair production.

We propose making use of the same variables which we employed in Chapter 4 for tW^- production, but for a study CP violation, we would also need analogous variables for $\bar{t}W^+$ production. The difference (in certain cases the sum) of these variables for the cases of tW^- and $\bar{t}W^+$ production would be a measure of CP violation. For convenience, in this work we will adopt a linear approximation for the couplings. This enables determination of limits on the CP-violating parameter which are independent of the parameter itself.

The measurement of CP violation at e^+e^-, $\gamma\gamma$ and $p\bar{p}$ colliders is straightforward because the initial state being self-conjugate, a study of CP-conjugate final-state particles can reveal the extent of CP violation, if present. However, in case of the LHC, the intial state being pp is not self-conjugate. Since a CP transformation relates a pp state to a $\bar{p}\bar{p}$ state, a naive comparison of processes related by CP is not possible. However, the trick is to consider either a partonic initial state which is self-conjugate (gg or $q\bar{q}$), or one whose densities in pp and $p\bar{p}$ initial states can be related to each other in a simple way. The former possibility is realized in case of $t\bar{t}$ pair production. In the case of single-top production, however, the initial state partonic state is not self-conjugate. However, if associated tW^- production is considered, the relevant partons are b and g, whose respective densities in p and $\bar{p}$ are equal, and also equal to those of the conjugates $\bar{b}$ and g, from simple charge conjugation invariance of strong interactions governing parton distributions in hadrons.

To elaborate on this further, consider a partial cross section for tW^- inclusive production at the LHC:

$$\begin{aligned} d\sigma\left(p(p_1)p(p_2) \to t(p_t, h_t)W^-(p_{W^-})X\right) &= \int dx_1\, dx_2\, f_b(x_1) f_g(x_2) \\ &\quad \times\, d\hat{\sigma}_{bg\to tW^-}(x_1p_1, x_2p_2, p_t, h_t, p_{W^-}), \end{aligned} \tag{5.1}$$

where $d\hat{\sigma}_{bg\to tW^-}$ is the corresponding parton-level partial cross section, and f_b, f_g are the densities of b, g partons in the proton. p_1, p_2, p_t and p_{W^-} are respectively the momenta of the two protons, t and W^-, and h_t is the helicity of t. Under CP this partial cross section is related to that for the process $\bar{p}\bar{p} \to \bar{t}W^+\bar{X}$:

$$d\sigma\left(\bar{p}(p_1)\bar{p}(p_2) \to \bar{t}(p_{\bar{t}}, h_{\bar{t}})W^+(p_{W^+})\bar{X}\right) = \int dx_1\, dx_2\, \bar{f}_{\bar{b}}(x_1)\bar{f}_g(x_2) \times d\hat{\sigma}_{\bar{b}g\to\bar{t}W^+}(x_1p_1, x_2p_2, p_{\bar{t}}, -h_{\bar{t}}, p_{W^+}), \tag{5.2}$$

where, now, $\bar{f}$ represents the parton density in an anti-proton. If we assume that

$$f_{\bar{b}}(x) = \bar{f}_{\bar{b}}(x), \quad f_g(x) = \bar{f}_g(x), \tag{5.3}$$

we can equate the partial cross section of the above $\bar{p}\bar{p}$-initiated process to that of a pp-initiated process:

$$d\sigma(\bar{p}\bar{p} \to \bar{t}W^+\bar{X}) = d\sigma(pp \to \bar{t}W^+\bar{X}). \tag{5.4}$$

Thus, CP invariance at the parton level, which implies

$$d\hat{\sigma}_{bg\to tW^-}(x_1p_1, x_2p_2, p_t, h_t, p_{W^-}) = d\hat{\sigma}_{\bar{b}g\to\bar{t}W^+}(x_1p_1, x_2p_2, p_{\bar{t}}, -h_{\bar{t}}, p_{W^+}), \tag{5.5}$$

gives, for the hadron-level cross sections,

$$d\sigma(pp \to t(p_t, h_t)W^-(p_{W^-})X) = d\sigma(pp \to \bar{t}(p_{\bar{t}}, -h_{\bar{t}})W^+(p_{W^+})\bar{X}). \tag{5.6}$$

A violation of this relation would signal CP violation. Thus, CP implies equal and opposite longitudinal polarizations for t and $\bar{t}$ in the two processes.

The assumptions regarding equality of b-quark and gluon distributions in p and $\bar{p}$ depend on C invariance of strong interactions responsible for the structure of the proton. In principle, there could be small weak-inteaction corrections which violate C invariance. These are difficult to estimate, and in this work we assume that these corrections are small compared to CP-violation effects we investigate. The relations (5.3) are equivalent to equality of b and $\bar{b}$ densities in the proton, and in practice, all parametrizations of parton distributions obey the equality. This is the assumption we make in our calculations.

5.1 The structure of tbW vertex

For the on-shell top, bottom and W, we write the most general effective vertices for the tbW interaction up to dimension five as

$$V_{t\to bW^+} = \frac{-g}{\sqrt{2}}V_{tb}\left[\gamma^\mu(\mathrm{f}_{1\mathrm{L}}P_L + \mathrm{f}_{1\mathrm{R}}P_R) - \frac{i\sigma^{\mu\nu}}{m_W}(p_t - p_b)_\nu(\mathrm{f}_{2\mathrm{L}}P_L + \mathrm{f}_{2\mathrm{R}}P_R)\right] \tag{5.7}$$

for the decay $t \to bW^+$, and

$$V_{b\to tW^-} = \frac{-g}{\sqrt{2}} V_{tb}^* \left[\gamma^\mu(\mathrm{f}_{1\mathrm{L}}^* P_L + \mathrm{f}_{1\mathrm{R}}^* P_R) - \frac{i\sigma^{\mu\nu}}{m_W}(p_t - p_b)_\nu(\mathrm{f}_{2\mathrm{R}}^* P_L + \mathrm{f}_{2\mathrm{L}}^* P_R)\right] \quad (5.8)$$

for tW^- production from a virtual b, where V_{tb} is the Cabibbo-Kobayashi-Maswkawa matrix element, and $\mathrm{f}_{1\mathrm{L}},\ \mathrm{f}_{2\mathrm{L}},\ \mathrm{f}_{1\mathrm{R}},\ \mathrm{f}_{2\mathrm{R}}$ are anomalous couplings of top quarks.

Similarly, the most general effective vertices for the $\bar{t}\bar{b}W$ interaction up to dimension five can be written as

$$V_{\bar{t}\to\bar{b}W^-} = \frac{-g}{\sqrt{2}} V_{tb} \left[\gamma^\mu(\bar{\mathrm{f}}_{1\mathrm{L}} P_L + \bar{\mathrm{f}}_{1\mathrm{R}} P_R) - \frac{i\sigma^{\mu\nu}}{m_W}(p_t - p_b)_\nu(\bar{\mathrm{f}}_{2\mathrm{R}} P_L + \bar{\mathrm{f}}_{2\mathrm{L}} P_R)\right] \quad (5.9)$$

for the decay $\bar{t} \to \bar{b}W^-$, and

$$V_{\bar{b}\to\bar{t}W^+} = \frac{-g}{\sqrt{2}} V_{tb}^* \left[\gamma^\mu(\bar{\mathrm{f}}_{1\mathrm{L}}^* P_L + \bar{\mathrm{f}}_{1\mathrm{R}}^* P_R) - \frac{i\sigma^{\mu\nu}}{m_W}(p_t - p_b)_\nu(\bar{\mathrm{f}}_{2\mathrm{L}}^* P_L + \bar{\mathrm{f}}_{2\mathrm{R}}^* P_R)\right] \quad (5.10)$$

for $\bar{t}W^+$ production from a virtual $\bar{b}$, where V_{tb} is the Cabibbo-Kobayashi-Maswkawa matrix element, and $\bar{\mathrm{f}}_{1\mathrm{L}},\ \bar{\mathrm{f}}_{2\mathrm{L}},\ \bar{\mathrm{f}}_{1\mathrm{R}},\ \bar{\mathrm{f}}_{2\mathrm{R}}$ are anomalous couplings for anti-top quarks.

We write anomalous tbW and $\bar{t}\bar{b}W$ couplings in terms of modulus and phase as

$$\begin{aligned}
\mathrm{f}_{1\mathrm{L}} &= |\mathrm{f}_{1\mathrm{L}}|\mathrm{e}^{\mathrm{i}\phi_{1\mathrm{L}}} & \bar{\mathrm{f}}_{1\mathrm{L}} &= |\bar{\mathrm{f}}_{1\mathrm{L}}|\mathrm{e}^{\mathrm{i}\bar{\phi}_{1\mathrm{L}}} \\
\mathrm{f}_{1\mathrm{R}} &= |\mathrm{f}_{1\mathrm{R}}|\mathrm{e}^{\mathrm{i}\phi_{1\mathrm{R}}} & \bar{\mathrm{f}}_{1\mathrm{R}} &= |\bar{\mathrm{f}}_{1\mathrm{R}}|\mathrm{e}^{\mathrm{i}\bar{\phi}_{1\mathrm{R}}} \\
\mathrm{f}_{2\mathrm{L}} &= |\mathrm{f}_{2\mathrm{L}}|\mathrm{e}^{\mathrm{i}\phi_{2\mathrm{L}}} & \bar{\mathrm{f}}_{2\mathrm{L}} &= |\bar{\mathrm{f}}_{2\mathrm{L}}|\mathrm{e}^{\mathrm{i}\bar{\phi}_{2\mathrm{L}}} \\
\mathrm{f}_{2\mathrm{R}} &= |\mathrm{f}_{2\mathrm{R}}|\mathrm{e}^{\mathrm{i}\phi_{2\mathrm{R}}} & \bar{\mathrm{f}}_{2\mathrm{R}} &= |\bar{\mathrm{f}}_{2\mathrm{R}}|\mathrm{e}^{\mathrm{i}\bar{\phi}_{2\mathrm{R}}} \qquad (5.11)
\end{aligned}$$

where ϕ's and $\bar{\phi}$'s denote the phases in the anomalous couplings of top and antitop respectively.

CP invariance requires, apart from V_{tb} to be real, that

$$\mathrm{f}_{1\mathrm{L}} = \bar{\mathrm{f}}_{1\mathrm{L}}, \quad \mathrm{f}_{1\mathrm{R}} = \bar{\mathrm{f}}_{1\mathrm{R}}, \quad \mathrm{f}_{2\mathrm{L}} = \bar{\mathrm{f}}_{2\mathrm{R}}, \quad \mathrm{f}_{2\mathrm{R}} = \bar{\mathrm{f}}_{2\mathrm{L}}. \quad (5.12)$$

which further implies that

$$|\mathrm{f}_{1\mathrm{L}}| = |\bar{\mathrm{f}}_{1\mathrm{L}}| \qquad \phi_{1\mathrm{L}} = \bar{\phi}_{1\mathrm{L}} \quad (5.13)$$

$$|\mathrm{f}_{1\mathrm{R}}| = |\bar{\mathrm{f}}_{1\mathrm{R}}| \qquad \phi_{1\mathrm{R}} = \bar{\phi}_{1\mathrm{R}} \quad (5.14)$$

$$|\mathrm{f}_{2\mathrm{L}}| = |\bar{\mathrm{f}}_{2\mathrm{R}}| \qquad \phi_{2\mathrm{L}} = \bar{\phi}_{2\mathrm{R}} \quad (5.15)$$

$$|\mathrm{f}_{2\mathrm{R}}| = |\bar{\mathrm{f}}_{2\mathrm{L}}| \qquad \phi_{2\mathrm{R}} = \bar{\phi}_{2\mathrm{L}} \quad (5.16)$$

Another useful set of relations follows from CPT invariance (in the absence of absorptive parts):

$$\mathrm{f}_{1\mathrm{L}}^{*} = \bar{\mathrm{f}}_{1\mathrm{L}}; \quad \mathrm{f}_{1\mathrm{R}}^{*} = \bar{\mathrm{f}}_{1\mathrm{R}}; \quad \mathrm{f}_{2\mathrm{R}}^{*} = \bar{\mathrm{f}}_{2\mathrm{L}}; \quad \mathrm{f}_{2\mathrm{L}}^{*} = \bar{\mathrm{f}}_{2\mathrm{R}} \tag{5.17}$$

which implies

$$|\mathrm{f}_{1\mathrm{L}}| = |\bar{\mathrm{f}}_{1\mathrm{L}}| \qquad \phi_{1\mathrm{L}} = -\bar{\phi}_{1\mathrm{L}} \tag{5.18}$$

$$|\mathrm{f}_{1\mathrm{R}}| = |\bar{\mathrm{f}}_{1\mathrm{R}}| \qquad \phi_{1\mathrm{R}} = -\bar{\phi}_{1\mathrm{R}} \tag{5.19}$$

$$|\mathrm{f}_{2\mathrm{L}}| = |\bar{\mathrm{f}}_{2\mathrm{R}}| \qquad \phi_{2\mathrm{L}} = -\bar{\phi}_{2\mathrm{R}} \tag{5.20}$$

$$|\mathrm{f}_{2\mathrm{R}}| = |\bar{\mathrm{f}}_{2\mathrm{L}}| \qquad \phi_{2\mathrm{R}} = -\bar{\phi}_{2\mathrm{L}} \tag{5.21}$$

One can write the phase ϕ's as a sum of two phases, the CP-violating phase δ and the phase corresponding to absorptive part α. Then, we have

$$\phi_{1\mathrm{L}} = \delta_{1\mathrm{L}} + \alpha_{1\mathrm{L}} \qquad \bar{\phi}_{1\mathrm{L}} = -\delta_{1\mathrm{L}} + \alpha_{1\mathrm{L}} \tag{5.22}$$

$$\phi_{1\mathrm{R}} = \delta_{1\mathrm{R}} + \alpha_{1\mathrm{R}} \qquad \bar{\phi}_{1\mathrm{R}} = -\delta_{1\mathrm{R}} + \alpha_{1\mathrm{R}} \tag{5.23}$$

$$\phi_{2\mathrm{L}} = \delta_{2\mathrm{L}} + \alpha_{2\mathrm{L}} \qquad \bar{\phi}_{2\mathrm{L}} = -\delta_{2\mathrm{R}} + \alpha_{2\mathrm{R}} \tag{5.24}$$

$$\phi_{2\mathrm{R}} = \delta_{2\mathrm{R}} + \alpha_{2\mathrm{R}} \qquad \bar{\phi}_{2\mathrm{R}} = -\delta_{2\mathrm{L}} + \alpha_{2\mathrm{L}} \tag{5.25}$$

Hence, $\delta = 0$ signifies no CP violation and $\alpha = 0$ signifies no absorptive parts.

From Eqn. 5.12, we see that any CP-violating observable must be proportional to the combinations: $(\mathrm{f}_{1\mathrm{L}} - \bar{\mathrm{f}}_{1\mathrm{L}})$, $(\mathrm{f}_{1\mathrm{R}} - \bar{\mathrm{f}}_{1\mathrm{R}})$, $(\mathrm{f}_{2\mathrm{L}} - \bar{\mathrm{f}}_{2\mathrm{R}})$ and $(\mathrm{f}_{2\mathrm{R}} - \bar{\mathrm{f}}_{2\mathrm{L}})$. In the presence of absorptive parts, these observables are proportional to the real parts of these combinations and signal CP violation. The real part of $(\mathrm{f}_{2\mathrm{R}} - \bar{\mathrm{f}}_{2\mathrm{L}})$ can be written as

$$\mathrm{Ref}_{2\mathrm{R}} - \mathrm{Re}\bar{\mathrm{f}}_{2\mathrm{L}} = -2|\mathrm{f}_{2\mathrm{R}}| \sin\delta_{2\mathrm{R}} \sin\alpha_{2\mathrm{R}}. \tag{5.26}$$

Thus, we must have both δ and α to be nonzero simultaneously to have non-vanishing values of CP-violating observables if they are to arise from absorptive parts.

5.2 CP-violating observables in tW channel of single-top production

We study the single-top production process $gb \to tW^-$ and its CP-conjugated process $g\bar{b} \to \bar{t}W^+$ to study CP violation. We assume that anomalous tbW couplings contributing in the production and in the decay are CP violating and arise from the absorptive parts of the amplitudes. In Chapter 4, we have obtained analytical expressions for the spin density matrix for the top quark produced in the process $gb \to tW^-$ and for the top decay including the full contribution of anomalous tbW couplings. The corresponding expressions for the CP-conjugated process $g\bar{b} \to \bar{t}W^+$ and $\bar{t} \to \bar{b}W^-$ can be obtained from those expressions by replacing $\mathrm{Re}f_{2R}$ by $\mathrm{Re}\bar{f}_{2L}$ taking appropriate helicity of the antitop.

We obtain the contribution of CP-violating tbW couplings in sums or differences of observables in tW^- and $\bar{t}W^+$ production and decay, and examine how well the couplings can be constrained by them. We will assume that the anomalous couplings are small and work in a linear approximation of the couplings. We also retain only $\mathrm{Re}f_{2R}$ and $\mathrm{Re}\bar{f}_{2L}$, since these are the only ones which contribute in the limit of vanishing bottom mass, which we set to zero.

For our numerical analysis, we use the leading-order parton distribution function (PDF) sets of CTEQ6L [79] with a factorization scale of $m_t = 172.6$ GeV. We also evaluate the strong coupling at the same scale, $\alpha_s(m_t) = 0.1085$. We make use of the following values of other parameters: $M_W = 80.403$ GeV, the electromagnetic coupling $\alpha_{em}(m_Z) = 1/128$ and $\sin^2\theta_W = 0.23$.

We study the sensitivities of the observables discussed in Chapter 4 to CP violation at the LHC for two cm of energies viz., 7 TeV and 14 TeV, with integrated luminosities 2 fb^{-1} and 10 fb^{-1}, respectively. For the case of 7 TeV LHC, we also quote limits with 5 fb^{-1} of integrated luminosity. To obtain the 1σ limit on anomalous tbW couplings from a measurement of an observable, we find those values of the couplings for which the observable deviates by 1σ from its SM value. The statistical uncertainty σ_i in the measurement of the sum or difference any two generic asymmetries is given by $\sigma_i = \sqrt{2/\mathcal{N}}$, where $\mathcal{N}$ is the total number of events predicted in the SM. We apply this to the various cases we have discussed. In the case of the top polarization asymmetry, the limits are obtained on the assumption that the polarization can be measured with 100% accuracy.

5.2.1 Production rate asymmetry

The simplest asymmetry we consider is the rate asymmetry in the production of tW^- and $\bar{t}W^+$. We define

$$\sigma^- \equiv \sigma(pp \to tW^-X) \tag{5.27}$$

and

$$\sigma^+ \equiv \sigma(pp \to \bar{t}W^+X). \tag{5.28}$$

As stated before, we assume the equality of b and $\bar{b}$ densities in the proton. Then, at linear order in anomalous couplings,

$$\sigma^- = \sigma_0 + \mathrm{Ref}_{2\mathrm{R}}\ \sigma_1 \tag{5.29}$$

$$\sigma^+ = \sigma_0 + \mathrm{Re}\bar{\mathrm{f}}_{2\mathrm{L}}\ \sigma_1. \tag{5.30}$$

Here σ_0 is the SM cross section, which is identical for $pp \to tW^-X)$ as well as $pp \to \bar{t}W^+X$. σ_1 is the cross section arising from interference of the anomalous contribution with the SM amplitude, for unit anomalous coupling.

We consider the rate asymmetry

$$A_\sigma = \frac{\sigma^+ - \sigma^-}{\sigma^+ + \sigma^-}, \tag{5.31}$$

which is, in the linear approximation,

$$A_\sigma = \frac{(\mathrm{Re}\bar{\mathrm{f}}_{2\mathrm{L}} - \mathrm{Ref}_{2\mathrm{R}})\ \sigma_1}{2\sigma_0} = \frac{\Delta_{2\mathrm{R}}\ \sigma_1}{\sigma_0} \tag{5.32}$$

where $\Delta_{2\mathrm{R}}$ is the CP-violating parameter defined by

$$\Delta_{2\mathrm{R}} = (\mathrm{Re}\bar{\mathrm{f}}_{2\mathrm{L}} - \mathrm{Ref}_{2\mathrm{R}}) \equiv -2|\mathrm{f}_{2\mathrm{R}}| \sin\alpha_{2\mathrm{R}} \sin\delta_{2\mathrm{R}}. \tag{5.33}$$

σ_0 and σ_1 can be obtained by numerical integration over parton densities of analytical expressions for the corresponding parton-level quantities. The latter may be easily found from expressions in Appendix III.

We plot the asymmetry A_σ^{CPV} in Fig. 5.1 as a function of the CP-violating parameter $\Delta_{2\mathrm{R}}$ for the two cm of energies 7 TeV and 14 TeV. We also show the 1σ fluctuation in the measurement of the asymmetry with 2 fb^{-1} and 10 fb^{-1} of integrated luminosities for 7 and 14 TeV LHC respectively. 1σ fluctuation from the SM asymmetry with 5 fb^{-1} of luminosity is also shown in the case of 7 TeV. We find that 1σ limit of $\pm 5.42 \times 10^{-3}$ on $\Delta_{2\mathrm{R}}$ can be obtained from $\mathrm{A}_\sigma^{\mathrm{CPV}}$ at 14 TeV LHC with 10 fb^{-1} of integrated luminosity. At 7 TeV LHC, the limits on $\Delta_{2\mathrm{R}}$ are $\pm 2.89 \times 10^{-2}$ and $\pm 1.83 \times 10^{-2}$ with 2 fb^{-1} and 5 fb^{-1} of integrated luminosities.

5.2.2 CP-violating asymmetry – Production and decay

Since the top quark decays into b and W via tbW interactions, we also consider CP violation in top decay. Here, we construct an asymmetry in single-top production with subsequent decay of the top quark into charged leptons, assuming CP violation

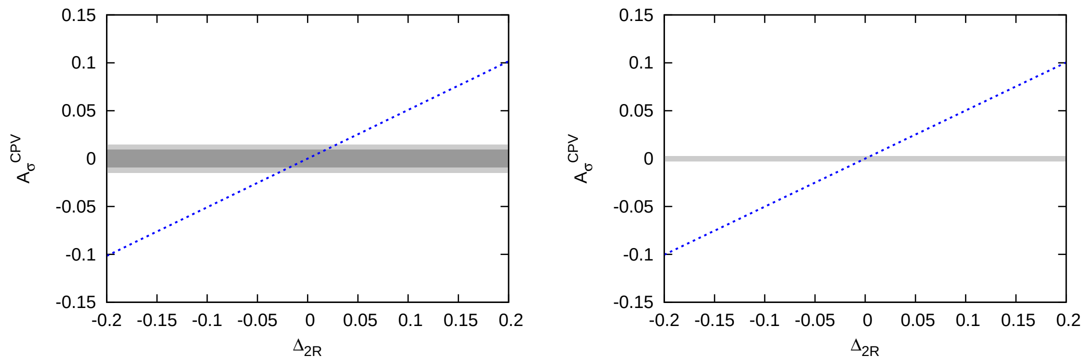

Figure 5.1: *The CP asymmetry in tW production at the LHC as a function of Δ_{2R} for the cm energies 7 TeV (left) and 14 TeV (right). In the left plot, the outer and inner grey bands correspond to the 1σ error intervals for the asymmetry predicted in the SM with 2 fb^{-1} and 5 fb^{-1} of integrated luminosity respectively.*

in both production and decay. Using the narrow-width approximation (NWA), we can write the cross section for the process $pp \to tW^-X \to b\ell^+\nu W^-$ as

$$\sigma^-(pp \to b\ell^+\nu W^- X) = \frac{1}{\Gamma_t}\left[\rho(pp \to tW^-X) \otimes \Gamma(t \to b\ell^+\nu)\right], \tag{5.34}$$

where Γ_t is total decay width of the top. $\rho(pp \to tW^-X)$, $\Gamma(t \to b\ell^+\nu)$ are respectively the production and decay density matrices (with appropriate integration of the phase space carried out), and $\otimes$ denotes a matrix product. The density matrix formalism is used here to ensure proper spin coherence between production and decay.

We can write down an analogous expression for the cross section σ^+ of conjugate process of $\bar{t}$ production, with decay into a state containing ℓ^+. We then define the asymmetry in charged-lepton production rates as

$$A_d = \frac{\sigma^-(pp \to b\ell^+\nu W^- X) - \sigma^+(pp \to \bar{b}\ell^-\bar{\nu}W^+\bar{X})}{\sigma^-(pp \to b\ell^+\nu W^- X) + \sigma^+(pp \to \bar{b}\ell^-\bar{\nu}W^+\bar{X})} \tag{5.35}$$

Hence, the asymmetry A_d, in linear approximation of anomalous couplings, again turns out to be proportional to $(\mathrm{Re}\bar{\mathrm{f}}_{2\mathrm{L}} - \mathrm{Re}\mathrm{f}_{2\mathrm{R}}) = -2|\mathrm{f}_{2\mathrm{R}}| \sin\delta_{2\mathrm{R}} \sin\alpha_{2\mathrm{R}}$.

We plot the asymmetry A_d^{CPV} in Fig. 5.2 as a function of the CP-violating parameter $\Delta_{2\mathrm{R}}$ for the two cm energies 7 TeV and 14 TeV. We also show the 1σ fluctuation in the measurement of the asymmetry with 2 fb^{-1} and 10 fb^{-1} of integrated luminosities for 7 and 14 TeV LHC respectively. 1σ fluctuation from the SM asymmetry with 5 fb^{-1} of luminosity is also shown in the case of 7 TeV. We find that 1σ limit of $\pm 2.43 \times 10^{-2}$ on $\Delta_{\rm 2R}$ can be obtained from $\rm A_d^{CPV}$ at 14 TeV LHC with 10 fb^{-1} of integrated luminosity. At 7 TeV LHC, the limits on $\Delta_{\rm 2R}$ are $\pm 1.37 \times 10^{-1}$ and $\pm 8.67 \times 10^{-2}$ with 2 fb^{-1} and 5 fb^{-1} of integrated luminosities.

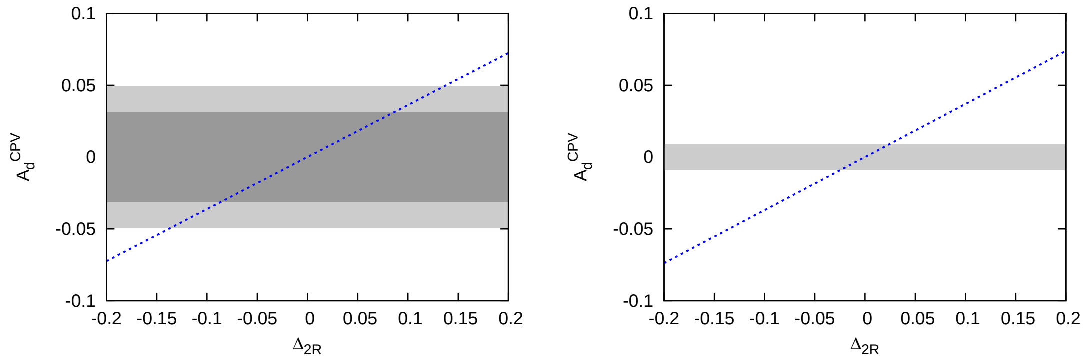

Figure 5.2: *The CPV asymmetry in tW production and top-decay at LHC as a function of Δ_{2R} for the cm energies 7 TeV (left) and 14 TeV (right). In the left plot, the outer and inner grey bands correspond to the 1σ error intervals for the asymmetry predicted in the SM with 2 fb^{-1} and 5 fb^{-1} of integrated luminosity respectively.*

5.2.3 Top Polarization asymmetry

We define the degree of longitudinal polarization P_t of the top as

$$P_t = \frac{\mathcal{N}_t^+ - \mathcal{N}_t^-}{\mathcal{N}_t^+ + \mathcal{N}_t^-}. \tag{5.36}$$

where $\mathcal{N}_t^+$ and $\mathcal{N}_t^-$ are the numbers for the positive and negative helicity tops and $\mathcal{N} = \mathcal{N}_t^+ + \mathcal{N}_t^-$ is the total number of events.

In the linear approximation of anomalous couplings, the polarization P_t for the top and $P_{\bar{t}}$ for the antitop can be written as

$$P_t = P_t^0 + {\rm Re} f_{\rm 2R}\, P_t^1, \tag{5.37}$$
$$P_{\bar{t}} = -P_t^0 - {\rm Re}\bar{f}_{\rm 2L}\, P_t^1, \tag{5.38}$$

where P_t^0 and P_t^1 are contributions from the SM and from the interference of anomalous contribution with the SM amplitude, for unit value of anomalous couplings, respectively.

We define CP-violating asymmetry in top and antitop polarization as

$$A_{P_t} \;=\; P_{\bar{t}} + P_t \tag{5.39}$$

which in the linear order in anomalous couplings takes the form

$$A_{P_t} = -(\mathrm{Re}\bar{\mathrm{f}}_{2\mathrm{L}} - \mathrm{Re}\mathrm{f}_{2\mathrm{R}})P_t^1 = -\Delta_{2\mathrm{R}} P_t^1. \tag{5.40}$$

In Fig. 5.3, we show the asymmetry A_{P_t} as a function of $\Delta_{2\mathrm{R}}$ for the two cm energies 7 TeV and 14 TeV with 1σ fluctuations in the measurement of the asymmetry. We find that the asymmetry constructed using top polarization is a sensitive probe of CP violation. We obtain the 1σ limit of $\pm 5.06 \times 10^{-3}$ on $\Delta_{2\mathrm{R}}$ at 14 TeV LHC with 10 fb^{-1} of integrated luminosity. At 7 TeV, the limits are $\pm 2.85 \times 10^{-2}$ and $\pm 1.80 \times 10^{-2}$ with 2 fb^{-1} and 5 fb^{-1} of integrated luminosities.

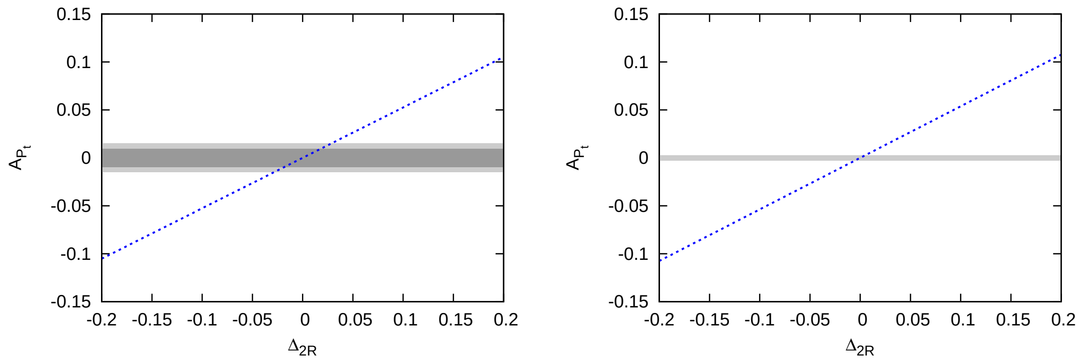

Figure 5.3: *The CP-violating top-polarization asymmetry in tW^- and $\bar{t}W^+$ production at the LHC as a function of Δ_{2R} for the cm energies 7 TeV (left) and 14 TeV (right). In the left plot, the outer and inner grey bands correspond to the 1σ error intervals for the asymmetry predicted in the SM with 2 fb^{-1} and 5 fb^{-1} of integrated luminosity respectively.*

5.3 CP-violating observables from top-decay products

5.3.1 Azimuthal asymmetry of charged lepton

In Chapter 4, we studied azimuthal distributions of the charged lepton from top-quark decay in the single-top production process in the presence of anomalous *tbW* couplings. We found that the charged-lepton azimuthal distributions are sensitive to anomalous couplings and the distributions show deviation from the SM distribution. So, to quantify this deviation and make the best use of statistics, we define a charged-lepton azimuthal asymmetry in single-top production process as

$$A_\phi = \frac{\sigma(\cos\phi_\ell > 0) - \sigma(\cos\phi_\ell < 0)}{\sigma(\cos\phi_\ell > 0) + \sigma(\cos\phi_\ell < 0)} \tag{5.41}$$

where ϕ is the azimuthal angle of charged lepton w.r.t. the top/antitop production plane. In the linear order in anomalous *tbW* couplings, this asymmetry can be written as

$$A_\phi^- = A_\phi^0 + \mathrm{Ref_{2R}A_\phi^1}, \tag{5.42}$$

$$A_\phi^+ = A_\phi^0 + \mathrm{Re\bar{f}_{2L}A_\phi^1}, \tag{5.43}$$

where A_ϕ^- and A_ϕ^+ are azimuthal asymmetries of the charged lepton coming from top/antitop decays respectively. The A_ϕ^0 and A_ϕ^1 denote contributions to the asymmetry from the SM and and from the interference of anomalous contribution with the SM amplitude respectively, for unit value of anomalous couplings.

We define a CP-violating asymmetry A_ϕ^{CPV}

$$A_\phi^{CPV} = A_\phi^+ - A_\phi^- \tag{5.44}$$

which in linear approximation of anomalous couplings can be written as

$$A_\phi^{CPV} = (\mathrm{Re\bar{f}_{2L}} - \mathrm{Ref_{2R}})A_\phi^1 = \Delta_{\mathrm{2R}} A_\phi^1. \tag{5.45}$$

In Fig. 5.4, we show the asymmetry A_ϕ^{CPV} as a function of Δ_{2R} for the two cm energies 7 TeV and 14 TeV together with 1σ fluctuations in measurement of the asymmetry. From the figure, it can be seen that the asymmetry A_ϕ^{CPV} shows low sensitivity to CP violation at 7 TeV. We obtain 1σ limit of $\pm 2.80 \times 10^{-2}$ on CP-violating parameter Δ_{2R} at 14 TeV with 10 fb^{-1} of integrated luminosity. At 7 TeV, the limits are $\pm 2.07 \times 10^{-1}$ and $\pm 1.43 \times 10^{-1}$ with 2 fb^{-1} and 5 fb^{-1} of integrated luminosities.

5.3.2 Energy asymmetry of charged lepton

In Chapter 4, we found that the charged-lepton energy distribution is sensitive to anomalous *tbW* couplings and the curves for the E_ℓ distribution for anomalous *tbW* couplings of ± 0.2 and the SM are well separated from each other and intersect at

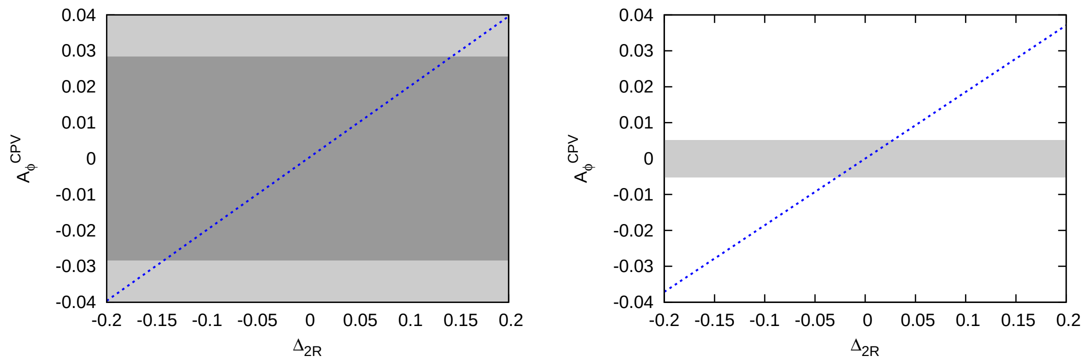

Figure 5.4: *The CP-violating azimuthal asymmetry of the charged lepton from top/antitop decay in tW^- and $\bar{t}W^+$ production at the LHC as a function of Δ_{2R} for the cm energies 7 TeV (left) and 14 TeV (right). In the left plot, the outer and inner grey bands correspond to the 1σ error intervals for the asymmetry predicted in the SM with 2 fb^{-1} and 5 fb^{-1} of integrated luminosity respectively.*

about $E_\ell^C = 62$ GeV. We constructed an asymmetry around the intersection point of the curves, defined by

$$A_{E_\ell} = \frac{\sigma(E_\ell < E_\ell^C) - \sigma(E_\ell > E_\ell^C)}{\sigma(E_\ell < E_\ell^C) + \sigma(E_\ell > E_\ell^C)}. \tag{5.46}$$

We define a CP-violating asymmetry utilizing the energy asymmetry of the charged lepton coming from top/antitop decay in single-top production as

$$A_{E_\ell}^{CPV} = A_{E_{\ell^-}} - A_{E_{\ell^+}} = \Delta_{2\mathrm{R}} A_{E_\ell}^1, \tag{5.47}$$

where ℓ^+ and ℓ^- come from top and antitop decay respectively.

We plot the asymmetry $A_{E_\ell}^{CPV}$ in Fig. 5.5 as a function of CP-violating parameter $\Delta_{2\mathrm{R}}$ for two cm energies 7 TeV and 14 TeV. We also show the 1σ fluctuation in the measurement of the asymmetry with 2 fb^{-1} and 10 fb^{-1} of integrated luminosities for 7 and 14 TeV respectively. 1σ fluctuation with 5 fb^{-1} of luminosity is also shown in the case of 7 TeV. We find that 1σ limit of $\pm 1.86 \times 10^{-2}$ on $\Delta_{2\mathrm{R}}$ can be obtained from $A_{E_\ell}^{CPV}$ at 14 TeV with 10 fb^{-1} of integrated luminosity. At 7 TeV, the limits on $\Delta_{2\mathrm{R}}$ are $\pm 9.68 \times 10^{-2}$ and $\pm 6.12 \times 10^{-2}$ with 2 fb^{-1} and 5 fb^{-1} of integrated luminosities.

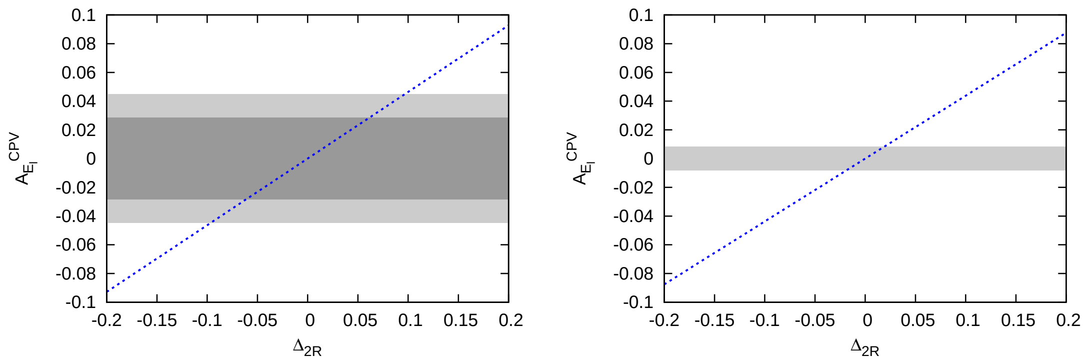

Figure 5.5: *The CP-violating energy asymmetry of the charged lepton from top/antitop decay in* tW^- *and* $\bar{t}W^+$ *production at the LHC as a function of* Δ_{2R} *for the cm energies 7 TeV (left) and 14 TeV (right). In the left plot, the outer and inner grey bands correspond to the* 1σ *error intervals for the asymmetry predicted in the SM with 2 fb*$^{-1}$ *and 5 fb*$^{-1}$ *of integrated luminosity respectively.*

5.3.3 Azimuthal asymmetry of b quark

In Chapter 4, we found that the b-quark azimuthal distribution is sensitive to anomalous tbW couplings and the curves for the distribution for anomalous tbW couplings of ± 0.2 and the SM are well separated from each other. We constructed an asymmetry around the intersection point of the curves, defined by

$$A_b = \frac{\sigma(\cos\phi_b > 0) - \sigma(\cos\phi_b < 0)}{\sigma(\cos\phi_b > 0) + \sigma(\cos\phi_b < 0)} \tag{5.48}$$

where ϕ is the azimuthal angle of b quark w.r.t. the top/antitop production plane. In the linear order in anomalous tbW couplings, this asymmetry can be written as

$$A_b^- = A_b^0 + \mathrm{Re} f_{2\mathrm{R}} A_b^1, \tag{5.49}$$

$$A_b^+ = A_b^0 + \mathrm{Re} \bar{f}_{2\mathrm{L}} A_b^1, \tag{5.50}$$

where A_b^- and A_b^+ are azimuthal asymmetries of b quark coming from top/antitop decays respectively. The A_b^0 and A_b^1 denote contributions to the asymmetry from the SM and and from the interference of anomalous contribution with the SM amplitude respectively, for unit value of anomalous couplings.

We define a CP-violating asymmetry A_b^{CPV}

$$A_b^{CPV} = A_b^+ - A_b^- \tag{5.51}$$

which in the linear approximation of anomalous couplings can be written as

$$A_b^{CPV} \;=\; (\mathrm{Re}\bar{\mathrm{f}}_{2\mathrm{L}} - \mathrm{Re}\mathrm{f}_{2\mathrm{R}})A_b^1 = \Delta_{2\mathrm{R}} A_b^1. \tag{5.52}$$

In Fig. 5.6, we show the asymmetry A_b^{CPV} as a function of $\Delta_{2\mathrm{R}}$ for two cm of energies 7 TeV and 14 TeV with the 1σ fluctuations in the measurement of the asymmetry. From the figure, it can be seen that the asymmetry A_b^{CPV} shows low sensitivity to CP violation at 7 TeV. We obtain 1σ limit of $\pm 3.15 \times 10^{-2}$ on CP-violating parameter $\Delta_{2\mathrm{R}}$ at 14 TeV with 10 fb^{-1} of integrated luminosity. At 7 TeV, the limits are $\pm 1.65 \times 10^{-1}$ and $\pm 1.04 \times 10^{-1}$ with 2 fb^{-1} and 5 fb^{-1} of integrated luminosities.

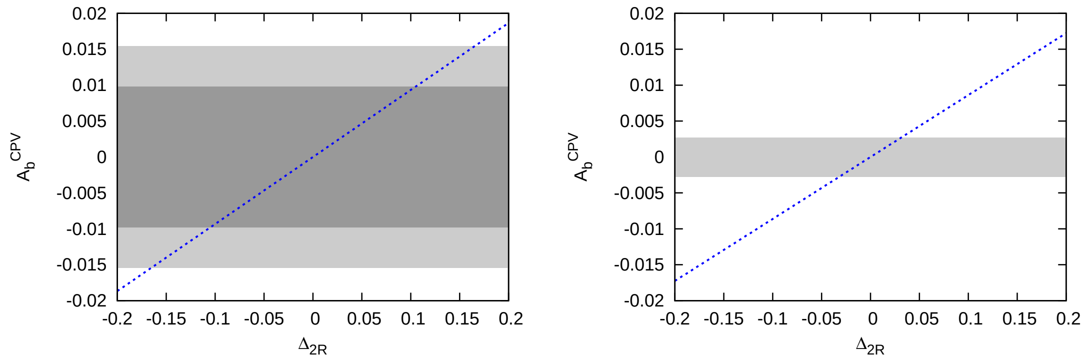

Figure 5.6: *The CP-violating asymmetry of the b quark coming from top/antitop decay in tW^- and $\bar{t}W^+$ production at the LHC as a function of Δ_{2R} for the cm energies 7 TeV (left) and 14 TeV (right). In the left plot, the outer and inner grey bands correspond to the 1σ error intervals for the asymmetry predicted in the SM with 2 fb^{-1} and 5 fb^{-1} of integrated luminosity respectively.*

5.4 Summary and conclusions

We have investigated the possibility of measuring CP-violating tbW couplings at the LHC through the conjugate processes of tW^- and $\bar{t}W^+$ production. We proposed a number of CP-violating asymmetries which would be sensitive to the CP-odd combination of couplings $\Delta_{2\mathrm{R}} \equiv \bar{\mathrm{f}}_{2\mathrm{L}} - \mathrm{f}_{2\mathrm{R}}$, the difference of the couplings associated with top and antitop. The results for the 1σ limits coming from the various asymmetries for the chosen combinations of cm energy and integrated luminosity are summarized in Table 5.1.

Asymmetry	$\sqrt{s} = 7$ TeV		$\sqrt{s} = 14$ TeV
	$L = 2$ fb^{-1}	$L = 5$ fb^{-1}	$L = 10$ fb^{-1}
A_{σ}^{CPV}	2.89×10^{-2}	1.83×10^{-2}	5.42×10^{-3}
A_{P_t}	2.85×10^{-2}	1.80×10^{-2}	5.06×10^{-3}
A_{d}^{CPV}	0.137	8.67×10^{-2}	2.43×10^{-2}
$A_{\phi_\ell}^{CPV}$	0.207	0.143	2.80×10^{-2}
$A_{E_\ell}^{CPV}$	9.68×10^{-2}	6.12×10^{-2}	1.86×10^{-2}
$A_{\phi_b}^{CPV}$	0.165	0.104	3.15×10^{-2}

Table 5.1: 1σ *limits on the magnitude of the CP-violating combination of couplings,* $|\Delta_{2\mathrm{R}}|$*, possible at the LHC from various asymmetries defined in the text.*

We see from the table that 1σ limits on $\Delta_{2\mathrm{R}}$ possible for $\sqrt{s} = 7$ TeV, even with $L = 5$ fb^{-1}, are of the order of about 0.1, perhaps at the limit of validity of our linear approximation. The limit from A_{P_t} is nominally better, but cannot be realized since the polarization cannot be measured with 100% accuracy. For $\sqrt{s} = 14$ TeV, on the other hand, the limits are of the order of a few times 10^{-2}, well within the validity range of the approximation. The best limit, 1.86×10^{-2}, would come from the measurement of $A_{E_\ell}^{CPV}$.

We conclude from our analysis that the tW mode of single-top production would be an alternative place to look for CP-violating tbW couplings apart from the decay of top and antitop produced as a $t\bar{t}$-pair. We find that the energy asymmetry, $A_{E_\ell}^{CPV}$, is the most sensitive to the CP-violating parameter and would enable a limit of about 1.86×10^{-2} to be placed on $|\Delta_{2\mathrm{R}}|$, for a cm energy of 14 TeV and integrated luminosity of 10 fb^{-1}. The limits possible for an operational energy of 7 TeV for integrated luminosity of up to 5 fb^{-1} are not as good, being at the level of 10-20%.

Our limits would no doubt be somewhat worse when relevant detection efficiencies of the W produced in association with the top and the b-quark are taken into account (see [58, 94] for a discussion on backgrounds for the process). However, we do not expect the limits to be much worse, since we do not require full reconstruction of the top momentum. Moreover, we have been conservative in that we have included only one charged lepton in our analysis – including other charged-lepton would improve the limits. It is also likely that the integrated luminosity collected by the LHC at $\sqrt{s} = 14$ TeV will be better than the 10 fb^{-1} assumed by us. All in all we conclude that it would be possible to obtain limits on the CP-violating anomalous coupling in the region of 10^{-2} by employing the energy asymmetry of the charged lepton. It would be worthwhile carrying out a more detailed and refined analysis.

We adopted a linear approximation in the couplings, which in Chapter 4 was found to be strictly valid for $|\mathrm{Re} f_{2R}|$, $|\mathrm{Re} \bar{f}_{2L}| < 0.05$. It is straightforward to do away with approximation. However, that would make an interpretation of results somewhat more complicated. Our results may be taken to be indicative of the results of a full calculation without approximation.

Chapter 6

Associated production of single top with charged Higgs in 2HDM at the LHC

In the SM, the EW symmetry is broken through a single $SU(2)$ scalar doublet, i.e., through the Higgs mechanism. However, while the SM Higgs mechanism is the simplest way to break the EW symmetry, there are reasons to consider an enlarged Higgs sector [95]. Models with two Higgs doublets can address the strong CP problem and generate additional sources of CPV needed for baryogenesis [96]. Moreover, the most popular paradigm for addressing the gauge hierarchy problem, supersymmetry (SUSY), contains two Higgs doublets in its simplest formulation [95, 97]. The spectrum of two Higgs doublet models (THDM) involves three neutral and two charged Higgs bosons. Different versions of the THDM also have different couplings of the scalars to fermions. Thus, even if scalar particles were to be discovered at the LHC, it is necessary to probe in detail the precise couplings to these particles to establish the underlying model and pinpoint the exact mechanism of EW symmetry breaking. Charged Higgs particles exist even in extensions of the SM which involve the introduction of a $SU(2)$ triplet of scalars, which are also interesting from the point of view of obtaining a small Majorana mass for neutrinos in the type-II see-saw mechanism [98]. It is possible to produce a single top quark in association with a charged Higgs in such models. We study, in this work, such a process in the context of a type II THDM or SUSY models, where the up-type quarks couple to one of the Higgs doublets and down- type quarks couple to the other Higgs doublet [95].

In this chapter, we investigate top polarization in the single production of the top in association with a charged Higgs of the type II THDM or the MSSM. Single-top production in association with a charged Higgs can be used to probe the size and nature of the tbH coupling in the type II THDM. Apart from the cross section, the angular distribution of the top, and even the polarization of the top would give additional information enabling the determination of the tbH coupling. Here we concentrate on the polarization of the top in the process, which would be a measure of the extent of parity violation in the couplings. It will be seen that polarization gives a handle on the combination $A_L^2 - A_R^2$ of the left-handed and right-handed couplings, $A_L \equiv m_t \cot\beta$ and $A_R \equiv m_b \tan\beta$ of the charged Higgs to the top, where $\tan\beta$ is the ratio of the vacuum expectation values (vevs) of the Higgs doublets, in contrast to the combination $A_L^2 + A_R^2$ measured by the cross section or angular distribution.

As stated earlier, the angular distribution of the charged lepton has a special property $-$ it is independent of new physics in the tbW decay vertex, to linear order in the anomalous couplings, and is thus a pure probe of new physics in top production alone. We show that the azimuthal distribution of the lepton is sensitive to top polarization and can be used to probe the coupling parameter $\tan\beta$ in the type II THDM. This approach has been recently used to probe new physics in the case of top pair production in a model with an extra heavy vector resonance (Z') with chiral couplings [51]. The effects of top polarization in tW and tH^- production have been studied previously in [77], where the effects of 1-loop electroweak SUSY corrections have been considered; however, they do not consider top decay. Top polarization in different modes of single top production has also been studied in [99], where spin sensitive variables are used to analyze effective left- and right-handed couplings of the top coming from BSM physics.

6.1 Two-Higgs Doublet Model of Type II

The Higgs sector of the SM can be minimally extended by including another Higgs doublet which is a replica of the first doublet, so that the modified Higgs sector contains two Higgs doublets with the same quantum numbers

$$\Phi_1 = \begin{pmatrix} \phi_1^+ \\ \phi_1^0 \end{pmatrix}, \qquad \Phi_2 = \begin{pmatrix} \phi_2^+ \\ \phi_2^0 \end{pmatrix}, \tag{6.1}$$

with hypercharges $Y_1 = Y_2 = 1$. In general, both doublets could acquire vev,

$$\langle\Phi_1\rangle = \frac{v_1}{\sqrt{2}}\ ;\ \langle\Phi_2\rangle = \frac{v_2}{\sqrt{2}}. \tag{6.2}$$

Depending on how these Higgs doublets couple to the up and the down sectors of quarks and leptons, there can be four different types of THDM. In this chapter, we focus top-charged Higgs production in the type II THDM.

In the type II THDM, one Higgs doublet, say Φ_1 couples to the down sector of fermions while the other Higgs doublet i.e., Φ_2 couples to the up sector. The Lagrangian for the Yukawa sector can be written as :

$$-\mathcal{L}_Y = \mathcal{Y}^U_{ij}\bar{Q}_{iL}\tilde{\Phi}_2 U_{jR} + \mathcal{Y}^D_{ij}\bar{Q}_{iL}\Phi_1 D_{jR} + h.c., \tag{6.3}$$

In the expanded form when written in terms of mass eigenstates, it is:

$$\begin{aligned}
-\mathcal{L}_Y &= \frac{g}{2m_W\cos\beta}\bar{D}M_D D\left[\cos\alpha H^0 - \sin\alpha h^0\right] - \frac{ig\tan\beta}{2m_W}\bar{D}M_D\gamma_5 D A^0 \\
&+ \frac{g}{2M_W\sin\beta}\bar{U}M_U U\left[\sin\alpha H^0 + \cos\alpha h^0\right] - \frac{ig\cot\beta}{2m_W}\bar{U}M_U\gamma_5 U A^0 \\
&+ \frac{g}{\sqrt{2}m_W}\bar{U}\left[\cot\beta M_U P_L + \tan\beta M_D P_R\right] D H^+ + h.c.
\end{aligned} \tag{6.4}$$

where $\tan\beta$ is the ratio of vevs of two Higgs doublets i.e., $\tan\beta = v_2/v_1$, and α is the mixing angle of CP-even Higgs bosons.

6.2 Top polarization in the two Higgs doublet model

We consider the process of single-top production in association with a charged Higgs in the type II THDM or the MSSM. For our purposes, the model is completely characterized by two parameters, the mass of the charged Higgs M_{H^-} and the ratio of the vacuum expectation values of the Higgs doublets $\tan\beta$. At the parton level, single-top production proceeds via

$$g(p_1)\, b(p_2) \to t(p_3, \lambda_t) H^-(p_4), \tag{6.5}$$

where $\lambda_t = \pm 1$ is the sign of the helicity of the top. The tree level s and t channel diagrams contributing to the above process are shown in Fig. 6.1.

As mentioned in Chapter 4, a study of top polarization using angular distributions of the top decay products requires computing the spin density matrix for top

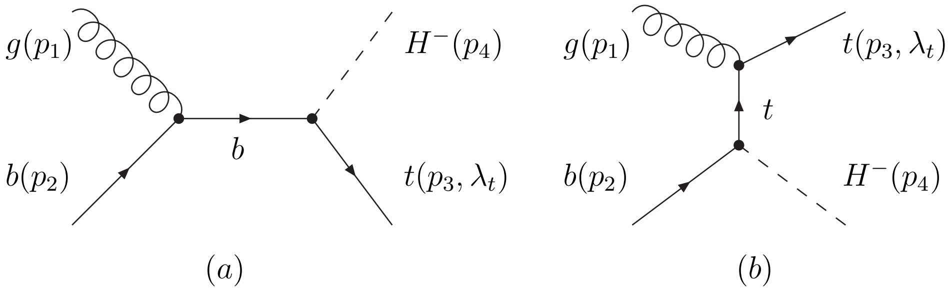

Figure 6.1: *Feynman diagrams contributing to the top charged-Higgs production at the LHC.*

production and decay. We have obtained simple analytic expressions for the top production density matrix. In the type II THDM the tbH^- coupling is

$$g_{tbH^-} = \frac{g}{\sqrt{2}m_W}(m_t \cot\beta P_L + m_b \tan\beta P_R), \tag{6.6}$$

where g is the $SU(2)$ gauge coupling and P_L and P_R are the left and right handed projection operators respectively, $P_{L,R} = (1 \mp \gamma^5)/2$. One can immediately see that at $\tan\beta = \sqrt{m_t/m_b}$, the pseudoscalar part of the coupling, which is proportional to γ^5, vanishes and the coupling (6.6) is purely scalar. Since polarization is parity violating we expect that the polarized cross section (4.4) should vanish for this value of $\tan\beta$ and we indeed find this to be the case, as will be shown later in Fig. 6.3.

Denoting the energy, momentum and scattering angle of the top in the parton center-of-mass (cm) frame by E_t, p_t and θ_t respectively and the parton level Mandelstam variable by $\hat{s}$, the diagonal elements of the top-production density matrix are given by

$$\rho(+,+) = F_1\, m_t^2 \cot^2\beta + F_2\, m_b^2 \tan^2\beta \tag{6.7}$$

$$\rho(-,-) = F_2\, m_t^2 \cot^2\beta + F_1\, m_b^2 \tan^2\beta, \tag{6.8}$$

where F_1 and F_2 are defined by

$$\begin{aligned}
F_1 &= \left(\frac{gg_s}{2m_W}\right)^2 \frac{1}{6\sqrt{\hat{s}}(E_t - p_t\cos\theta_t)^2}\Big\{p_t^2(E_t+p_t)\sin^2\theta_t\cos^2\frac{\theta_t}{2} \\
&+ \big[4E_t(E_t+p_t)(E_t-\sqrt{\hat{s}}) - pt + 2m_t^2\sqrt{\hat{s}} + (\hat{s}(E_t+p_t) \\
&+ m_t^2(E_t-p_t) - 4m_t^2E_t)\big]\sin^2\frac{\theta_t}{2}\Big\} \qquad (6.9) \\
F_2 &= \left(\frac{gg_s}{2m_W}\right)^2 \frac{1}{6\sqrt{\hat{s}}(E_t - p_t\cos\theta_t)^2}\Big\{p_t^2(E_t-p_t)\sin^2\theta_t\sin^2\frac{\theta_t}{2} \\
&+ \big[4E_t(E_t-p_t)(E_t-\sqrt{\hat{s}}) - pt + 2m_t^2\sqrt{\hat{s}} + (\hat{s}(E_t-p_t) \\
&+ m_t^2(E_t+p_t) - 4m_t^2E_t)\big]\cos^2\frac{\theta_t}{2}\Big\}. \qquad (6.10)
\end{aligned}$$

The off-diagonal elements are

$$\begin{aligned}
\rho(+,-) = \rho(-,+) = -\left(\frac{gg_s}{2m_W}\right)^2 \frac{1}{6\sqrt{\hat{s}}(E_t - p_t\cos\theta_t)^2}(m_t^2\cot^2\beta - m_b^2\tan^2\beta) \\
\times\, m_t\sin\theta_t(2E_t\sqrt{\hat{s}} - m_t^2 - \hat{s} + p_t^2\sin^2\theta_t). \qquad (6.11)
\end{aligned}$$

In deriving the above expressions we have neglected the kinematic effects of the b-quark mass but kept factors of m_b occurring in the tbH^- coupling (6.6). Analytic expressions for the helicity amplitudes for associated tH^- production can be found in [77], where a similar convention for retaining factors of m_b is used; our density matrix elements (6.8) and (6.11), obtained by an independent method, agree with those obtained using the helicity amplitudes of [77]. A plot of the cross section as a function of the coupling $\tan\beta$ is shown in Fig. 6.2 for various values of charged Higgs masses. We show the cross section for two different centre of mass energies of 7 TeV and 14 TeV and have used the leading-order PDF sets of CTEQ6L1 [100]. We see that the cross sections have a similar profile for various M_{H^-} values and fall sharply for larger M_{H^-}. The cross sections are proportional to $(m_t^2\cot^2\beta + m_b^2\tan^2\beta)$, which is minimized for $\tan\beta = \sqrt{\frac{m_t}{m_b}} \simeq 6.41$, independent of the cm energy and the value of M_{H^-}. This can indeed be seen from Fig. 6.2. Here we have taken the top mass to be 172.6 GeV and have evaluated the PDF's at the same scale.

The tbH^- vertex has a scalar-pseudoscalar $(A + B\gamma^5)$ chiral structure which is different from vector-axial vector coupling of the tbW and $t\bar{t}Z^0$ vertices. One thus expects a very different longitudinal polarization asymmetry given by Eqn. (4.4) for top charged-Higgs production compared to $t\bar{t}$ production, and for the closely

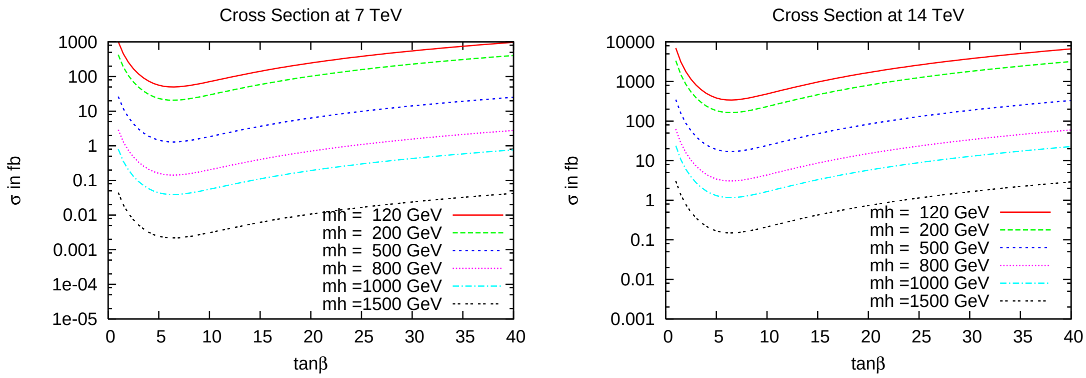

Figure 6.2: *The cross section for top charged-Higgs production at LHC for two different cm energies, 7 TeV (left) and 14 TeV (right), as a function of* $\tan\beta$ *for various charged Higgs masses.*

related process of associated tW production in the SM proceeding via $gb \to tW$. For SM tW production we find the longitudinal polarization to be $P_t \simeq -0.25$; for $t\bar{t}$ production it is $\mathcal{O}(-10^{-4})$. The very small value of P_t for top pair production in the SM is because the dominant contribution for both $gg \to t\bar{t}$ and $q\bar{q} \to t\bar{t}$ comes from chirality conserving s-channel gluon exchange processes, resulting in the production of largely unpolarized tops. These values of P_t have also been calculated in [50], where top polarization effects for top-slepton production in R-parity violating SUSY was considered. We show the polarization asymmetry for tH^- production in Fig. 6.3 as a function of $\tan\beta$ for both $\sqrt{s} = 7$ and 14 TeV. In

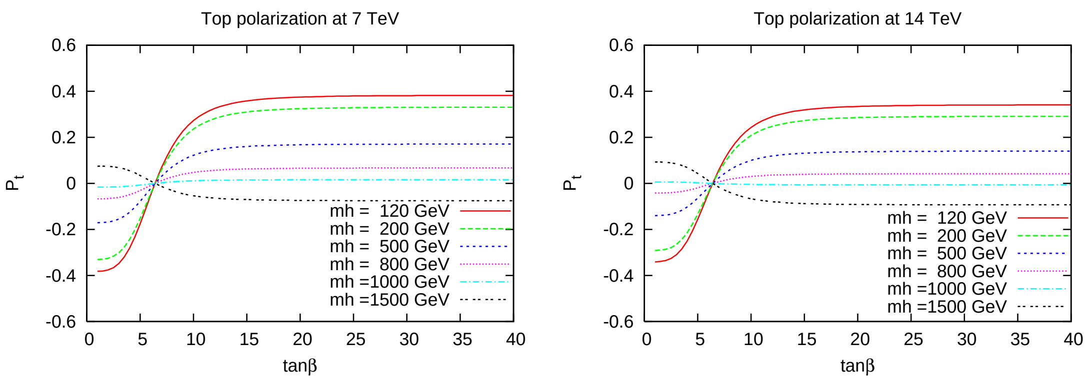

Figure 6.3: *The polarization asymmetries for top charged-Higgs production at LHC for two different cm energies, 7 TeV (left) and 14 TeV (right), as a function of* $\tan\beta$ *for various charged Higgs masses.*

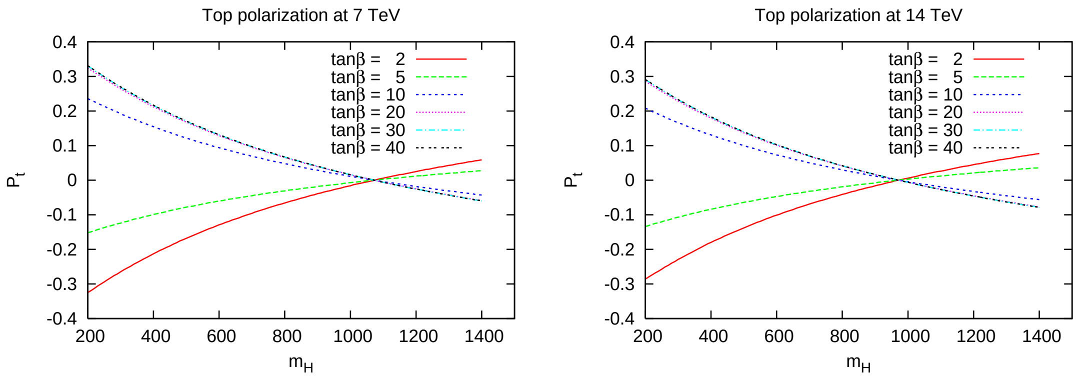

Figure 6.4: *The polarization asymmetry for top charged-Higgs production at LHC for a cm energy of 7 TeV (left) and 14 TeV (right), as a function of M_{H^-} for various* $\tan\beta$ *values.*

contrast to the related case of top-slepton production considered in [50] where P_t was found to be independent of the R-parity violating SUSY $tb\tilde{l}$ coupling, here P_t does have an interesting dependence on $\tan\beta$. As mentioned previously, we notice the interesting feature that the polarization vanishes at $\tan\beta = \sqrt{\frac{m_t}{m_b}}$ for all M_{H^-} and $\hat{s}$, as expected from the vanishing of the chiral part of the coupling (6.6) at this $\tan\beta$ value, the same value for which the cross sections are minimized. The curves change sign at this point and saturate rapidly for larger $\tan\beta$ values.

A plot of P_t vs the charged Higgs mass for various values of $\tan\beta$ is shown in Fig. 6.4, for $\sqrt{s} = 7$ and 14 TeV. We notice that the polarization asymmetry vanishes for a charged Higgs mass close to 1100 GeV for $\sqrt{s} = 7$ TeV and around 1000 GeV for the 14 TeV case, for all $\tan\beta$, and changes sign as M_{H^-} is increased. This can be understood as follows. In the expression for the polarization asymmetry $P_t \propto \rho(+,+) - \rho(-,-)$, the angular integrals can be done analytically. Since the parton distributions of the gluon and the b quark peak at low x, the remaining PDF integrals over the momentum fractions of the gluon and b are dominated at low x, i.e, at the threshold for top charged-Higgs production. One can show that the expressions for P_t, expanded in powers of the top momentum p_t (i.e, evaluated close to $\hat{s} = (m_t + M_{H^-})^2$), vanishes for $M_{H^-} = 6m_t \simeq 1035.6$ GeV at leading order in p_t, for all $\tan\beta$, in reasonable agreement with Fig. 6.4. Of course, one cannot get an exact analytic expression for M_{H^-} when P_t vanishes without doing the numerical integrals over the gluon and b quark PDF's. Still, the above argument, which is independent of the cm energy of the colliding protons, is useful for understanding why the polarization vanishes close to $M_{H^-} \simeq 1000$ GeV for both $\sqrt{s} = 7$ and 14 TeV.

The important point to note is that the magnitude and sign of these asymmetries are sensitively dependent on M_{H^-} and $\tan\beta$ values and are significantly different from the case of tW and $t\bar{t}$ production, because of the different chiral structure of the tbW vertex.

6.3 Azimuthal distributions of decay leptons

As mentioned in previous sections, the top quark decays rapidly and its properties have to be deduced from its decay products. The top polarization can be determined by the angular distribution of its decay products using Eqn. (1.66). The lab frame polar distribution of the lepton is independent of the anomalous tbW decay vertex. However, we find that it is not sensitive to model parameters and is largely indistinguishable from the tW case in the SM.

As shown in [76] and references therein, the azimuthal angle of the decay lepton in the lab frame is sensitive to the top polarization and independent of possible new physics in the tbW decay vertex and is thus a convenient probe. The lepton azimuthal angle ϕ_ℓ is defined with respect to the top production plane chosen as the $x - z$ plane, with the beam direction as the z axis and the convention that the x component of the top momentum is positive. Since at the LHC, one cannot uniquely define a positive direction of z axis, the lepton azimuthal distribution is identical for ϕ_l and $2\pi - \phi_l$ and is symmetric around $\phi_l = \pi$.

The ϕ_ℓ distribution for a pure, i.e, 100% positively or negatively polarized top quark ensemble is obtained by using only the $(+,+)$ or $(-,-)$ density matrix elements respectively in Eqn. (4.7). This is, of course, expected to be different from that for an ensemble with a partial degree of polarization P_t. In computing the ϕ_ℓ distributions we have taken into account the full spin coherence effects of the top encoded in the diagonal and off-diagonal elements of the production and decay spin density matrices.

With the above choice of frame, the normalized lepton azimuthal distributions for $\sqrt{s} = 7$ TeV are shown in Fig. 6.5 for small and large values of $\tan\beta$, for various M_{H^-} values. The corresponding plots for a cm energy of 14 TeV is shown in Fig. 6.6. The ϕ_ℓ distribution for tW^- production in the SM is also shown for comparison.

The ϕ_ℓ distributions for other values of $\tan\beta$ and M_{H^-} have a similar profile,

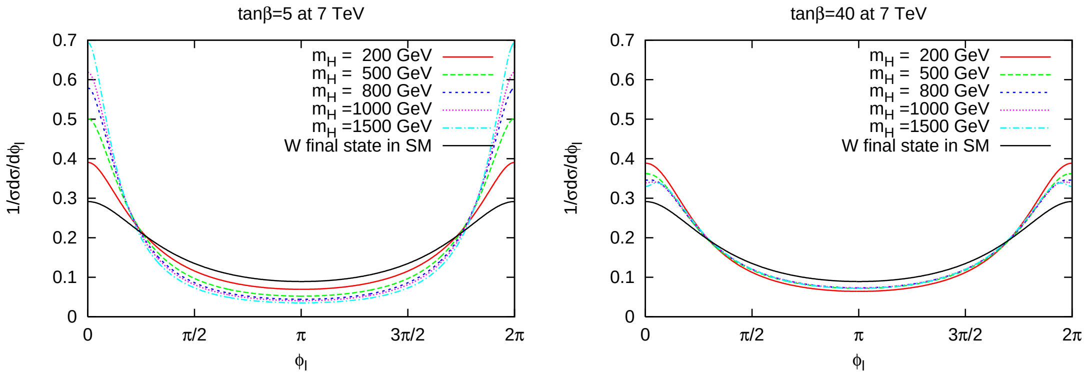

Figure 6.5: *The normalized lepton azimuthal distribution for* $\tan\beta = 5$ *(left) and* $\tan\beta = 40$ *(right) for various charged Higgs masses at a cm energy of 7 TeV.*

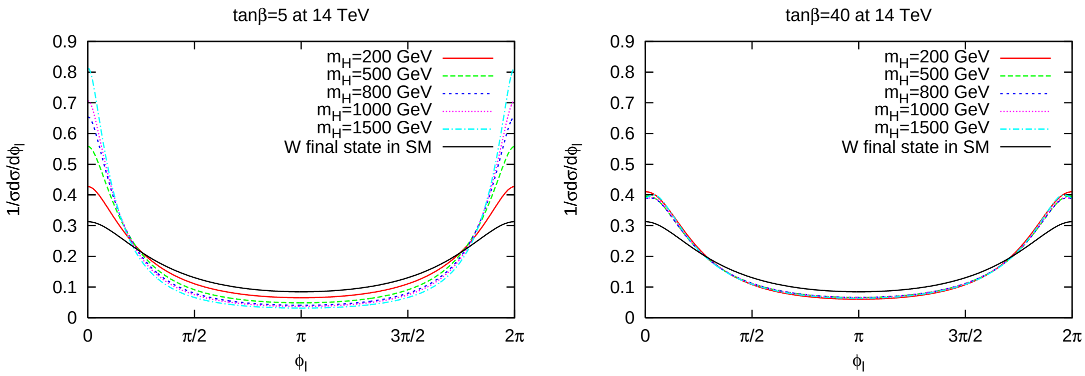

Figure 6.6: *The normalized lepton azimuthal distribution for* $\tan\beta = 5$ *(left) and* $\tan\beta = 40$ *(right) for various charged Higgs masses at a cm energy of 14 TeV.*

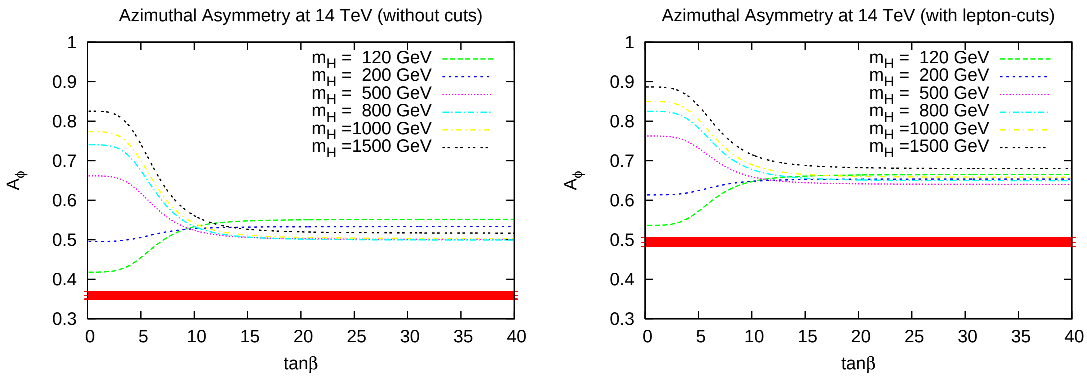

Figure 6.7: *A_ϕ as a function of* $\tan\beta$ *and different charged Higgs masses at* $\sqrt{s} = 14$ *TeV without lepton cuts (left) and with cuts (right). The red band corresponds to the azimuthal asymmetry for tW production in the SM with a 2σ error interval.*

with a peak at $\phi_\ell = 0$ and 2π. The ϕ_ℓ distribution depends on both kinematic and top polarization effects and the factors which influence its shape have been explained in chapter 4. The angular distribution of the charged lepton coming from top decay in any generic top-production process is written in parton cm frame in Eqn. 4.13 with the angular parts described by Eqs. 4.14 and 4.15. The rest-frame forward (backward) peak corresponds to a peak for $\cos\theta_{t\ell} = \pm 1$, as seen from the factor $(1 \pm \cos\theta_{t\ell})$ in the numerator of Eqn. 4.14. This is the effect of polarization. The kinematic effect is seen in the factor $(1 - \beta_t \cos\theta_{t\ell})^3$ in the denominator of Eqns. 4.14 and 4.15, which again gives rise to peaking for large $\cos\theta_{t\ell}$. Eqn. 4.15 therefore implies peaking for small ϕ_ℓ. This is borne out by the numerical results.

We notice that the curves are separated at the peaks for different M_{H^-} values and are very different from the tW case in the SM. As in [51, 76, 101, 102], we can quantify this difference by defining a normalized azimuthal asymmetry for the lepton as

$$A_\phi = \frac{\sigma(\cos\phi_\ell > 0) - \sigma(\cos\phi_\ell < 0)}{\sigma(\cos\phi_\ell > 0) + \sigma(\cos\phi_\ell < 0)}, \tag{6.12}$$

where the denominator is the total cross section. Plots for A_ϕ as a function of $\tan\beta$ with and without cuts on the lepton momenta are shown in Fig. 6.7 for a cm energy of 14 TeV. We have used the following rapidity and transverse momentum acceptance cuts on the decay lepton: $|\eta| < 2.5$, $p_T^\ell > 20$ GeV. Also shown is the SM value for A_ϕ for tW production with a 2σ error band.

The lepton cuts only mildly increase the value of A_ϕ for the charged Higgs case and the value for tW production in the SM is also enhanced from about

0.35 without cuts to about 0.5 with cuts, as can been seen from Fig. 6.7. The azimuthal asymmetry also shows considerable variation, as a function of $\tan\beta$, roughly in the range $3 \lesssim \tan\beta \lesssim 15$ and becomes flat for values outside this range and almost independent of M_{H^-}. From Fig. 6.3, we see that this is the same range of $\tan\beta$ for which the polarization P_t shows variation, becoming constant for roughly $\tan\beta > 15$; thus, the azimuthal asymmetry follows the same trends as the top polarization. If the mass of the charged Higgs is known, from a measurement of A_ϕ it would be easier to determine $\tan\beta$ if it lies within this range.

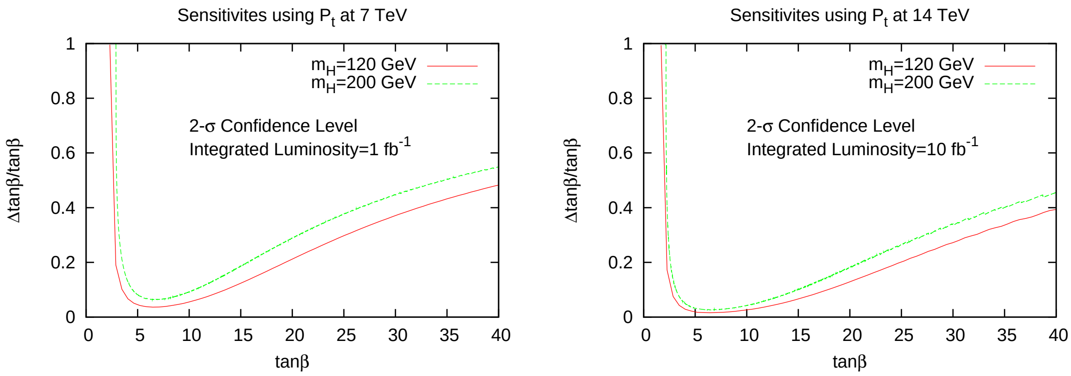

Figure 6.8: *The fractional accuracy of* $\tan\beta$ *at* 2σ *CL as a function of* $\tan\beta$ *for* $\sqrt{s} = 7$ *TeV (left) and 14 TeV (right) using the polarization* P_t*, with* $\int \mathcal{L}dt = 1$ *fb*$^{-1}$ *and* 10 *fb*$^{-1}$ *respectively.*

We now investigate the accuracy to which one can determine $\tan\beta$ from the top polarization, P_t, and the azimuthal asymmetry A_ϕ. The accuracy of the determination of parameter $\tan\beta$ at $\tan\beta_0$, from the measurement of an observable $O(\tan\beta)$, is $\Delta\tan\beta$ if $|O(\tan\beta) - O(\tan\beta_0)| < \Delta O(\tan\beta_0)$ for $|\tan\beta_0 - \tan\beta| < \Delta\tan\beta$, where $\Delta O(\tan\beta_0)$ is the statistical fluctuation in O at an integrated luminosity $\mathcal{L}$. The corresponding fractional accuracy is then $\Delta\tan\beta/\tan\beta_0$. For top-polarization, P_t and azimuthal asymmetry, A_ϕ, the statistical fluctuations at a level of confidence f are given by $\Delta O = f/\sqrt{\mathcal{L}\sigma} \times \sqrt{1 - O^2}$, where O denotes P_t or A_ϕ.

In Fig. 6.8, we show the fractional accuracy $\Delta\tan\beta/\tan\beta$ in the determination of the coupling $\tan\beta$ from the polarization P_t at the 2σ confidence level (CL). We choose, for illustration, charged Higgs masses of 120 and 200 GeV and an integrated luminosity of 1 fb^{-1} and 10 fb^{-1} for $\sqrt{s} = 7$ and 14 TeV respectively. We use, for convenience, the criterion $\Delta\tan\beta/\tan\beta < 0.3$ for an accurate determination of

$\tan\beta$ since this corresponds to a relative accuracy of about 1% in the determination of physical quantities, which are proportional to the square of the couplings.

Then, we see that at $\sqrt{s} = 7$ TeV, $\tan\beta$ can be determined accurately for values between roughly 3 and 25 for $M_{H^-} = 120$ GeV and between 3 and 20 for $M_{H^-} = 200$ GeV. The corresponding range for $\tan\beta$ determination for the LHC running at 14 TeV are 3 to 30 for $M_{H^-} = 120$ GeV and 3 to 25 for $M_{H^-} = 200$ GeV. For larger $\tan\beta$ (and even for very low $\tan\beta$) the sensitivity worsens since the P_t curves become flat and do not show much variation as a function of $\tan\beta$, as can be seen from Fig. 6.3. One can, of course, choose a different value for $\Delta\tan\beta/\tan\beta$ as a measure of $\tan\beta$ accuracy in which case the corresponding limits on $\tan\beta$ will be different as can be read from the plots.

We now consider the accuracy to which $\tan\beta$ can be determined from the more conveniently measurable azimuthal asymmetry. Plots of the fractional accuracy for this case are shown in Fig. 6.9 and Fig. 6.10 for the cases of $\sqrt{s} = 7$ TeV and 14 TeV respectively and with the indicated charged Higgs masses and luminosities. If we use the same criterion for $\tan\beta$ accuracy as before, $\Delta\tan\beta/\tan\beta < 0.3$,

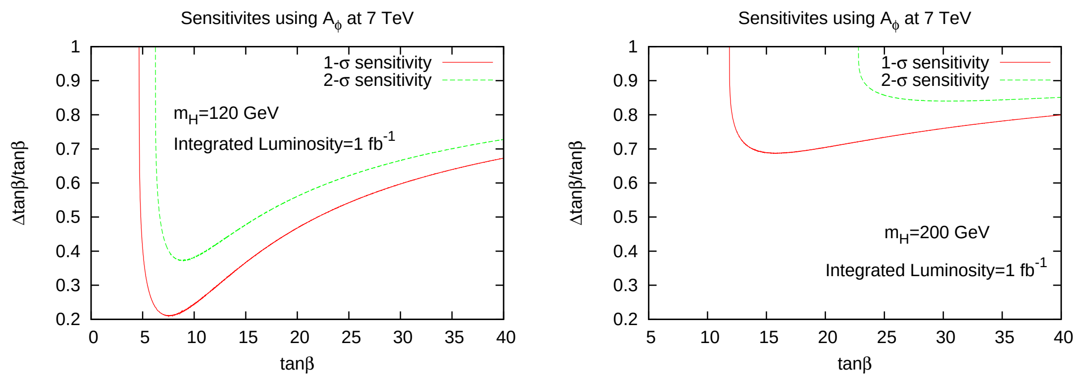

Figure 6.9: *The fractional accuracy of* $\tan\beta$ *as a function of* $\tan\beta$ *for* $\sqrt{s} = 7$ *TeV using the azimuthal asymmetry* A_ϕ *for* $M_{H^-} = 120$ *GeV (left) and* $M_{H^-} = 200$ *GeV (right).*

we notice that for a cm energy of 7 TeV and an integrated luminosity of 1 fb^{-1}, the azimuthal asymmetry is not a very sensitive measure of $\tan\beta$. For the lower charged Higgs mass of 120 GeV, and at the 1σ CL, $\tan\beta$ can be probed roughly in the range 6 to 12; the sensitivity worsens for larger charged Higgs masses or CL's. Top polarization is a better probe of $\tan\beta$ than the azimuthal asymmetry. However, this is due to the fact that in constructing the asymmetry only the semi-

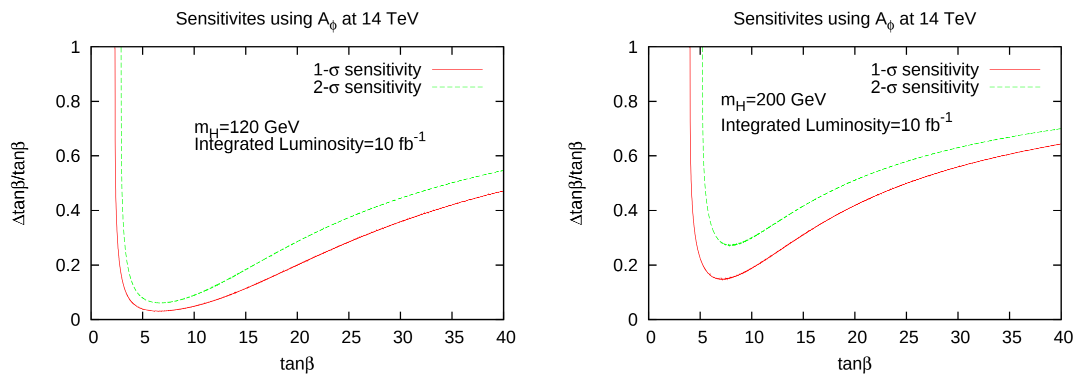

Figure 6.10: *The fractional accuracy of* $\tan\beta$ *as a function of* $\tan\beta$ *for* $\sqrt{s} = 14$ *TeV using the azimuthal asymmetry* A_ϕ *for* $M_{H^-} = 120$ *GeV (left) and* $M_{H^-} = 200$ *GeV (right).*

leptonic decay modes of the top have been considered, which reduces the cross section by a factor of 3. The sensitivities are considerably enhanced if we include all decay channels of the top. But it must be remembered that using any decay product of the top other than ℓ^+ and $\bar{d}$ to construct the azimuthal asymmetry will make A_ϕ dependent on new physics in the tbW vertex. For the LHC running at $\sqrt{s} = 14$ TeV, A_ϕ is a more sensitive measure of $\tan\beta$ compared to the 7 TeV case, at least for the lower charged Higgs mass of 120 GeV. For this case $\tan\beta$ can be probed in the range 3 to 25 at the 1σ CL and between 3 and 20 at a 2σ CL. For $M_{H^-} = 200$ GeV, A_ϕ is sensitive to $\tan\beta$ only at the 1σ CL for a smaller range of 5 to 15.

As is to be expected, $\tan\beta$ can be determined to a higher accuracy and for a larger range using the top polarization P_t, compared to the azimuthal asymmetry constructed from the decay lepton; the restriction to semi-leptonic decay modes of the top further reduces the sensitivity to A_ϕ. However, it is interesting to note that the profile of the plots of $\Delta\tan\beta/\tan\beta$ vs $\tan\beta$ computed by using A_ϕ, shown in Fig. 6.9 and 6.10, is similar to that obtained by using the polarization P_t, shown in Fig. 6.8. A_ϕ follows the change in P_t as a function of the coupling $\tan\beta$ and is thus a faithful probe of the top polarization itself. At least for $\sqrt{s} = 14$ TeV and $M_{H^-} = 120$ GeV, the range in which $\tan\beta$ can be probed accurately using A_ϕ or P_t is roughly similar for both variables.

Thus, the azimuthal asymmetry can be a convenient and sensitive probe of both the top polarization and the coupling parameter $\tan\beta$ in the THDM, at least in the regions of parameter space mentioned above.

6.4 Backgrounds and Next-to-leading order corrections

It is worthwhile to comment on the dominant backgrounds to our signal process $gb \to tH^- \to t\bar{t}b$. When $M_{H^-} > m_t + m_b$, we require the top to decay semi-leptonically and the anti-top to decay hadronically to trigger on the charged Higgs signal, as well as for the purpose of reconstruction of the top quarks and the charged Higgs. The complete final state therefore consists of 3 b jets + 2 light jets + 1 lepton + missing energy. The main background for this signal would come from next-to-leading order NLO QCD processes, which are (a) $gg \to t\bar{t}b\bar{b}$, (b) $gb \to t\bar{t}b$, and (c) $gg \to t\bar{t}g$, where in the first case, one of the b jets is missed and in the last case the gluon jet is mis-tagged as a b jet (with probability of around 1%). Refs. [103, 104, 105] have investigated the charged-Higgs signal in this process in great detail for the LHC with triple b-tagging. They have used kinematical cuts of $p_T > 30$ GeV and $|\eta| < 2.5$ for all jets and assume b-tagging efficiency of 40% in their analysis. The conclusion from their analysis for 30 fb^{-1} of accumulated data is that there are enough number of events for charged Higgs discovery in this channel at the 5-σ level upto a mass of 600 GeV for very large values of $\tan\beta$ (> 25) and very small values of $\tan\beta$ (< 5). We can expect better visibility for the charged Higgs when the b-tagging efficiency increases in future. Backgrounds from weak processes like $tW + X$, $b\bar{b} + X$ and $W + 2j$ would be suppressed because we choose the signal to consist of 3 b jets and an isolated lepton.

When $M_{H^-} < m_t + m_b$, the dominant decay of the H^- is into $\tau + \bar{\nu}_\tau$. Our signal in this will be $gb \to tH^- \to t\tau^-\bar{\nu}_\tau \to b\ell^+\nu_\ell\tau^-\bar{\nu}_\tau$. For this final state of b + lepton + τ + missing energy, the background now comes from the processes of $t\bar{t}$ production with the $\bar{t}$ decaying into a τ and tW^- production with W^- decaying into a τ. In both these cases, since the τ comes from W^- decay, τ polarization can be used to suppress the background [106]. While the presence of two neutrinos in the final state would seem to make it impossible to reconstruct the top production plane needed for our analysis, we are helped by the fact that the tH^- events are produced close to the threshold because of the sharp peaking of the initial-state partons at low x. Thus it is a reasonable approximation to treat the top quark and the charged Higgs as at rest, enabling approximate determination of the energy and momenta of both neutrinos on an event-by-event basis.

The NLO QCD corrections to the process $gb \to tH^-$ have been studied in Refs. [107, 108] and next-to-next-to-leading-order (NNLO) soft gluon corrections have been evaluated in Ref. [109]. These corrections are shown to be substantial, upto 85% of the LO cross section for large Higgs masses. It has been also shown that the K-factor in this process is proportional to the mass of charged Higgs and do not depend on $\tan\beta$. As QCD corrections are model independent, one can use the K-factor appropriately in the analysis to rescale the LO result to the NLO order. The normalized differential cross sections and the asymmetries we calculate would be insensitive to the higher order corrections. We have not used any K-factor in our analysis. Including NLO QCD corrections through the naive use of K-factor would increase our signal cross section by a factor of 1.5-1.85 depending upon the charged Higgs mass and hence sensitivity to the parameters would increase.

The complete NLO EW calculations for the process $gb \to tH^-$ have been done in Ref. [110] for type II 2HDM. They have reported that the NLO EW correction to the total cross section is very mild. It varies from less than 1% for low values of $\tan\beta$ to less than 4% for higher values of $\tan\beta$. The effects of NLO EW corrections to observables like top polarization, normalized angular distributions and angular asymmetries are expected to be small. For example, in Ref. [77], it has been shown that NLO EW supersymmetric effects on top polarization is almost zero for all values of charged Higgs masses and all values of $\tan\beta$ except for $\tan\beta \approx 10$, for which correction is around -1% to -3%.

Any NLO corrections to top decay will not affect our analysis of charged-lepton angular distributions and asymmetries as it has been proven that charged-lepton angular distributions are independent of any corrections to form factors in top decay. There can also be NLO corrections from non-factorizable diagrams. However, this analysis has not been done in the literature so far and it would be interesting to see the effect of these non-factorizable diagrams to our analysis which is beyond the scope of this work.

6.5 Summary

We have studied the issue of using the polarization of the top quark produced in association with a charged Higgs in the type II THDM or SUSY models as a probe of the coupling parameter $\tan\beta$ occurring in such models. Since the top decays before it has the time to hadronize, its polarization, reflected in the angular distribution of its decay products, can be a probe of new physics underlying its production. We have derived analytic expressions for left and right polarized tH^- production (and the off-diagonal elements as well in the spin density matrix). Essentially because of the scalar-pseudoscalar coupling (6.6) of the tbH^- vertex, compared to the vector-axial vector couplings of the top in the SM, the resulting polarizations are vastly different from that expected in the SM and are sensitively dependent on the charged Higgs mass and $\tan\beta$, as shown in Figs. 6.3 and 6.4, where we considered both the cm energies of 7 and 14 TeV at which the LHC is planned to run. The degree of longitudinal top polarization can be as large as 0.3 to 0.4 (for a charged Higgs mass of 120 GeV and for $\tan\beta$ values less than 5 and greater than 10), compared to the SM values of -0.25 for tW production or $\mathcal{O}(-10^{-4})$ for $t\bar{t}$ production. Characteristic of the tbH^- coupling in the THDM, the $2 \to 2$ top production cross sections are minimized and the polarizations vanish and change sign as a function of $\tan\beta$ at $\tan\beta = \sqrt{\frac{m_t}{m_b}}$.

We then investigated to what extent top polarization is reflected in the angular distribution of the decay lepton in the process $t \to bW^+ \to b\nu_\ell \ell^+$, with inclusive decay of the b and H^-. Since it is known that the laboratory frame angular distributions of the charged lepton in top decay depends only on the top production process and are independent of new physics in the tbW vertex, we considered the azimuthal distribution of the lepton from top decay, A_ϕ, as a probe of new physics in its production (we find the polar distribution of the lepton in the THDM insensitive to $\tan\beta$ and the charged Higgs mass and almost identical to tW production in the SM). A_ϕ is sensitive to $\tan\beta$ values roughly in the range $3 \lesssim \tan\beta \lesssim 15$, for different charged Higgs masses considered and becomes constant for larger $\tan\beta$ values. This is the same range in which the top polarization shows variation as a function of $\tan\beta$; A_ϕ thus captures the dependence of P_t on $\tan\beta$. If the charged Higgs mass is already known, a measurement of A_ϕ can help measure $\tan\beta$ if it lies in the above range.

We also computed the fractional accuracy to which $\tan\beta$ can be measured, as a function of $\tan\beta$, from the top polarization P_t and a measurement of the azimuthal asymmetry A_ϕ. Using the criterion that $\Delta\tan\beta/\tan\beta < 0.3$ for an accurate determination of $\tan\beta$, we find that P_t can help determine $\tan\beta$ lying in the range between 3 and 25 for a cm energy of 7 TeV and between 3 and 30 for the 14 TeV case, at the 2σ CL for $M_{H^-} = 120$ GeV; the range is only slightly smaller for a larger M_{H^-} of 200 GeV. While the azimuthal asymmetry is not very sensitive to an accurate measurement of $\tan\beta$ for the LHC running at 7 TeV, we find that at 14 TeV one can use the azimuthal asymmetry to probe $\tan\beta$ up to 25 at the 1σ CL and for $M_{H^-} = 120$ GeV; for $M_{H^-} = 200$ GeV the corresponding range is 5 to 15. Including both leptonic and hadronic decay modes of the top is expected to increase the sensitivity of the azimuthal asymmetry to $\tan\beta$; however, this renders the asymmetry sensitive to new physics in the tbW decay vertex, apart from new physics in top production.

The sensitivity plot for $\tan\beta$ determination using A_ϕ follows roughly the one obtained by using P_t. Thus, the azimuthal asymmetry of the decay lepton can be a convenient and accurate probe of the top polarization and the coupling parameter $\tan\beta$ of the THDM or SUSY models for the LHC running at $\sqrt{s} = 14$ TeV and for smaller charged Higgs masses.

Chapter 7

Summary

The Standard Model (SM) has been extremely successful in explaining the fundamental interactions among elementary particles: quarks and leptons. Quarks interact through electroweak and color interactions while leptons interact only through electroweak interactions. However, some aspects of the SM have not been fully established yet. For example, the electroweak symmetry breaking (EWSB) sector of the SM remains untested yet. The central pillar of the EWSB, known as the Higgs, has not been discovered so far. That is why the most important goal of the current and future colliders like the Large Hadron Collider (LHC) at CERN, International Linear Collider (ILC) and Compact Linear Collider (CLIC) is to discover the Higgs and study its properties with great precision so as to ascertain it to be the SM Higgs as different alternate scenarios beyond the SM (BSM) allow for a number of Higgs particles e.g., Minimal Supersymmetric Standard Model (MSSM), Two Higgs Doublet Model (THDM) etc. Also, the top quark, because of its large mass (close to EWSB scale), is considered to be a window to probe the EWSB. In this thesis, we study Higgs boson and top quark couplings in various scenarios and at different colliders to probe the EWSB utilizing the polarization of the final state top quark at the LHC and the polarization of the initial beams at the ILC.

In the first two chapters of the thesis, we study anomalous ZZH and γZH couplings in the process $e^+e^- \to ZH$ at the ILC with polarized beams. We consider both electron and positron beams to be polarized simultaneously and have studied longitudinal and transverse polarization of the beams separately. We assume all anomalous couplings to be complex and consider their real and imaginary parts to be independent parameters. Our main emphasis in this work is to obtain simultaneous limits on the couplings to the extent possible making use of combination of the observables and/or polarizations. We study angular distributions of the Z using both longitudinally as well as transversely polarized beams and construct various asymmetries. We also study the angular correlations of the charged leptons coming from Z-decay. Using the momenta of the charged leptons, we construct various correlations having definite CP and T transformation properties which thence probe the couplings having the same transformation properties under CP and T. We find that the longitudinal polarization helps to enhance the sensitivities of the couplings relative to the unpolarized case. The most remarkable result from the study of transverse polarization is that it helps to probe a specific coupling Ima_γ which is inaccessible in the distributions with longitudinally polarized as well as unpolarized beams.

In the next two chapters, we study the sensitivity of the LHC to anomalous tbW couplings in single-top production in association with a W^- boson followed by semileptonic decay of the top. We calculate top polarization and the effects of these anomalous couplings to it at two centre-of-mass (cm) energies of 7 TeV and 14 TeV. As a measure of top polarization, we look at various laboratory frame distributions of its decay products, viz., lepton angular and energy distributions and b-quark angular distributions, without requiring reconstruction of the rest frame of the top, and study the effect of anomalous couplings on these distributions. We construct certain asymmetries to study the sensitivity of these distributions to anomalous tbW couplings. We find that 1σ limits on real and imaginary parts of the dominant anomalous coupling $\mathrm{f}_{2\mathrm{R}}$ which may be obtained by utilizing these asymmetries at the LHC with cm energy of 14 TeV and an integrated luminosity of 10 fb^{-1} are at least as good as the expectations from other direct measurements at the LHC and at over an order of magnitude better than the expected indirect search limits. We also study the possibility of CP-violation in anomalous tbW couplings in the single top production process. We construct all the observables (as discussed above) in the case of CP-violation and find that these observables are proportional to the difference of the couplings $\mathrm{f}_{2\mathrm{R}}$ and $\bar{\mathrm{f}}_{2\mathrm{L}}$. We study the sensitivities of these observables to the CP-violation at two configurations of the LHC and probe the difference, $\mathrm{f}_{2\mathrm{R}} - \bar{\mathrm{f}}_{2\mathrm{L}}$, which would be a signal of CP-violation.

We study single top production in association with a charged Higgs in the type II THDM at the Large Hadron Collider. The polarization of the top, reflected in the angular distributions of its decay products, can be a sensitive probe of new physics in its production. We present theoretically expected polarizations of the top for top charged-Higgs production, which is significantly different from that in the closely related process of tW production in the Standard Model. We then show that an azimuthal asymmetry, constructed from the decay lepton angular distribution in the laboratory frame, is a sensitive probe of top polarization and can be used to constrain parameters involved in top charged-Higgs production.

To summarize, we explore different possible ways to probe the mechanism of EWSB through the study of polarization of initial beams in the context of ILC and final state polarization of the top quark in the context of the LHC.

Appendix I

Cross section using longitudinally polarized beams

The expression for the cross section for process $e^-(p_1)e^+(p_2) \to \ell^-(p_3)\ell^+(p_4)H$ with longitudinal polarizations P_L and $\overline{P}_L$ for e^- and e^+ beams respectively is

$$\begin{aligned}\sigma_L &= \int \frac{d^3p_3}{2p_3^0} \int \frac{d^3p_4}{2p_4^0} \Big(\frac{e}{4\sin\theta_W\cos\theta_W}\Big)^2 \\ &\times \frac{1}{(q^2-m_Z^2)^2+\Gamma_Z^2}(1-P_L\overline{P}_L)\left[\mathcal{F}_{SM}^L+\mathcal{F}_Z^L+\mathcal{F}_\gamma^L\right]\end{aligned}$$

where $\mathcal{F}_{SM}^L$, $\mathcal{F}_Z^L$ and $\mathcal{F}_\gamma^L$ are the contributions from the SM alone, interference between the SM and the ZZH terms and interference between the SM and the γZH terms respectively.

Let us first denote :

$$\begin{aligned}
C_Z^{V1} &= ({g_V^f}^2+{g_A^f}^2)\{({g_V^e}^2+{g_A^e}^2)-2g_V^e g_A^e P_L^{\text{eff}}\}, &(7.1)\\
C_Z^{A1} &= 2g_V^f g_A^f\{({g_V^e}^2+{g_A^e}^2)P_L^{\text{eff}}-2g_V^e g_A^e\}, &(7.2)\\
C_\gamma^{V1} &= 2g_V^f g_A^f(g_A^e-g_V^e P_L^{\text{eff}}), &(7.3)\\
C_\gamma^{A1} &= ({g_V^f}^2+{g_A^f}^2)(g_V^e-g_A^e P_L^{\text{eff}}), &(7.4)\\
C_Z^{V2} &= ({g_V^f}^2+{g_A^f}^2)\{({g_V^e}^2+{g_A^e}^2)P_L^{\text{eff}}-2g_V^e g_A^e\}, &(7.5)\\
C_Z^{A2} &= 2g_V^f g_A^f\{({g_V^e}^2+{g_A^e}^2)-2g_V^e g_A^e P_L^{\text{eff}}\}, &(7.6)\\
C_\gamma^{V2} &= 2g_V^f g_A^f(g_V^e-g_A^e P_L^{\text{eff}}), &(7.7)\\
C_\gamma^{A2} &= ({g_V^f}^2+{g_A^f}^2)(g_V^e P_L^{\text{eff}}-g_A^e), &(7.8)\\
\mathcal{E} &= \epsilon_{\alpha\beta\sigma\rho}p_1^\alpha p_2^\beta p_3^\sigma p_4^\rho, &(7.9)\\
s_{ij} &= (p_i\cdot p_j), &(7.10)\\
B_Z &= \frac{m_Z}{s-m_Z^2}\Big(\frac{e}{2\sin\theta_W\cos\theta_W}\Big)^2, &(7.11)\\
B_\gamma &= e^2\frac{m_Z}{s}. &(7.12)
\end{aligned}$$

where g_V^e and g_A^e are the vector and the axial-vector couplings of intial electron and positron with Z while g_V^f and g_A^f are the vector and the axial-vector couplings of final-state fermions with Z. The e and θ_W is the electromagnetic coupling and the weak-mixing angle respectively.

Using the above notations, we write the analytical expressions of the SM contribution $\mathcal{F}^L_{SM}$

$$\mathcal{F}^L_{SM} \;=\; 8B_Z^2\Big[C_Z^{V1}(s_{13}s_{24}+s_{14}s_{23}) - C_Z^{A1}(s_{13}s_{24}-s_{14}s_{23})\Big],$$

the contribution from interference between the SM and the ZZH terms

$$\begin{aligned}
\mathcal{F}^L_Z \;=\;& \frac{8B_Z^2}{m_Z^2}\Big[2m_Z^2\mathrm{Re}\Delta a_Z[C_Z^{V1}\{s_{13}s_{24}+s_{14}s_{23}\} \\
&+ C_Z^{A1}\{s_{14}s_{23}-s_{13}s_{24}\}] \qquad (7.13)\\
&+ \mathrm{Re}b_Z\big\{s_{12}s_{34}[C_Z^{V1}\mathcal{S}_1 - C_Z^{A1}\mathcal{S}_2] \\
&- (s_{14}s_{23}-s_{13}s_{24})[C_Z^{V1}\mathcal{S}_2 - C_Z^{A1}\mathcal{S}_1]\big\} \\
&+ \mathcal{E}\big[\mathrm{Im}b_Z\{C_Z^{V2}\mathcal{S}_4 + C_Z^{A2}\mathcal{S}_3\} - \mathrm{Re}\tilde{b}_Z\{C_Z^{A1}\mathcal{S}_1 - C_Z^{V1}\mathcal{S}_2\}\big] \\
&+ \mathrm{Im}\tilde{b}_Z\{s_{12}s_{34}[C_Z^{A2}\mathcal{S}_3 - C_Z^{V2}\mathcal{S}_4] \\
&+ (s_{14}s_{23}-s_{13}s_{24})[C_Z^{V2}\mathcal{S}_3 - C_Z^{A2}\mathcal{S}_4]\}\Big], \qquad (7.14)
\end{aligned}$$

and the contribution from interference between the SM and the γZH terms

$$\begin{aligned}
\mathcal{F}^L_\gamma \;=\;& \frac{8B_ZB_\gamma}{m_Z^2}\Big[2m_Z^2\mathrm{Re}a_\gamma[C_\gamma^{A1}\{s_{13}s_{24}+s_{14}s_{23}\}] \\
&+ C_\gamma^{V1}\{s_{14}s_{23}-s_{13}s_{24}\}] \\
&+ \mathrm{Re}b_\gamma\big\{s_{12}s_{34}[C_\gamma^{A1}\mathcal{S}_1 - C_\gamma^{V1}\mathcal{S}_2] \\
&- (s_{14}s_{23}-s_{13}s_{24})[C_\gamma^{A1}\mathcal{S}_2 - C_\gamma^{V1}\mathcal{S}_1]\big\} \\
&+ \mathcal{E}\big[\mathrm{Im}b_\gamma\{C_\gamma^{A2}\mathcal{S}_4 + C_\gamma^{V2}\mathcal{S}_3\} - \mathrm{Re}\tilde{b}_\gamma\{C_\gamma^{V1}\mathcal{S}_1 - C_\gamma^{A1}\mathcal{S}_2\}\big] \\
&+ \mathrm{Im}\tilde{b}_\gamma\{s_{12}s_{34}[C_\gamma^{V2}\mathcal{S}_3 - C_\gamma^{A2}\mathcal{S}_4] \\
&+ (s_{14}s_{23}-s_{13}s_{24})[C_\gamma^{A2}\mathcal{S}_3 - C_\gamma^{V2}\mathcal{S}_4]\}\Big]. \qquad (7.15)
\end{aligned}$$

Appendix II

Cross section using transversely polarized beams

The expression for the cross section for process $e^-(p_1)e^+(p_2) \to \ell^-(p_3)\ell^+(p_4)H$ with transverse polarizations P_T and $\overline{P}_T$ for e^- and e^+ beams respectively is

$$\sigma_T = \int \frac{d^3p_3}{2p_3^0} \int \frac{d^3p_4}{2p_4^0} \Big(\frac{e}{4\sin\theta_W \cos\theta_W}\Big)^2 \frac{1}{(q^2 - m_Z^2)^2 + \Gamma_Z^2} \left[\mathcal{F}^T_{SM} + \mathcal{F}^T_Z + \mathcal{F}^T_\gamma\right]$$

where $\mathcal{F}^T_{SM}$, $\mathcal{F}^T_Z$ and $\mathcal{F}^T_\gamma$ are the contributions from the SM alone, interference between the SM and the ZZH terms and interference between the SM and the γZH terms respectively.

Let us first denote :

$$\begin{aligned}
\mathcal{E}3 &= \epsilon_{\alpha\beta\sigma\rho} n^\alpha p_3^\beta p_1^\sigma p_2^\rho & (7.16)\\
\mathcal{E}4 &= \epsilon_{\alpha\beta\sigma\rho} n^\alpha p_4^\beta p_1^\sigma p_2^\rho & (7.17)\\
\mathcal{S}_1 &= s_{13} + s_{14} + s_{23} + s_{24} & (7.18)\\
\mathcal{S}_2 &= s_{13} - s_{14} - s_{23} + s_{24} & (7.19)\\
\mathcal{S}_3 &= s_{13} - s_{14} + s_{23} - s_{24} & (7.20)\\
\mathcal{S}_4 &= s_{13} + s_{14} - s_{23} - s_{24} & (7.21)\\
s_{in} &= p_i \cdot n & (7.22)
\end{aligned}$$

where n is the spin four vector of the inital electron and positron.

Using the above notations, we write the analytical expressions of the SM contribution $\mathcal{F}^T_{SM}$

$$\begin{aligned}
\mathcal{F}^T_{\mathrm{SM}} &= 8B_Z^2\Big[({g_V^f}^2 + {g_A^f}^2)\{[({g_V^e}^2 + {g_A^e}^2) - P_T\overline{P}_T({g_V^e}^2 - {g_A^e}^2)]\}\\
&\times\ (s_{14}s_{23} + s_{13}s_{24}) + 4g_V^f g_A^f g_V^e g_A^e (s_{14}s_{23} - s_{13}s_{24})\\
&+\ P_T\overline{P}_T({g_V^f}^2 + {g_A^f}^2)({g_V^e}^2 - {g_A^e}^2) s_{12}(2s_{3n}s_{4n} + s_{34})\Big], \qquad (7.23)
\end{aligned}$$

the $\mathcal{F}^T_Z$ which comes from interference between the SM and the ZZH terms

$$\mathcal{F}^T_Z = \mathcal{F}^T_{\mathrm{Re}\Delta a_Z} + \mathcal{F}^T_{\mathrm{Re}b_Z} + \mathcal{F}^T_{\mathrm{Im}b_Z} + \mathcal{F}^T_{\mathrm{Re}\tilde{b}_Z} + \mathcal{F}^T_{\mathrm{Im}\tilde{b}_Z} \qquad (7.24)$$

where

$$\begin{aligned}
\mathcal{F}^T_{\mathrm{Re}\Delta a_Z} &= 16B_Z^2 \mathrm{Re}\Delta a_Z\Big[({g_V^f}^2 + {g_A^f}^2)\{[({g_V^e}^2 + {g_A^e}^2) - P_T\overline{P}_T({g_V^e}^2 - {g_A^e}^2)]\}\\
&\times(s_{14}s_{23} + s_{13}s_{24}) + 4g_V^f g_A^f g_V^e g_A^e (s_{14}s_{23} - s_{13}s_{24})\\
&+P_T\overline{P}_T({g_V^f}^2 + {g_A^f}^2)({g_V^e}^2 - {g_A^e}^2) s_{12}(2s_{3n}s_{4n} + s_{34})\Big] \qquad (7.25)
\end{aligned}$$

$$\begin{aligned}
\mathcal{F}^T_{\mathrm{Re}b_Z} &= \frac{8B_Z^2}{m_Z^2}\mathrm{Re}b_Z\Big[(g_V^{f\,2}+g_A^{f\,2})\Big\{(g_V^{e\,2}+g_A^{e\,2})[s_{12}s_{34}\mathcal{S}_1-(s_{14}s_{23}-s_{13}s_{24})\mathcal{S}_2] \\
&- P_T\overline{P}_T(g_V^{e\,2}-g_A^{e\,2})[s_{12}s_{34}\mathcal{S}_1+(s_{14}s_{23}-s_{13}s_{24})\mathcal{S}_2 \\
&+ 2s_{12}s_{3n}s_{4n}\mathcal{S}_1-2s_{12}(s_{13}+s_{23})s_{4n}^2-2s_{12}s_{3n}^2(s_{14}+s_{24})]\Big\} \\
&+ 4g_V^f g_A^f g_V^e g_A^e\left\{(s_{14}s_{23}-s_{13}s_{24})\mathcal{S}_1-s_{12}s_{34}\mathcal{S}_2\right\}\Big] \qquad (7.26)
\end{aligned}$$

$$\begin{aligned}
\mathcal{F}^T_{\mathrm{Im}b_Z} &= \frac{8B_Z^2}{m_Z^2}\mathrm{Im}b_Z\Big[(g_V^{f\,2}+g_A^{f\,2})(2g_V^e g_A^e)(\mathcal{E}4s_{3n}-\mathcal{E}3s_{4n})\mathcal{S}_3 \\
&+ 2g_V^f g_A^f(g_V^{e\,2}+g_A^{e\,2})(\mathcal{E}_3s_{4n}-\mathcal{E}_4s_{3n})\mathcal{S}_4+2g_V^f g_A^f(g_V^{e\,2}-g_A^{e\,2})P_T\overline{P}_T \\
&\times [(\mathcal{E}3s_{4n}+\mathcal{E}4s_{3n})\mathcal{S}_2+2s_{3n}(s_{24}-s_{14})\mathcal{E}3+2s_{4n}(s_{13}-s_{23})\mathcal{E}4]\Big] \qquad (7.27)
\end{aligned}$$

$$\begin{aligned}
\mathcal{F}^T_{\mathrm{Re}\tilde{b}_Z} &= \frac{8B_Z^2}{m_Z^2}\mathrm{Re}\tilde{b}_Z\Big[(g_V^{f\,2}+g_A^{f\,2})(g_V^{e\,2}+g_A^{e\,2})\mathcal{S}_2(s_{3n}\mathcal{E}4-s_{4n}\mathcal{E}3) \\
&- 2g_V^f g_A^f 2g_V^e g_A^e\mathcal{S}_1(s_{4n}\mathcal{E}3-s_{3n}\mathcal{E}4)-P_T\overline{P}_T(g_V^{f\,2}+g_A^{f\,2}) \\
&\times (g_V^{e\,2}-g_A^{e\,2})[(s_{4n}\mathcal{E}3+s_{3n}\mathcal{E}4)\mathcal{S}_4-2\mathcal{E}3s_{3n}(s_{14}-s_{24}) \\
&- 2\mathcal{E}4s_{4n}(s_{13}-s_{23})]\Big] \qquad (7.28)
\end{aligned}$$

$$\begin{aligned}
\mathcal{F}^T_{\mathrm{Im}\tilde{b}_Z} &= \frac{8B_Z^2}{m_Z^2}\mathrm{Im}\tilde{b}_Z\Big[2g_V^f g_A^f(g_V^{e\,2}+g_A^{e\,2})\{s_{12}s_{34}\mathcal{S}_3-(s_{14}s_{23}-s_{13}s_{24})\mathcal{S}_4\} \\
&- P_T\overline{P}_T 2g_V^f g_A^f(g_V^{e\,2}-g_A^{e\,2})\{(s_{14}s_{23}-s_{13}s_{24})\mathcal{S}_4 \\
&+ s_{12}s_{34}\mathcal{S}_3+2s_{12}[s_{3n}^2(s_{14}+s_{24})-s_{4n}^2(s_{13}+s_{23})-s_{3n}s_{4n}\mathcal{S}_3]\} \\
&+ 2(g_V^{f\,2}+g_A^{f\,2})g_V^e g_A^e\{(s_{14}s_{23}-s_{13}s_{24})\mathcal{S}_3-s_{12}s_{34}\mathcal{S}_4\}\Big] \qquad (7.29)
\end{aligned}$$

and the F^T_γ which comes from interference between the SM and the γZH terms

$$\mathcal{F}^T_\gamma = \mathcal{F}^T_{\mathrm{Re}a_\gamma}+F^T_{\mathrm{Im}a_\gamma}+\mathcal{F}^T_{\mathrm{Re}b_\gamma}+\mathcal{F}^T_{\mathrm{Im}b_\gamma}+\mathcal{F}^T_{\mathrm{Re}\tilde{b}_\gamma}+\mathcal{F}^T_{\mathrm{Im}\tilde{b}_\gamma} \qquad (7.30)$$

where

$$\begin{aligned}
\mathcal{F}^T_{\mathrm{Re}a_\gamma} &= 16B_ZB_\gamma\mathrm{Re}a_\gamma\Big[g_V^e(1+P_T\overline{P}_T)\}(s_{14}s_{23}+s_{13}s_{24}) \\
&\quad +2g_V^f g_A^f g_A^e(s_{14}s_{23}-s_{13}s_{24}) \\
&\quad +P_T\overline{P}_T(g_V^{f\,2}+g_A^{f\,2})g_V^e s_{12}(2s_{3n}s_{4n}+s_{34})\Big] \qquad (7.31)
\end{aligned}$$

$$\mathcal{F}^T_{\mathrm{Im}a_\gamma} = 8B_ZB_\gamma\Big[2g_A^e(g_V^{f\,2}+g_A^{f\,2})P_T\overline{P}_T\{s_{3n}\mathcal{E}4+s_{4n}\mathcal{E}3\}\Big]\mathrm{Im}a_\gamma \qquad (7.32)$$

$$
\begin{aligned}
\mathcal{F}^T_{\mathrm{Re}b_\gamma} &= \frac{8B_ZB_\gamma}{m_Z^2}\mathrm{Re}b_\gamma\Big[({g_V^f}^2+{g_A^f}^2)\Big\{g_V^e[s_{12}s_{34}\mathcal{S}_1-(s_{14}s_{23}-s_{13}s_{24})\mathcal{S}_2] \\
&- g_V^eP_T\overline{P}_T[s_{12}s_{34}\mathcal{S}_1+(s_{14}s_{23}-s_{13}s_{24})\mathcal{S}_2 \\
&+ 2s_{12}s_{3n}s_{4n}\mathcal{S}_1-2s_{12}(s_{13}+s_{23})s_{4n}^2-2s_{12}s_{3n}^2(s_{14}+s_{24})]\Big\} \\
&+ 2g_V^fg_A^fg_A^e[(s_{14}s_{23}-s_{13}s_{24})\mathcal{S}_1-s_{12}s_{34}\mathcal{S}_2] \\
&- 2g_V^fg_A^fg_A^eP_T\overline{P}_T[(s_{14}s_{23}-s_{13}s_{24})\mathcal{S}_1+s_{12}s_{34}\mathcal{S}_2 \\
&+ 2s_{12}\{s_{3n}s_{4n}\mathcal{S}_2-s_{3n}^2(s_{14}-s_{24})+s_{4n}^2(s_{13}-s_{23})\}]\Big] \qquad (7.33)
\end{aligned}
$$

$$
\begin{aligned}
\mathcal{F}^T_{\mathrm{Im}b_\gamma} &= \frac{8B_ZB_\gamma}{m_Z^2}\mathrm{Im}b_\gamma\Big[({g_V^f}^2+{g_A^f}^2)g_A^e(\mathcal{E}4s_{3n}-\mathcal{E}3s_{4n})\mathcal{S}_3 \\
&+ 2g_V^fg_A^fg_V^e(\mathcal{E}_3s_{4n}-\mathcal{E}_4s_{3n})\mathcal{S}_4-2g_V^eg_V^fg_A^fP_T\overline{P}_T \\
&\times [(\mathcal{E}3s_{4n}+\mathcal{E}4s_{3n})\mathcal{S}_2+2s_{3n}(s_{24}-s_{14})\mathcal{E}3+2s_{4n}(s_{13}-s_{23})\mathcal{E}4] \\
&+ P_T\overline{P}_Tg_A^e({g_V^f}^2+{g_A^f}^2)(\mathcal{E}4s_{3n}+\mathcal{E}3s_{4n})\mathcal{S}_1 \\
&- 2\mathcal{E}4s_{4n}(s_{13}+s_{23})-2\mathcal{E}3s_{3n}(s_{14}+s_{24})\Big] \qquad (7.34)
\end{aligned}
$$

$$
\begin{aligned}
\mathcal{F}^T_{\mathrm{Re}\tilde{b}_\gamma} &= \frac{8B_ZB_\gamma}{m_Z^2}\mathrm{Re}\tilde{b}_\gamma\Big[({g_V^f}^2+{g_A^f}^2)g_V^e\mathcal{S}_2(s_{3n}\mathcal{E}4-s_{4n}\mathcal{E}3) \\
&- 2g_V^fg_A^fg_A^e\mathcal{S}_1(s_{4n}\mathcal{E}3-s_{3n}\mathcal{E}4)+P_T\overline{P}_T({g_V^f}^2+{g_A^f}^2) \\
&\times g_V^e[(s_{4n}\mathcal{E}3+s_{3n}\mathcal{E}4)\mathcal{S}_4-2\mathcal{E}3s_{3n}(s_{14}-s_{24}) \\
&- 2\mathcal{E}4s_{4n}(s_{13}-s_{23})]-2P_T\overline{P}_Tg_V^fg_A^fg_A^e\{s_{4n}\mathcal{E}_3+s_{3n}\mathcal{E}_4\}\mathcal{S}_3 \\
&- 2\mathcal{E}4s_{4n}(s_{13}+s_{23})+2\mathcal{E}3s_{3n}(s_{14}+s_{24})\Big] \qquad (7.35)
\end{aligned}
$$

$$
\begin{aligned}
\mathcal{F}^T_{\mathrm{Im}\tilde{b}_\gamma} &= \frac{8B_ZB_\gamma}{m_Z^2}\mathrm{Im}\tilde{b}_\gamma\Big[2g_V^fg_A^fg_V^e\{s_{12}s_{34}\mathcal{S}_3-(s_{14}s_{23}-s_{13}s_{24})\mathcal{S}_4\} \\
&- 2g_V^fg_A^fg_V^eP_T\overline{P}_T\{(s_{14}s_{23}-s_{13}s_{24})\mathcal{S}_4+s_{12}s_{34}\mathcal{S}_3 \\
&+ 2s_{12}[s_{3n}^2(s_{14}+s_{24})-s_{4n}^2(s_{13}+s_{23})-s_{3n}s_{4n}\mathcal{S}_3]\} \\
&+ ({g_V^f}^2+{g_A^f}^2)g_A^e\{(s_{14}s_{23}-s_{13}s_{24})\mathcal{S}_3-s_{12}s_{34}\mathcal{S}_4\} \\
&- g_A^e({g_V^f}^2+{g_A^f}^2)P_T\overline{P}_T\{(s_{14}s_{23}-s_{13}s_{24})\mathcal{S}_3+s_{12}s_{34}\mathcal{S}_4 \\
&+ 2s_{12}[s_{3n}^2(s_{14}-s_{24})+s_{4n}^2(s_{13}-s_{23})-s_{3n}s_{4n}\mathcal{S}_4]\}\Big]. \qquad (7.36)
\end{aligned}
$$

Appendix III

In this appendix, we give the spin density matrix elements for the single-top production process. For this we use the following notation for scalar products of four-momenta involved in the process: $(p_t \cdot p_b) = \mathcal{S}_{tb}$, $(p_t \cdot p_g) = \mathcal{S}_{tg}$ and $(p_b \cdot p_g) = \mathcal{S}_{bg}$. Also, we use the following expressions :

$$\begin{aligned}
\mathcal{F}_1 &= \frac{g^2 g_s^2}{24\mathcal{S}_{tg}^2\mathcal{S}_{bg}^2}\left[\left\{|\mathrm{f_{1L}}|^2\left(1+\frac{m_t^2}{2m_W^2}\right)+3\mathrm{Ref_{1L}f_{2R}^*}\frac{m_t}{m_W}+3|\mathrm{f_{2R}}|^2\frac{m_t^2}{2m_W^2}\right\}\right.\\
&\times \left\{[\mathcal{S}_{tb}+\mathcal{S}_{tg}-\mathcal{S}_{bg}]\left[2\mathcal{S}_{tg}\mathcal{S}_{tb}\mathcal{S}_{bg}-m_t^2\mathcal{S}_{bg}^2\right]-\mathcal{S}_{tg}\mathcal{S}_{bg}\left[\mathcal{S}_{bg}^2-\mathcal{S}_{tg}^2\right]\right\}\\
&- |\mathrm{f_{1L}}|^2\frac{m_t^2}{m_W^2}\mathcal{S}_{tg}^2\mathcal{S}_{bg}^2+\mathrm{Ref_{1L}f_{2R}^*}\frac{m_t}{m_W}\left\{2\mathcal{S}_{tg}\mathcal{S}_{bg}^2[\mathcal{S}_{bg}-\mathcal{S}_{tg}]\right\}\\
&+ \frac{|\mathrm{f_{2R}}|^2}{m_W^2}\left\{m_t^2[-\mathcal{S}_{bg}^2(\mathcal{S}_{bg}\mathcal{S}_{tg}-\mathcal{S}_{tb}^2+\mathcal{S}_{bg}^2)]+\mathcal{S}_{tg}\mathcal{S}_{bg}\left[\mathcal{S}_{tb}(\mathcal{S}_{tg}+\mathcal{S}_{tb}-\mathcal{S}_{bg})\right.\right.\\
&\times \left.\left.\left.\{3(\mathcal{S}_{bg}-\mathcal{S}_{tg})-\mathcal{S}_{tb}\}+\{(\mathcal{S}_{bg}+\mathcal{S}_{tg})(\mathcal{S}_{bg}^2-\mathcal{S}_{tg}^2)-\mathcal{S}_{tg}^3\}\right]\right\}\right]
\end{aligned}$$

$$\begin{aligned}
\mathcal{F}_2 &= \frac{g^2 g_s^2}{12\mathcal{S}_{tg}^2\mathcal{S}_{bg}^2}\left[\left\{|\mathrm{f_{1L}}|^2\left(1-\frac{m_t^2}{2m_W^2}\right)+\mathrm{Ref_{1L}f_{2R}^*}\frac{m_t}{m_W}+|\mathrm{f_{2R}}|^2\frac{m_t^2}{2m_W^2}\right\}m_t\mathcal{S}_{bg}\right.\\
&\times \left[(\mathcal{S}_{bn}+\mathcal{S}_{gn})\mathcal{S}_{tg}(\mathcal{S}_{tb}+\mathcal{S}_{tg})-\mathcal{S}_{bg}\left(\mathcal{S}_{tb}\mathcal{S}_{gn}+\mathcal{S}_{tg}\mathcal{S}_{bn}+m_t^2\mathcal{S}_{bn}-\mathcal{S}_{gn}\right)+\mathcal{S}_{tb}\mathcal{S}_{tg}\mathcal{S}_{bn}\right]\\
&- |\mathrm{f_{1L}}|^2\frac{m_t^2}{m_W^2}\mathcal{S}_{tg}\mathcal{S}_{bg}^2\mathcal{S}_{gn}+\mathrm{Ref_{1L}f_{2R}^*}\frac{1}{m_W}\left\{2\mathcal{S}_{tg}^2\mathcal{S}_{bg}[\mathcal{S}_{tb}\mathcal{S}_{gn}-\mathcal{S}_{tg}\mathcal{S}_{bn}]\right\}\\
&+ |\mathrm{f_{2R}}|^2\left\{\mathcal{S}_{bn}(\mathcal{S}_{tb}-\mathcal{S}_{bg}+\mathcal{S}_{tg})(m_t^2\mathcal{S}_{bg}^2-3\mathcal{S}_{bg}\mathcal{S}_{tg}^2+\mathcal{S}_{bg}^2\mathcal{S}_{tg}-2\mathcal{S}_{bg}\mathcal{S}_{tg}\mathcal{S}_{tb})\right.\\
&+ 2\mathcal{S}_{bg}\mathcal{S}_{tg}^2\mathcal{S}_{tb}+\mathcal{S}_{gn}(\mathcal{S}_{tb}-\mathcal{S}_{bg}-\mathcal{S}_{tg})(-\mathcal{S}_{bg}\mathcal{S}_{tg}\mathcal{S}_{tb}+\mathcal{S}_{bg}\mathcal{S}_{tg}^2-\mathcal{S}_{bg}^3)-2\mathcal{S}_{bg}\mathcal{S}_{tg}^3\\
&+ \left.\left.\mathcal{S}_{bg}^2(\mathcal{S}_{tb}\mathcal{S}_{bg}+2\mathcal{S}_{bg}\mathcal{S}_{tg}+\mathcal{S}_{bg}^2+m_t^2\mathcal{S}_{tg})\right\}\right]
\end{aligned}$$

The diagonal elements of the spin density matrix for single-top production in tW channel can be written as

$$\rho(\pm,\pm) = \mathcal{F}_1 \pm \mathcal{F}_2 \tag{7.37}$$

with $\mathcal{S}_{gn} = (p_g.n_3)$ and $\mathcal{S}_{bn} = (p_b.n_3)$ and the off-diagonal elements are

$$\rho(\pm,\mp) = \mathcal{F}_2 \tag{7.38}$$

with $\mathcal{S}_{gn} = (p_g \cdot (n_1 \pm in_2))$ and $\mathcal{S}_{bn} = (p_b \cdot (n_1 \pm in_2))$ where n_i^μ's $(i = 1, 2, 3)$ are the four-vectors with the properties $n_i \cdot n_j = -\delta_{ij}$ and $n_i \cdot p_t = 0$. n_1, n_2 and n_3 represent spin four-vectors of the top quark with spin respectively along the x, y and z axis in the top rest frame.

Bibliography

[1] P. W. Higgs, Phys. Rev. Lett. **13**, 508 (1964); Phys. Rev. **145**, 1156 (1966); F. Englert and R. Brout, Phys. Rev. Lett. **13**, 321 (1964); G. S. Guralnik, C. R. Hagen and T. W. B. Kibble, Phys. Rev. Lett. **13**, 585 (1964).

[2] S. Glashow, Nucl. Phys. 22 (1961) 579; S. Weinberg, Phys./ Rev./ Lett. 19 (1967) 1264; A. Salam, in "Elementary Particle Theory", ed. by N. Svartholm, Almqvist and Wiksells, Stockholm (1969) p. 367.

[3] C. N. Yang and R. L. Mills, Phys. Rev. **96**, 191 (1954).

[4] T. P. Cheng, E. Eichten and L. F. Li, Phys. Rev. D **9**, 2259 (1974); B. Pendleton and G. G. Ross, Phys. Lett. B **98**, 291 (1981); J. Bagger, S. Dimopoulos and E. Masso, Nucl. Phys. B **253**, 397 (1985); A. Djouadi, Phys. Rept. **457**, 1 (2008) [arXiv:hep-ph/0503172].

[5] T. Hambye and K. Riesselmann, arXiv:hep-ph/9708416; Phys. Rev. D **55**, 7255 (1997) [arXiv:hep-ph/9610272].

[6] R. Barate *et al.* [LEP Working Group for Higgs boson searches and ALEPH Collaboration and and], Phys. Lett. B **565**, 61 (2003) [arXiv:hep-ex/0306033].

[7] [CDF and D0 Collaboration], arXiv:0903.4001 [hep-ex].

[8] J. Alcaraz *et al.* [LEP Collaborations and ALEPH Collaboration and DELPHI Collaboration an], arXiv:0712.0929 [hep-ex].

[9] P. C. Rowson, D. Su, S. Willocq, Ann. Rev. Nucl. Part. Sci. **51**, 345-412 (2001). [hep-ph/0110168].

[10] N. Phinney, ICFA Beam Dyn. Newslett. **42**, 7 (2007).

[11] Presentation slides by Jim Clarke at ILC/LCWS10:
`http://ilcagenda.linearcollider.org/materialDisplay.py?contribId=379&sessionId=8&materialId=slides&confId=4175`

[12] G. Moortgat-Pick *et al.*, Phys. Rept. **460**, 131 (2008) [arXiv:hep-ph/0507011].

[13] I. I. Y. Bigi, Y. L. Dokshitzer, V. A. Khoze, J. H. Kuhn and P. M. Zerwas, Phys. Lett. B **181**, 157 (1986).

[14] W. Bernreuther, J. Phys. G **35**, 083001 (2008) [arXiv:0805.1333 [hep-ph]];

[15] M. Beneke *et al.*, arXiv:hep-ph/0003033;

[16] W. Wagner, Rept. Prog. Phys. **68**, 2409 (2005) [arXiv:hep-ph/0507207].

[17] G. Mahlon and S.J. Parke, Phys. Rev. D **53**, 4886 (1996) [arXiv:hep-ph/9512264]; Phys. Lett. B **411**, 173 (1997) [arXiv:hep-ph/9706304]; T. Stelzer and S. Willenbrock, Phys. Lett. B **374**, 169 (1996) [arXiv:hep-ph/9512292]; W. Bernreuther, A. Brandenberg, Z.G. Si and P. Uwer, Phys. Rev. Lett. **87**, 242002 (2001) [arXiv:hep-ph/0107086]; Nucl. Phys. B **690**, 81 (2004) [arXiv:hep-ph/0403035]; M. Arai, N. Okada, K. Smolek and V. Simak, Phys. Rev. D **75**, 095008 (2007) [arXiv:hep-ph/0701155].

[18] P. Achard *et al.* [L3 Collaboration], Phys. Lett. B **589**, 89 (2004) [arXiv:hep-ex/0403037].

[19] A. Djouadi, J. Lykken, K. Monig, Y. Okada, M. J. Oreglia, S. Yamashita *et al.*, arXiv:0709.1893 [hep-ph].

[20] V. D. Barger, K. m. Cheung, A. Djouadi, B. A. Kniehl and P. M. Zerwas, Phys. Rev. D **49**, 79 (1994) [arXiv:hep-ph/9306270]. W. Kilian, M. Kramer and P. M. Zerwas, arXiv:hep-ph/9605437; Phys. Lett. B **381**, 243 (1996) [arXiv:hep-ph/9603409]. J. F. Gunion, B. Grzadkowski and X. G. He, Phys. Rev. Lett. **77**, 5172 (1996) [arXiv:hep-ph/9605326]. M. C. Gonzalez-Garcia, S. M. Lietti and S. F. Novaes, Phys. Rev. D **59**, 075008 (1999) [arXiv:hep-ph/9811373]. V. Barger, T. Han, P. Langacker, B. McElrath and P. Zerwas, Phys. Rev. D **67**, 115001 (2003). [arXiv:hep-ph/0301097];

[21] A. Gutierrez-Rodriguez, J. Montano and M. A. Perez, arXiv:1009.4354 [hep-ph].

[22] K. Hagiwara and M. L. Stong, Z. Phys. C **62**, 99 (1994) [arXiv:hep-ph/9309248].

[23] A. Skjold and P. Osland, Nucl. Phys. B **453**, 3 (1995) [arXiv:hep-ph/9502283].

[24] G. J. Gounaris, F. M. Renard and N. D. Vlachos, Nucl. Phys. B **459**, 51 (1996) [arXiv:hep-ph/9509316].

[25] T. Han and J. Jiang, Phys. Rev. D **63**, 096007 (2001) [arXiv:hep-ph/0011271].

[26] S. S. Biswal, R. M. Godbole, R. K. Singh and D. Choudhury, Phys. Rev. D **73**, 035001 (2006) [Erratum-ibid. D **74**, 039904 (2006)] [arXiv:hep-ph/0509070]; S. S. Biswal, D. Choudhury, R. M. Godbole and Mamta, arXiv:0809.0202 [hep-ph].

[27] S. S. Biswal and R. M. Godbole, Phys. Lett. B **680**, 81 (2009) [arXiv:0906.5471 [hep-ph]].

[28] Q. H. Cao, F. Larios, G. Tavares-Velasco and C. P. Yuan, Phys. Rev. D **74**, 056001 (2006) [arXiv:hep-ph/0605197].

[29] K. Hagiwara, S. Ishihara, J. Kamoshita and B. A. Kniehl, Eur. Phys. J. C **14**, 457 (2000) [arXiv:hep-ph/0002043].

[30] S. Dutta, K. Hagiwara and Y. Matsumoto, arXiv:0808.0477 [hep-ph].

[31] K. Rao and S. D. Rindani, Phys. Lett. B **642**, 85 (2006) [arXiv:hep-ph/0605298].

[32] K. Rao and S. D. Rindani, Phys. Rev. D **77**, 015009 (2008) [arXiv:0709.2591 [hep-ph]].

[33] G. Moortgat-Pick *et al.*, Phys. Rept. **460**, 131 (2008) [arXiv:hep-ph/0507011].

[34] B. Ananthanarayan and S. D. Rindani, Phys. Rev. D **70**, 036005 (2004) [arXiv:hep-ph/0309260];

[35] B. Ananthanarayan, S. D. Rindani, R. K. Singh and A. Bartl, Phys. Lett. B **593**, 95 (2004) [Erratum-ibid. B **608**, 274 (2005)] [arXiv:hep-ph/0404106];

[36] S. D. Rindani, arXiv:hep-ph/0409014.

[37] B. Ananthanarayan and S. D. Rindani, Phys. Lett. B **606**, 107 (2005) [arXiv:hep-ph/0410084]; JHEP **0510**, 077 (2005) [arXiv:hep-ph/0507037];

[38] S. D. Rindani, Phys. Lett. B **602**, 97 (2004) [arXiv:hep-ph/0408083].

[39] T. G. Rizzo, JHEP **0302**, 008 (2003) [arXiv:hep-ph/0211374]; JHEP **0308**, 051 (2003) [arXiv:hep-ph/0306283]; J. Fleischer, K. Kolodziej and F. Jegerlehner, Phys. Rev. D **49**, 2174 (1994); M. Diehl, O. Nachtmann and F. Nagel, Eur. Phys. J. C **32**, 17 (2003) [arXiv:hep-ph/0306247]; S. Y. Choi, J. Kalinowski, G. Moortgat-Pick and P. M. Zerwas, Eur. Phys. J. C **22**, 563 (2001) [Addendum-ibid. C **23**, 769 (2002)] [arXiv:hep-ph/0108117]; A. Bartl, K. Hohenwarter-Sodek, T. Kernreiter and H. Rud, Eur. Phys. J. C **36**, 515 (2004) [arXiv:hep-ph/0403265]; J. Kalinowski, arXiv:hep-ph/0410137; P. Osland and N. Paver, arXiv:hep-ph/0507185; A. Bartl, H. Fraas, S. Hesselbach, K. Hohenwarter-Sodek, T. Kernreiter and G. Moortgat-Pick, JHEP **0601**, 170 (2006) [arXiv:hep-ph/0510029]; S. Y. Choi, M. Drees and J. Song, JHEP **0609**, 064 (2006) [arXiv:hep-ph/0602131]; K. Huitu and S. K. Rai, Phys. Rev. D **77**, 035015 (2008) [arXiv:0711.4754 [hep-ph]].

[40] B. Ananthanarayan and S. D. Rindani, Eur. Phys. J. C **46**, 705 (2006); [arXiv:hep-ph/0601199]. Eur. Phys. J. C **56**, 171 (2008) [arXiv:0805.2279 [hep-ph]].

[41] P. Poulose and S. D. Rindani, Phys. Lett. B **383**, 212 (1996) [arXiv:hep-ph/9606356]; Phys. Rev. D **54**, 4326 (1996) [Erratum-ibid. D **61**, 119901 (2000)] [arXiv:hep-ph/9509299]; Phys. Lett. B **349**, 379 (1995) [arXiv:hep-ph/9410357]; F. Cuypers and S. D. Rindani, Phys. Lett. B **343**, 333 (1995) [arXiv:hep-ph/9409243]. D. Choudhury and S. D. Rindani, Phys. Lett. B **335**, 198 (1994) [arXiv:hep-ph/9405242]; S. D. Rindani, Pramana **61**, 33 (2003) [arXiv:hep-ph/0304046].

[42] J. A. M. Vermaseren, arXiv:math-ph/0010025.

[43] K.-i. Hikasa, Phys. Rev. D **33**, 3203 (1986).

[44] See, for example, S.D. Rindani, Pramana **49**, 81 (1997); Pramana **45**, S263 (1995) [arXiv:hep-ph/9411398]; G. C. Branco, L. Lavoura and J. P. Silva, *Oxford, UK: Clarendon (1999) 511 p*

[45] P. Ciafaloni, D. Comelli and A. Vergine, JHEP **0407**, 039 (2004). [arXiv:hep-ph/0311260].

[46] R. S. Chivukula, E. Gates, E. H. Simmons and J. Terning, Phys. Lett. B **311**, 157 (1993) [arXiv:hep-ph/9305232].

[47] F. Abe *et al.* [CDF Collaboration], Phys. Rev. Lett. **73**, 225 (1994) [arXiv:hep-ex/9405005].

[48] [CDF and D0 Collaboration], arXiv:hep-ex/0703034.

[49] K. Huitu, S. K. Rai, K. Rao, S. D. Rindani, P. Sharma, JHEP **1104**, 026 (2011) [arXiv:1012.0527 [hep-ph]].

[50] M. Arai, K. Huitu, S. K. Rai, K. Rao, JHEP **1008**, 082 (2010) [arXiv:1003.4708 [hep-ph]].

[51] R. M. Godbole, K. Rao, S. D. Rindani, R. K. Singh, JHEP **1011**, 144 (2010) [arXiv:1010.1458 [hep-ph]].

[52] D. Choudhury, R. M. Godbole, S. D. Rindani, P. Saha, [arXiv:1012.4750 [hep-ph]].

[53] E. L. Berger, Q. -H. Cao, C. -R. Chen, H. Zhang, [arXiv:1103.3274 [hep-ph]].

[54] A. Heinson, A. S. Belyaev, E. E. Boos, Phys. Rev. **D56**, 3114-3128 (1997) [hep-ph/9612424].

[55] T. Stelzer, Z. Sullivan and S. Willenbrock, Phys. Rev. D **58**, 094021 (1998) [arXiv:hep-ph/9807340].

[56] A. S. Belyaev, E. E. Boos and L. V. Dudko, Phys. Rev. D **59**, 075001 (1999) [arXiv:hep-ph/9806332].

[57] E. Boos, L. Dudko and T. Ohl, Eur. Phys. J. C **11**, 473 (1999) [arXiv:hep-ph/9903215].

[58] T. M. P. Tait, Phys. Rev. D **61**, 034001 (2000) [arXiv:hep-ph/9909352].

[59] D. Espriu and J. Manzano, Phys. Rev. D **65**, 073005 (2002) [arXiv:hep-ph/0107112].

[60] D. Espriu and J. Manzano, Phys. Rev. D **66**, 114009 (2002) [arXiv:hep-ph/0209030].

[61] T. M. P. Tait and C. P. P. Yuan, Phys. Rev. D **63**, 014018 (2000) [arXiv:hep-ph/0007298].

[62] T. Aaltonen *et al.* [The CDF Collaboration], Phys. Rev. Lett. **105**, 042002 (2010) [arXiv:1003.0224 [hep-ex]].

[63] V. M. Abazov *et al.* [D0 Collaboration], Phys. Rev. D **83**, 032009 (2011) [arXiv:1011.6549 [hep-ex]].

[64] C. R. Chen, F. Larios and C. P. Yuan, Phys. Lett. B **631**, 126 (2005) [AIP Conf. Proc. **792**, 591 (2005)] [arXiv:hep-ph/0503040].

[65] G. Aad *et al.* [ATLAS Collaboration], Report No. ATLAS-CONF-2011-037; S. Chatrchyan *et al.* [CMS Collaboration], arXiv:1104.3829 [hep-ex].

[66] J. A. Aguilar-Saavedra, N. F. Castro and A. Onofre, Phys. Rev. D **83**, 117301 (2011) [arXiv:1105.0117 [hep-ph]].

[67] S. Chatrchyan *et al.* [CMS Collaboration], arXiv:1106.3052 [hep-ex].

[68] J. A. Aguilar-Saavedra, J. Carvalho, N. F. Castro, F. Veloso and A. Onofre, Eur. Phys. J. C **50**, 519 (2007) [arXiv:hep-ph/0605190].

[69] W. Bernreuther, P. Gonzalez, M. Wiebusch, Eur. Phys. J. **C60**, 197-211 (2009) [arXiv:0812.1643 [hep-ph]].

[70] P. L. Cho and M. Misiak, Phys. Rev. D **49**, 5894 (1994) [arXiv:hep-ph/9310332].

[71] F. Larios, M. A. Perez and C. P. Yuan, Phys. Lett. B **457**, 334 (1999) [arXiv:hep-ph/9903394].

[72] G. Burdman, M. C. Gonzalez-Garcia and S. F. Novaes, Phys. Rev. D **61**, 114016 (2000) [arXiv:hep-ph/9906329].

[73] B. Grzadkowski, M. Misiak, Phys. Rev. **D78**, 077501 (2008) [arXiv:0802.1413 [hep-ph]].

[74] J. Drobnak, S. Fajfer and J. F. Kamenik, Phys. Lett. B **701**, 234 (2011) [arXiv:1102.4347 [hep-ph]].

[75] B. Grzadkowski and Z. Hioki, Phys. Lett. **B476**, 87 (2000) [arXiv:hep-ph/9911505]; S. D. Rindani, Pramana **54**, 791 (2000) [arXiv:hep-ph/0002006]; B. Grzadkowski and Z. Hioki, Phys. Lett. **B529**, 82 (2002) [arXiv:hep-ph/0112361]; Phys. Lett. **B557**, 55 (2003) [arXiv:hep-ph/0208079]; Z. Hioki, arXiv:hep-ph/0104105 and arXiv:hep-ph/0210224; K. Ohkuma, Nucl. Phys. Proc. Suppl. **111**,285 (2002) [arXiv:hep-ph/0202126].

[76] R. M. Godbole, S. D. Rindani and R. K. Singh, JHEP **0612**, 021 (2006) [arXiv:hep-ph/0605100].

[77] M. Beccaria, F. M. Renard and C. Verzegnassi, Phys. Rev. D **71**, 033005 (2005) [arXiv:hep-ph/0410089].

[78] J. A. M. Vermaseren, arXiv:math-ph/0010025.

[79] J. Pumplin, A. Belyaev, J. Huston, D. Stump and W. K. Tung, JHEP **0602**, 032 (2006) [arXiv:hep-ph/0512167].

[80] F. Hubaut, E. Monnier, P. Pralavorio, K. Smolek and V. Simak, Eur. Phys. J. C **44S2**, 13 (2005) [arXiv:hep-ex/0508061].

[81] J. A. Aguilar-Saavedra, J. Carvalho, N. F. Castro, A. Onofre, F. Veloso, Eur. Phys. J. **C53**, 689-699 (2008) [arXiv:0705.3041 [hep-ph]].

[82] J. A. Aguilar-Saavedra, Nucl. Phys. **B804**, 160-192 (2008) [arXiv:0803.3810 [hep-ph]].

[83] J. A. Aguilar-Saavedra, J. Bernabeu, Nucl. Phys. **B840**, 349-378 (2010) [arXiv:1005.5382 [hep-ph]].

[84] M. M. Najafabadi, JHEP **0803**, 024 (2008) [arXiv:0801.1939 [hep-ph]].

[85] A. Lucotte, A. Llres, D. Chevallier, ATLAS note ATL-PHYS-PUB-2007-005.

[86] S. Zhu, arXiv:hep-ph/0109269.

[87] M. Beccaria, C. M. Carloni Calame, G. Macorini, G. Montagna, F. Piccinini, F. M. Renard, C. Verzegnassi, Eur. Phys. J. **C53**, 257-265 (2008) [arXiv:0705.3101 [hep-ph]].

[88] A. G. Cohen, D. B. Kaplan and A. E. Nelson, Ann. Rev. Nucl. Part. Sci. **43**, 27 (1993) [arXiv:hep-ph/9302210]; A. Riotto and M. Trodden, Ann. Rev. Nucl. Part. Sci. **49**, 35 (1999) [arXiv:hep-ph/9901362].

[89] A. E. Nelson, D. B. Kaplan and A. G. Cohen, Nucl. Phys. B **373**, 453 (1992). M. Aoki, A. Sugamoto and N. Oshimo, Prog. Theor. Phys. **98**, 1325 (1997) [arXiv:hep-ph/9706287].

[90] S. D. Rindani, arXiv:hep-ph/0202045; Pramana **54**, 791 (2000) [arXiv:hep-ph/0002006]; Pramana **61**, 33 (2003) [arXiv:hep-ph/0304046]; P. Poulose and S. D. Rindani, Phys. Lett. B **383**, 212 (1996) [arXiv:hep-ph/9606356]; Phys. Rev. D **54**, 4326 (1996) [Erratum-ibid. D **61**, 119901 (2000)] [arXiv:hep-ph/9509299]; Phys. Lett. B **349**, 379 (1995) [arXiv:hep-ph/9410357]; B. Ananthanarayan and S. D. Rindani, Phys. Rev. D **70**, 036005 (2004) [arXiv:hep-ph/0309260]; B. Grzadkowski, Phys. Lett. B **305**, 384 (1993) [arXiv:hep-ph/9303204]; M. S. Baek, S. Y. Choi and C. S. Kim, Phys. Rev. D **56**, 6835 (1997) [arXiv:hep-ph/9704312]; D. Chang, W. Y. Keung and I. Phillips, Nucl. Phys. B **408**, 286 (1993) [Erratum-ibid. B **429**, 255 (1994)] [arXiv:hep-ph/9301259]; B. Grzadkowski and Z. Hioki, Phys. Lett. B **391**, 172 (1997) [arXiv:hep-ph/9608306]; Nucl. Phys. B **484**, 17 (1997) [arXiv:hep-ph/9604301].

[91] H. Anlauf, W. Bernreuther and A. Brandenburg, Phys. Rev. D **52**, 3803 (1995) [Erratum-ibid. D **53**, 1725 (1996)] [Phys. Rev. D **53**, 1725 (1996)] [arXiv:hep-ph/9504424]; R. M. Godbole, S. D. Rindani and R. K. Singh, Phys. Rev. D **67**, 095009 (2003) [Erratum-ibid. D **71**, 039902 (2005)] [arXiv:hep-ph/0211136]; P. Poulose and S. D. Rindani, Phys. Lett. B **452**, 347 (1999) [arXiv:hep-ph/9809203]; Phys. Rev. D **57**, 5444 (1998) [Erratum-ibid. D **61**, 119902 (2000)] [arXiv:hep-ph/9709225].

[92] W. Khater and P. Osland, Nucl. Phys. B **661**, 209 (2003) [arXiv:hep-ph/0302004]; A. W. El Kaffas, W. Khater, O. M. Ogreid and P. Osland, Nucl. Phys. B **775**, 45 (2007) [arXiv:hep-ph/0605142]; W. Bernreuther, A. Brandenburg and M. Flesch, arXiv:hep-ph/9812387; H. Y. Zhou, Phys. Rev. D **58**, 114002 (1998) [arXiv:hep-ph/9805358].

[93] K. Y. Lee, D. W. Jung and H. S. Song, Phys. Rev. D **70**, 117701 (2004) [arXiv:hep-ph/0307246]; E. Christova, H. Eberl, E. Ginina and W. Majerotto, Phys. Rev. D **79**, 096005 (2009) [arXiv:0812.4392 [hep-ph]].

[94] A. Lucotte, A. Llres, D. Chevallier, ATLAS note ATL-PHYS-PUB-2007-005.

[95] J. F. Gunion, H. E. Haber, G. L. Kane and S. Dawson, *The Higgs Hunters Guide* (Westview Press, Boulder, CO, 2000).

[96] G. C. Branco, L. Lavoura and J. P. Silva, *CP Violation*, Int. Ser. Monogr. Phys. **103**, 1 (1999).

[97] A. Djouadi, Phys. Rept. **459**, 1-241 (2008). [hep-ph/0503173]; M. S. Carena and H. E. Haber, Prog. Part. Nucl. Phys. **50** (2003) 63 [arXiv:hep-ph/0208209].

[98] R. N. Mohapatra and G. Senjanovic, Phys. Rev. Lett. **44**, 912 (1980); R. N. Mohapatra and G. Senjanovic, Phys. Rev. D **23**, 165 (1981); M. Magg and C. Wetterich, Phys. Lett. B **94**, 61 (1980); G. Lazarides, Q. Shafi and C. Wetterich, Nucl. Phys. B **181**, 287 (1981); J. Schechter and J. W. F. Valle, Phys. Rev. D **22**, 2227 (1980).

[99] D. Espriu, J. Manzano, Phys. Rev. **D66**, 114009 (2002) [hep-ph/0209030]; D. Espriu, J. Manzano, [hep-ph/0109059]; D. Espriu, J. Manzano, Phys. Rev. **D65**, 073005 (2002) [hep-ph/0107112].

[100] J. Pumplin, A. Belyaev, J. Huston, D. Stump and W. K. Tung, JHEP **0602**, 032 (2006) [arXiv:hep-ph/0512167].

[101] B. C. Allanach *et al.*, arXiv:hep-ph/0602198.

[102] R. M. Godbole, S. D. Rindani, K. Rao and R. K. Singh, AIP Conf. Proc. **1200**, 682 (2010) [arXiv:0911.3622 [hep-ph]].

[103] S. Moretti and D. P. Roy, Phys. Lett. B **470**, 209 (1999) [arXiv:hep-ph/9909435].

[104] S. Lowette, J. Heyninck and P. Vanlaer, Report No. CMS CR 2004/031.

[105] K. A. Assamagan and N. Gollub, Eur. Phys. J. C **39S2**, 25 (2005) [arXiv:hep-ph/0406013].

[106] D. P. Roy, Mod. Phys. Lett. A **19**, 1813 (2004) [arXiv:hep-ph/0406102]; Phys. Lett. B **459**, 607 (1999) [arXiv:hep-ph/9905542].

[107] T. Plehn, Phys. Rev. D **67**, 014018 (2003) [arXiv:hep-ph/0206121].

[108] S. h. Zhu, Phys. Rev. D **67**, 075006 (2003) [arXiv:hep-ph/0112109].

[109] N. Kidonakis, JHEP **0505**, 011 (2005) [arXiv:hep-ph/0412422].

[110] M. Beccaria, G. Macorini, L. Panizzi, F. M. Renard and C. Verzegnassi, Phys. Rev. D **80**, 053011 (2009) [arXiv:0908.1332 [hep-ph]].